Department of Physics and Astronomy
University of Heidelberg

Bachelor Thesis in Physics
submitted by

Daniel Fan

born in Aachen (Germany)

2020

A few-level simulation of the time-dependent dynamics of singly excited resonances of molecular hydrogen under the influence of moderately strong, ultrashort laser pulses

This Bachelor Thesis has been carried out by
Daniel Fan
at the `Max-Planck Institut für Kernphysik` in Heidelberg
under the supervision of
Prof. Dr Thomas Pfeifer

Abstract

In this thesis a theoretical study of singly excited resonances of molecular hydrogen under the influence of moderately strong, ultrashort laser pulses was conducted. Motivated by a recent measurement of an absorption spectrum of H_2, a deeper investigation of this system was needed. All numerical calculations were performed within the framework of a few-level model including interactions with laser fields. Certain parameters, as well as the investigated vibronic states in the model system, are obtained from experimental data, so that the system can qualitatively reproduce the real hydrogen. Resonant line shapes were examined. An XUV field is used as an excitation pulse, while an NIR pulse is used to couple dark states with bright states. In absence of an NIR field, the expected Lorentzian line shape could be observed. The full width at half maximum is determined geometrically and its relation to the lifetime is demonstrated successfully. In the presence of the NIR field, the line form becomes asymmetrical - a fit was performed for the occuring `Fano` line shape. The main goal was to observe time-resolved absorption spectra. The absorption spectra showed rich dynamics. To conclude how the time-dependent structures come about, a systematic investigation is performed by forbidding couplings between certain dark and bright states. This break-down of the system to simpler ones enabled us to deduce which couplings between the considered vibronic states cause which time changing structures, imprinted by electronic and nuclear degrees of freedom, in the spectrum.

Zusammenfassung

In dieser Arbeit werden einfach angeregte Resonanzen von molekularem Wasserstoff unter Einfluss von moderat starken, ultrakurzen Laserpulsen theoretisch untersucht. Motiviert wird dies durch ein vor kurzem gemessenes Absorptionsspektrum von H_2, welches eine tiefere Untersuchung dieses Systems veranlasst. Dabei wurden alle numerischen Berechnung im Rahmen einer Few-Level-Simulation durchgeführt, welche die Wechselwirkung mit Laserfeldern berücksichtigt. Gewisse Parameter, sowie die zu untersuchenden Vibrationszustände im Modellsystem konnten unter Berücksichtigung von experimentellen Daten gewonnen werden, sodass das betrachtete System qualitativ das reale Wasserstoff reproduzieren kann. Untersucht wurden die resonanten Linienformen. Dabei dient ein XUV Puls als Anregungspuls, und ein NIR Puls wird verwendent um Kopplungen zwischen hellen und dunklen zu ermöglichen. Ohne Einfluss vom NIR Puls konnte eine zu erwartende Lorentzförmige Kurve beobachtet werden. Geometrisch wurde die Halbwertsbreite bestimmt und somit der Zusammenhang dieser Größe zur Lebenszeit bestätigt. Unter Einfluss des NIR Lasers ändert sich die Linie zu eine asymmetrische `Fano` förmige Linie, zu der auch ein Fit erstellt wurde. Das Hauptziel ist es nun zeitaufgelöste Absorptionsspektren im System zu betrachten. Ds Absorptionsspektrum zeigte eine reichhaltige Dynamik. Um Rückschlüsse auf die Ursachen der zeitabhängigen Strukturen zu ziehen, wurde eine systematische Untersuchung durchgeführt, indem man Kopplungen zwischen gewissen dunklen und hellen Zuständen verbietet. Durch diese Aufschlüsselung des gesamten Systems in kleinere Systeme, konnte abgeleitet werden, welche Kopplungen zwischen den betrachteten Vibrationszuständen welche zeitabhängigen Strukturen, geprägt von elektronischen und nuklearen Friheitsgeraden, im Spektrum verursachen.

Contents

1 Introduction

Atoms were believed to be indivisible particles. Over time, this hypothesis turned out to be wrong. In 1911, `Ernest Rutherford` was the first person to show experimentally that an atom consists of a positive charged nucleus, that contains almost the whole mass of the atom, surrounded by electrons, which compensate the nucleus' electric charge [1]. Numerous other atom models then were proposed. During the evolution of quantum mechanics, the atomic orbital model occurred. This model describes the wave-like behavior and the location of an electron in an atom and is still used nowadays for many calculations. The simplest atom is the hydrogen atom. It consists of a single proton as nucleus, surrounded by an electron. The new understanding of quantum mechanical behavior of atoms lead to an analytical solution of the `Schrödinger` equation for the nonrelativistic hydrogen atom. Moving on from the simplest atom to the simplest molecule, molecular hydrogen, consisting of two positively charged protons and two negatively charged electrons, one could ask, if the wavefunction for this molecule can be found easily, too. The answer is no, because when dealing with molecules, it is not possible to add properties known from atoms together. No exact analytical solution to the wavefunction for H_2 exists. This is why approximations are used, to simplify the molecular system. The most important approximation is the `Born-Oppenheimer` approximation, by assuming that the nuclei of a molecule are *fixed* in space, and their motion is independent of the motion of the electrons. Using this approximation the wavefunction could be split into a nuclear and electronic part using a product ansatz.

The study of atoms and molecules results to the question, how they behave in the free system as well under external influence. Electronic motions are in the order of femtoseconds to attoseconds. To get insights to the dynamics, interferometric methods proved to be the solution. In particular transient-absorption spectroscopy (TAS) is widely used. The temporal evolution of a wave function, describing the microscopic system within the framework of the non-relativistic quantum theory, is related to complex phase factors. Hence, when dealing with quantum mechanics, measuring time is strictly linked into measuring phases. Temporal phase information of an atom or a molecule can be gained by letting them interact with an external light source. Through this interaction, their relative phase shift, e.g. due to absorption, can be measured. This implies, that one needs a light source with high coherence, or perfect phase-relationship. Here, laser pulses come in handy, since they have a high coherence. The key ingredient in TAS is using ultrashort laser pulses, in order to resolve electronic motions within an atom or a molecule. An XUV pulse can be to used excite the system, while after a time delay, a second pulse, an NIR pulse, can be used to create a temporal overlap between the phases of the considered system and the NIR pulse. By comparing the initial intensity of the XUV pulse before it passes through the system with the intensity after travelling to the system, one can finally get insights to the dynamical processes after excitation.

A recent measured absorption spectrum of molecular hydrogen drew attention for a deeper investigation for the system (see figure 1). Since further experiments in our group are yet to be done, a theoretical consideration is needed for a better understanding. Also predicting experimental outcome and gaining understanding of not discussed effects in other experimental works, like [21, 22], is a goal to pursue.

The thesis is structured as follows: in section 2 the atomic units system is presented, before introducing a fundamental quantum mechanical description for quantum states. Light-matter interaction with linear absorption theory are discussed afterwards, along with the concept of transient-absorption spectroscopy.

Section 3 deals with basic concepts of the H_2 molecule, which is the investigated system through-

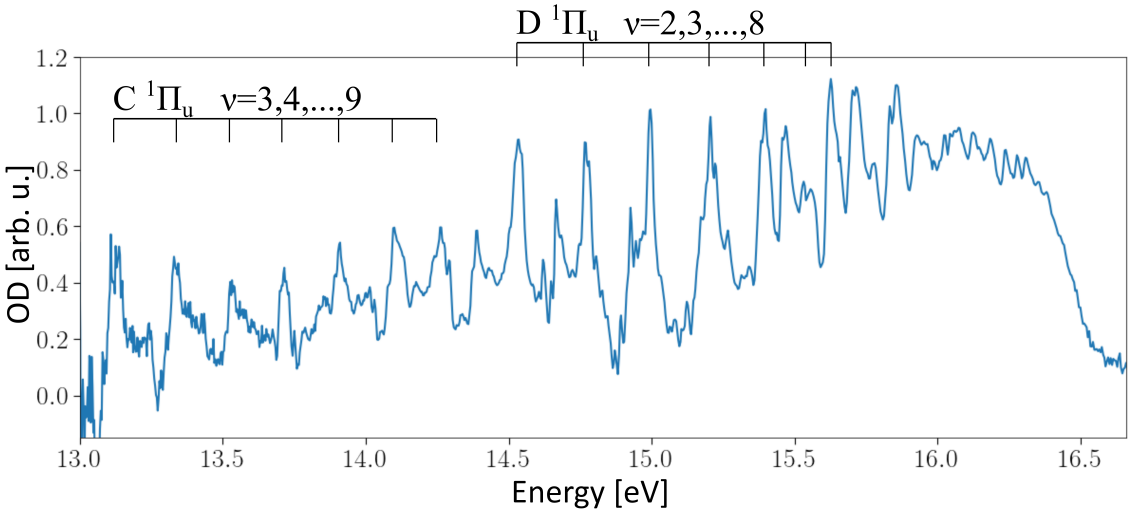

Figure 1: Absorption spectrum of H_2, measured by Gergana Borisova at the `Max-Planck-Intitut für Kernphysik Heidelberg`, in the division of Prof. Dr. Thomas Pfeifer. The OD [arb. u.] is plotted against the energy [eV]. Here, some spectral lines of the excited vibrational $C^1\Pi_u$- and $D^1\Pi_u$-states are visible.

out this thesis. Starting with introducing the common used molecular term symbols and introducing the states of interest for the simulation later, the `Born-Oppenheimer` approximation is explained in more detail. After that, the Hamiltonian and wave functions of molecular hydrogen are built in the framework of the mentioned approximation. The relevant energies in the system, potential curves and a level scheme for the considered 87 vibronic states are presented as well. Assuming a few-level model, which is the last point covered in this section, a numerical implementation aiming to solve the `Schrödinger` equation for our system is presented in section 4. The implementation is based on previous works by Paul Birk in our group.

There, it is also explained, how the Hamiltonian of the hydrogen system is built. The laser pulse configurations, parameters used in the simulation and the concept of zero-padding is outlined afterwards.

Section 5 presents the results of our calculated data. Taking a simplification into a five-level system, we are able to see population transfers between the ground electronic state and the bright states and the influence of an NIR pulse to the system. Resonant line shapes of the spectrum with and without an external NIR field are studied afterwards, both for the five-level system and as well for the full 87-level system. However, for the full system, we examine the time-resolved spectrum, if the NIR pulse is turned on. For different time delays between the XUV and NIR pulse, different scans are performed for different coupling configurations between certain bright and dark states. An outlook for possible further extensions to the simulation, like intensity scans and implementing `Franck-Condon` factors for the transitions between dark and bright states, is given at last.

A conclusion to sum up the presented ideas is given to close the thesis.

2 Theory

This section covers some theoretical aspects on light-matter interaction. It starts with an introduction to atomic units, before it turns to the basics of quantum mechanics. We give a short introduction in light-matter interactions, how one can quantify this interaction with linear absorption theory and finally how an experiment using **Transient-Absorption Spectroscopy (TAS)** enables access to the intrinsic dynamics of a quantum system.

2.1 Atomic Units

In atomic and molecular physics it is well established to use **atomic units (a.u.)**. These units are defined by properties of the electron of a hydrogen atom. We denote the mass of an electron with m_e, the elementary charge e, the reduced Planck constant $\hbar$ and the Bohr radius is a_0. Within the atomic unit system, these four values, and as well the factor $1/4\pi\epsilon_0$ (ϵ_0 = electric constant), are set to 1:

$$m_e = e = \hbar = a_0 = \frac{1}{4\pi\epsilon_0} = 1. \tag{1}$$

The speed of light c is defined by the inverse of the fine-structure constant α, so that $c \approx 137$. One time unit is $t = 1$ a.u. ≈ 24.189 as (attosecond), one energy unit is $E = 1$ a.u. ≈ 27.211 eV, the field strength is given by $\mathcal{E} = 1$ a.u. $\approx 5.142 \cdot 10^{11}$ V/m, while the intensity is $I = 1$ a.u. $\approx 3.51 \cdot 10^{16}$. In this thesis atomic units are used, if it is not mentioned otherwise.

2.2 Fundamental Quantum Mechanics

When dealing with non-relativistic quantum systems, the most fundamental time-dependent description of a quantum mechanical system is given by the `Schrödinger` equation

$$-i\frac{\partial}{\partial t}\left|\Psi(x,t)\right\rangle = \mathcal{H}(t)\left|\Psi(x,t)\right\rangle, \tag{2}$$

where $|\Psi(x,t)\rangle$ denotes a time-dependent state of the system. $\mathcal{H}(t)$ is the Hamiltonian, which corresponds to the underlying energies of the particles in the considered system. In the stationary case, equation (2) becomes an eigenvalue equation:

$$\mathcal{H}\left|\Psi_n\right\rangle = E_n\left|\Psi_n\right\rangle. \tag{3}$$

One obtains a set of n orthogonal eigenstates, each associated with an energy E_n. These energies are sorted by value, where the lowest energy E_0 corresponds to the ground state. A general solution of the `Schrödinger` equation can now be written as a superposition of all the eigenstates

$$\left|\Psi(x,t)\right\rangle = \sum_{i=0}^{n} c_i(t)\left|\Psi_i(x,t)\right\rangle. \tag{4}$$

The absolute squares of the coefficients $c_i = \langle\Psi_i|\Psi\rangle$ sum up to 1 ($\sum_{i=0}^{n}|c_i|^2 = 1$), if the normalization is given, since the physical interpretation of the expansion coefficients is the probability to find the considered system in a state $|\Psi_i\rangle$. For given initial conditions, the time propagation of a general state (equation (4)) is a phase evolution:

$$\left|\Psi(x,t)\right\rangle = \sum_{n} e^{-iE_n t/\hbar}\left|\Psi_n(x,t=0)\right\rangle. \tag{5}$$

2.3 Light-Matter interactions

To get insights of the dynamical behavior in an atom or molecule, one can use an external light source to interact with the considered system. If one knows how the incoming light source is changed after travelling through the system, one can quantify how the light is affected by the matter by looking at the absorbance. On needs to compare the intensity $I_0(\omega)$ of the transmitted light before travelling through a medium, and the intensity $I(\omega)$ that is actually transmitted through the medium. Here ω is the angular frequency of the light. Then calculating the ratio of these two intensities and taking the common logarithm results to the absorbance, also known as *optical density* (OD):

$$OD(\omega) = \log_{10} \frac{I_0(\omega)}{I(\omega)} = -\log_{10} \frac{I(\omega)}{I_0(\omega)}. \tag{6}$$

2.3.1 Linear Absorption

Light attenuation through an extended medium is described empirically by Beer-Lambert's law:

$$I(\omega, z) = I_0(\omega) \cdot e^{-\alpha(\omega) z}. \tag{7}$$

The attenuation is exponential and depends not only on the sample's length z, but also on an absorption coefficient $\alpha(\omega)$. This macroscopic quantity is related to the microscopic absorption cross section $\sigma(\omega)$ and the atomic number density ρ_N:

$$\alpha(\omega) = \rho_N \cdot \sigma(\omega). \tag{8}$$

As shown in [2], the cross section $\sigma(\omega)$ can be written via

$$\sigma(\omega) = \frac{\omega}{\epsilon_0 c} \mathrm{Im}\left(\frac{d(\omega)}{E(\omega)}\right), \tag{9}$$

while $E(\omega)$ is the electric field and $d(\omega)$ is the so called dipole moment expectation value. If one now insert Beer-Lamberts' law from equation (7) into the definition of the OD, equation (6), one gets:

$$OD(\omega) = \frac{\sigma(\omega)}{\ln 10} \cdot \rho_N \cdot l. \tag{10}$$

The optical density is hence proportional to $\sigma(\omega)$, for a propagation path of a length of l.

2.3.2 Transient-Absorption Spectroscopy

Since this thesis is about a numerical simulation of an experiment using **TAS**, a short overview on the experimental technique is covered here. More details can be found e.g. in [2] or in recent publications of our group [3, 4, 17]. A TAS experiment allows to get an insight into the time-dependent bound state dynamics of a system (e.g. how an atom or molecule is influenced by an NIR[1] laser field). The time-dependent dynamics is imprinted into the measured sample's absorbance or transmittance. TAS is a pump-probe technique, which means that two laser pulses are used - an excitation (pump) and a typically weaker probe pulse, measuring the absorbance. By applying different time delays τ between the pump and probe pulses, one is able to resolve the underlying

[1] Near-InfraRed

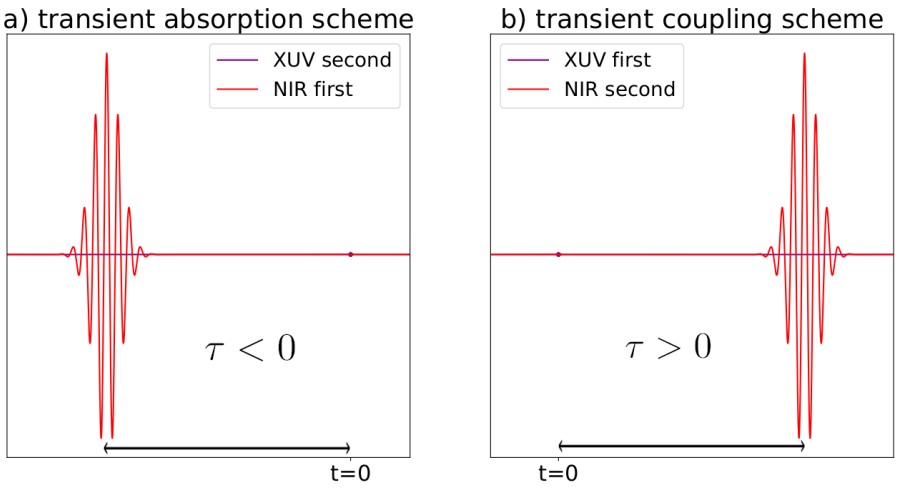

Figure 2: Laser pulse geometry used in the experiment. *Left:* a) Transient absorption scheme - NIR pulse is coming first, XUV pulse is second. This is defined as negative time delay between the pulses. *Right:* b) Transient coupling scheme - here the weaker XUV pulse comes first, then the NIR pulse is coming second. This is defined as positive time delay.

dynamics of the target in time. In a typical attosecond transient absorption setup, one of the pulses is a (moderately) strong NIR pulse pulse and the other a weak XUV[2] pulse. The XUV pulse is generated in the process of high-order harmonic generation, which is described in more details in e.g. [5]. The time delay τ is defined to be negative ($\tau < 0$, TAS scheme), if the NIR pulse comes first to start dynamical evolution of the target, before, after a delay of τ, the XUV pulse, probes the target, whose recorded signal provides information about the effect of the NIR. However, if the the time delay is positive ($\tau > 0$, transient coupling scheme), the first pulse is the weaker XUV pulse (see. fig. 2 for a visual representation). It can now excite the target, initiating temporal dynamics in the target. If a pertubation, by an NIR probe pulse, occurs within the lifetime of the dynamics induced by the XUV pulse, one can still recover the influence of the NIR in the measured absorption signal.

[2] eXtrem UltraViolet

3 Basic Concepts of Molecular Hydrogen and a Few-Level Model

This chapter gives an overview on the basic concepts to be considered for the treatment of molecules, since our system of interest is the hydrogen molecule. Here we follow [6]. The goal is to solve the `Schrödinger` equation using a few-level model, as will be explained in section 3.5. Before that, we introduce the molecular term symbols, a common notation used for molecules. For the description of H_2 as a diatomic molecule its Hamiltonian and wave functions are derived in the framework of the `Born-Oppenheimer` approximation. Also a level-scheme for molecular hydrogen is considered, to have a look of the different energy contributions.

3.1 Molecular Term Symbol

While the *spectroscopic notation* is used for atoms, in analogy for molecules one uses the following term symbol to characterize their electronic states:

$$^{2S+1}\Lambda^{\pm}_{g,u}. \tag{11}$$

S is the total spin quantum number, while Λ is the projection of the total angular momentum on the z-axis ($\Lambda \in \{\Sigma, \Pi, \Delta, ...\}$ with the identification $\Sigma = 0, \Pi = 1, \Delta = 2, ...$). The superscript defines the symmetry/antisymmetry and the subscript g, u refers to the parity of a state $\phi(\mathbf{r})$ for 'even' (g) or 'odd' (u):

$$\begin{aligned} \phi_g(\mathbf{r}) &= \phi_g(-\mathbf{r}) \qquad \text{even} \\ \phi_u(\mathbf{r}) &= -\phi_u(-\mathbf{r}) \qquad \text{odd} \end{aligned}$$

If one wants to specify a certain state, e.g. the ground electronic state, one adds the letter X before the term symbol: thus $X^1\Sigma^+_g$ is the ground state of H_2. The following excited states are labeled alphabetically $A, B, C, ...$ Note that capital letters are used, when dealing with singlet states (multiplicity = 1). However, triplet states (multiplicity = 3) are notated using lower case letters $a, b, c, ...$ Additionally one adds a molecular orbital designator, like $2p\sigma$, to characterize one electron wave functions. More details can be found in [6] as well.

The states of interest beside the ground state of H_2 are the three lowest excited states (Hydrogen does not have an A-state): $B^1\Sigma^+_u 2p\sigma$, $C^1\Pi_g 2p\pi$ and $D^1\Pi_u 3p\pi$, which can be populated from the ground state using an XUV-pulse. Furthermore, the $E, F^1\Sigma^+_g 2s\sigma + 2p\sigma^2$ and $H^1\Sigma^+_g 3s\sigma$ are studied, since they can couple to the excited states using an NIR-pulse.

For the sake of simplicity, the above mentioned states are abbreviated to B-/C-/D- state (*bright states*) or EF-/H- state (*dark states*).

3.2 Born-Oppenheimer Approximation

Molecular hydrogen consists of two protons and two electrons. As we will see in the following part, the description of such a simple molecule is not just adding properties, known from atoms, together. In molecular physics, the most important approximation uses the fact that the mass of an electron

m_e is much smaller than the mass of an atomic nucleus M, where

$$\frac{m_e}{M} \approx 10^{-3}...10^{-5}. \tag{12}$$

The Coulomb force is responsible for keeping the molecule together. This force acts identically on the electrons and to the nuclei and therefore the electrons movement is much faster than the movement of the nuclei. Hence, one can say that the nuclei are *fixed* and do not move, while the electrons orbit around them with a high speed. This leads to the assumption that one can treat the motion of the electrons and the movement of the nuclei *separately*. This ansatz was first introduced in 1927 by `Max Born` and `J. Robert Oppenheimer` [7] and named after them: the **`Born-Oppenheimer` approximation**.

3.3 Hamiltonian and Wave Functions

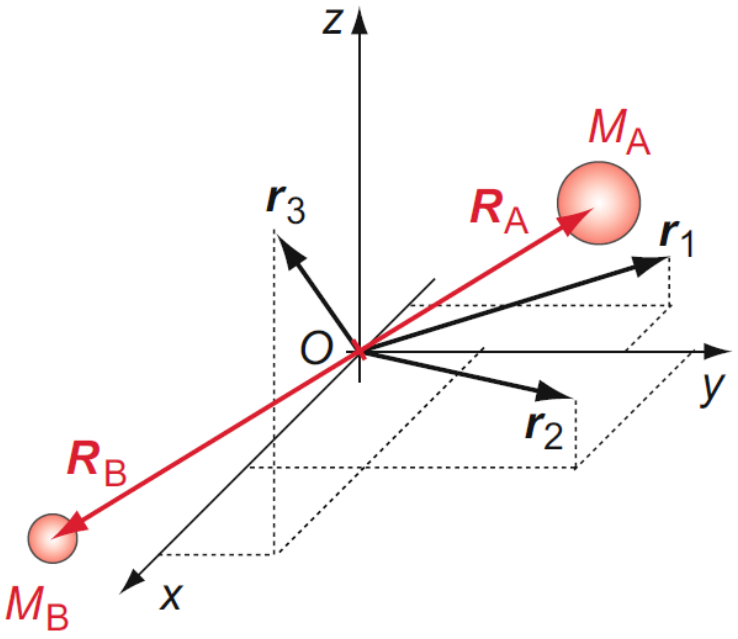

Figure 3: Relative coordinates for a diatomic molecule in respect to the centre of mass O. The big red dots represent the nuclei of atom A and B, with mass M_A and M_B, respectively. They are indicated by capital letters, while lower case letters stand for the coordinates of the electrons. The figure is taken from [6].

To derive the Hamiltonian of a diatomic molecule, we use relative coordinates, as shown in fig. 3, and atomic units. The kinetic energy of the two nuclei is

$$T_n = -\frac{1}{2\tilde{M}}\nabla^2_{\mathbf{R}}, \tag{13}$$

where $\tilde{M}$ is the reduced mass

$$\tilde{M} = \frac{M_A M_B}{M_a + M_B} \tag{14}$$

and $\mathbf{R} = \mathbf{R}_B - \mathbf{R}_A$ the distance between the nuclei. Since the nuclei of H_2 have the same mass, $M_A = M_B$, the reduced mass becomes

$$\tilde{M} = \frac{M_A^2}{2M_A} = \frac{M_A}{2}. \tag{15}$$

Also given the fact that H_2 has two electrons, the kinetic energy of the electrons reads

$$T_{el} = \sum_{i=1}^{2} \left(-\frac{1}{2} \nabla_{r_i}^2 \right), \tag{16}$$

for the coordinates $\mathbf{r}_i$ of the electrons. The potential energy caused by the `Coulomb` force is

$$V(\mathbf{r}, \mathbf{R}) = \underbrace{- \sum_{i \in \{A,B\}} \sum_{j=1}^{2} \frac{Z_i}{|\mathbf{R}_i - \mathbf{r}_j|}}_{U_{en}} + \underbrace{\sum_{\substack{i,k=1 \\ i<k}}^{2} \frac{e^2}{|\mathbf{r}_i - \mathbf{r}_k|}}_{U_{ee}} + \underbrace{\frac{Z_A Z_B}{\mathbf{R}}}_{U_{nn}}. \tag{17}$$

Z_i is the atomic number for nucleus i, whereby for molecular hydrogen it is $Z_A = Z_B = 1$. The term U_{en} describes the energy between an electron and a nucleus, U_{ee} and U_{nn} are the energies that occur due to the electron-electron and nuclear-nuclear repulsion, respectively. Together, these energies sum up to the total Hamiltonian:

$$\mathcal{H} = T_n(\mathbf{R}) + T_{el}(\mathbf{r}) + V(\mathbf{r}, \mathbf{R}). \tag{18}$$

The Schrödinger equation using this Hamiltonian transforms into

$$[T_n(\mathbf{R}) + T_{el}(\mathbf{r}) + V(\mathbf{r}, \mathbf{R})]\Psi(\mathbf{r}, \mathbf{R}) = E\Psi(\mathbf{r}, \mathbf{R}). \tag{19}$$

However, using the `Born-Oppenheimer` (BO) approximation, it is possible to split the Schrödinger equation into an electronic part and a nuclear part. This is achieved by using a product ansatz of the wavefunction in such a way that the electronic part and the nuclear part are separated:

$$\Psi(\mathbf{r}, \mathbf{R}) = \phi(\mathbf{r})\psi(\mathbf{R}). \tag{20}$$

As previously described, one can assume that the nuclei are fixed and not moving so that we can treat $\mathbf{R}$ now as a fixed value. The `Schrödinger` equation for the electronic part becomes

$$\mathcal{H}_{el}\phi_e(\mathbf{r}; \mathbf{R}) = V_e(R)\phi_e(\mathbf{r}; \mathbf{R}), \tag{21}$$

where

$$\mathcal{H}_{el} = \mathcal{H} - T_n(\mathbf{R}) = [T_{el} + V(\mathbf{r}; \mathbf{R})]. \tag{22}$$

The semicolon in the wavefunction $\phi(\mathbf{r}; \mathbf{R})$ and in the potential $V(\mathbf{r}; \mathbf{R})$ emphasizes again that $\mathbf{R}$ is simply a parameter. Therefore equation (21) needs to be solved for each $\mathbf{R}$ separately. The index e is the electronic quantum number. $V_e(R)$ is a continuous $\mathbf{R}$-dependent function and is

called molecular potential. This will be discussed in section 3.4. For the nuclear part we denote ν as the vibrational quantum number and J as the rotational quantum number (see section 3.4 for more details) and hence the `Schödinger` equation for the nuclear part with wave function $\psi_{\nu,J}(\mathbf{R})$ becomes:

$$\mathcal{H}_n \psi_{\nu,J}(\mathbf{R}) = W_{e\nu J} \psi_{\nu,J}(\mathbf{R}) \tag{23}$$

for

$$\mathcal{H}_n = -\frac{m_e}{2\tilde{M}} \nabla_r^2 + V_e(R). \tag{24}$$

3.4 Energies, Potential Curves and Level Scheme for H_2

In this section, we estimate the typical energy scales in the hydrogen molecule. The electronic energy W_e caused by the binding of the electrons, can be found in SI units as followed: let $\langle r \rangle$ be the average distance between an electron to its nucleus, where $\langle r \rangle \approx 0.074\text{nm}$ for H_2. The momentum p of the electron can be estimated by $p = \hbar/\langle r \rangle$, while the average kinetic energy is $\langle T \rangle = \frac{p^2}{2m_e}$. Using the *Virial theorem*, one finds: $2\langle T \rangle = -\langle V \rangle$, for a $-\frac{1}{r}$ potential. The total binding energy is the sum of potential and kinetic energy

$$W_e = \langle T \rangle + \langle V \rangle \approx -\frac{p^2}{2m_e} = -\frac{\hbar}{2m_e \langle r \rangle^2} \approx 7\text{eV}. \tag{25}$$

Not only the electron motion, but also the nuclear motion is relevant and contributes to the total energy of the molecule as well. The nuclei of an atom of a molecule can vibrate, since there is a force acting on the electrons and the two nuclei. Assume the force F is harmonic, such as $F = -kR$, for a constant k. The vibrational frequency of the nuclei can be found as $\omega_\nu = \sqrt{k/\tilde{M}}$, while the frequency of an electron is $\omega_e = \sqrt{k/\tilde{m_e}}$. The respective energy to those frequencies is given via $W_\nu = \hbar\omega_\nu$ and $W_e = \hbar\omega_e$ for the energy of vibrational motion and the electronic energy. Taking the ratio of theses energies one finds

$$W_\nu \approx \sqrt{m_e/\tilde{M}} W_e \lesssim 0.1\text{eV}, \tag{26}$$

where $\approx \sqrt{m_e/\tilde{M}} \lesssim 10^{-2}$, since $\tilde{M}$ is in the order of nuclear masses.

Also the whole nuclear structure can rotate in space, giving rise to the rotational energy W_J. A derivation for an estimate is found in [6]. The order of magnitude of the rotational energy is about

$$W_J \approx 1\text{meV to } 10\text{meV}. \tag{27}$$

The wave function is characterized by the quantum numbers e, ν, J: the electronic, vibrational and rotational quantum number, respectively. Each set of these quantum numbers correspond to a different state. The electronic energies depend on the distance to the nucleus and give rise to potential energy curves. Within the electronic potential, different vibrational states exists, while within the vibrational states there are different rotational states. In figure 4 the curves of the X-/B-/C-/D-/EF- states are plotted. Also the energy levels for all the vibrational states with $J = 1$ are visualized. The data for the curves are taken from [10]. The energies of the vibrational states for the B-/C-/D- state are calculated from experimental data from [11], while the energies of the EF-state are taken from [10]. The potential curves of the EF-/H- states have a double minimum, meaning

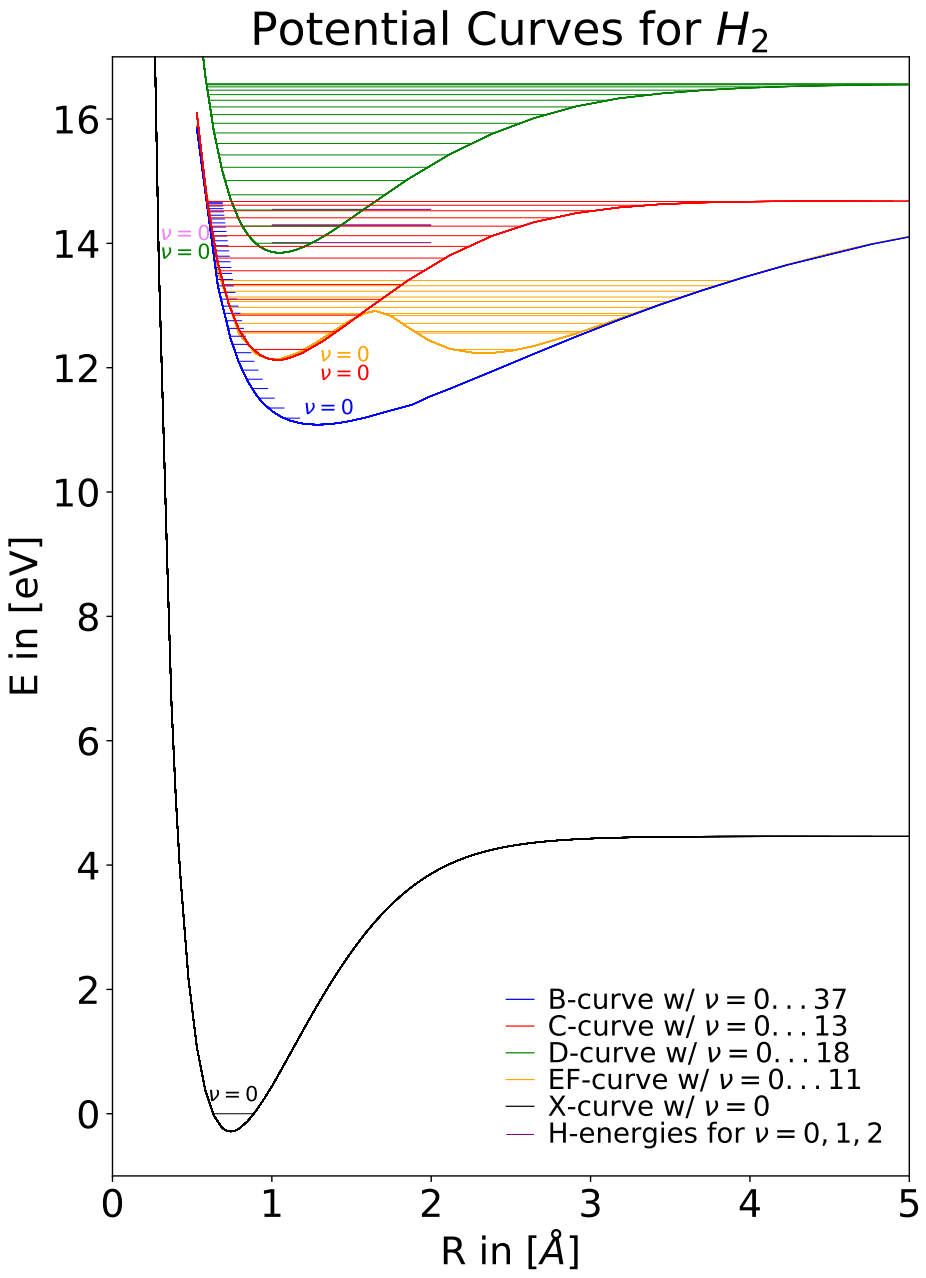

Figure 4: Potential energy curves of H_2 for the states of interest, with the energies of the vibrational states with $J = 1$ for the excited states. The ground state X has $J = 0, \nu = 0$. The potential energy E in eV is plotted against the nuclear distance $\boldsymbol{R}$ in $\mathring{A}$. The B-state has a minimum at around 11.1eV, for the C-state it is found at around 12.1eV, while the D-state's minimum is at 13.8eV. The EF-state has a double minimum at around 12.1eV. The states from both minima are each plotted in both potential wells, since we assume that each state can be populated due to tunneling. For the H-curve, which also has a double minimum, no data were found, but the considered vibrational ground state energies start at 14.0eV. The vibrational ground state for all states are indicated as well. For the ground electronic state X, the ground vibrational state is set to 0eV.

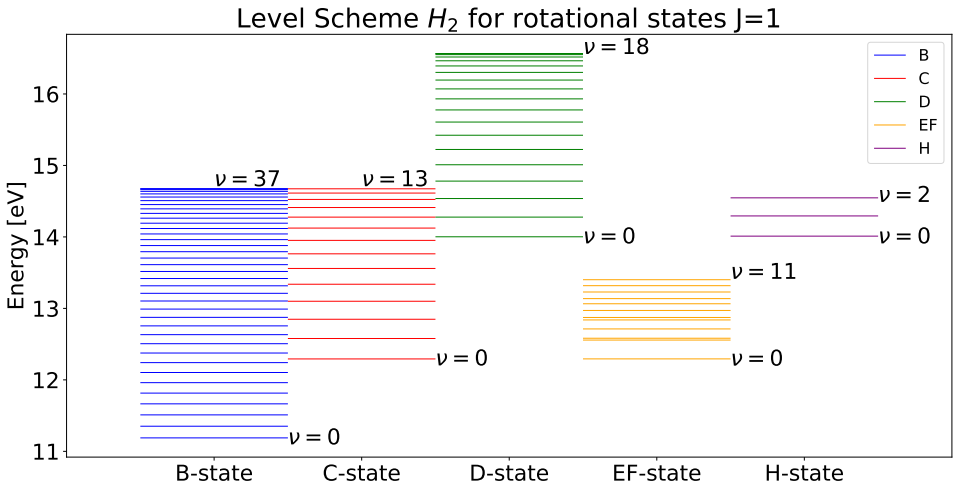

Figure 5: Level scheme for H_2, for the considered states. Only the states with $J = 1$ are considered, for different ν's. The energy levels are plotted side by side to avoid an overlap.

there are some states lying only in one of the potential wells. In this thesis an approximation is made that all states in both wells are considered equally, since due to tunneling it is possible to populate all states in both wells.

No data for the potential curves of the H-state were found. But the energies for the H-state are found in [12].

Since BO approximation is still assumed, we will only consider energies for a fixed $\mathbf{R}$ and treat any couplings between the dark and bright states equally (for the time being). For the states of interest, a level scheme is plotted in figure 5. The reason to choose vibrational states with $J = 1$ is due to the fact that the ground state of H_2 has $J = 0$ and out of it, transitions with $\Delta J = 1$ are allowed. The couplings of rotational states are neglected in this work, since these couplings are much smaller than the vibrational couplings. Also one needs to consider the *selection rules*: if one populates one of the excited (B-/C-/D-) states with an XUV-pulse from the ground state ($\Delta\Lambda \neq 0$), it is $\Delta\nu = 0, \pm1, \pm2, ...$ and $\Delta J = 0, \pm1$. This explains why all transitions from the ground state to any of the B-/C-/D- states are allowed, because all of these rules are fulfilled. Analogously the couplings from the EF-/H- states to excited states using a NIR-pulse are allowed, since the same selection rules can be applied here.

3.5 Few-Level Model

The system of interest, molecular hydrogen with its B-/C-/D- and as well EF-/H- states, is a finite system. This system can be studied using a few-level model, which aims to solve the `Schrödinger` equation (2). The Hamiltonian $\mathcal{H}(t)$ can be separated into an unpertubated part $\mathcal{H}_0$ and an interaction part $\mathcal{H}_{int}$:

$$\mathcal{H}(t) = \mathcal{H}_0 + \mathcal{H}_{int}(t). \tag{28}$$

The interaction part is in the dipole approximation $\mathcal{H}_{int} = \hat{\mathbf{d}} \cdot \mathbf{E}(t)$, where $\hat{\mathbf{d}}$ is the dipole-moment operator and $\mathbf{E}(t)$ is the electric field [9]. The general solution of the `Schrödinger` equation (4) is the wavefunction that represents the few-level system. Regarding a finite number of states, there is also a finite number of orthonormal eigenfunctions $\{|\Psi_i\rangle\}$

$$|\Psi(t)\rangle = \sum_{i=0}^{n} c_i(t)\,|\Psi_i\rangle\,. \tag{29}$$

By projecting $|\Psi(t)\rangle$ on $|\Psi_i\rangle$, the wavefunction can be expressed in the eigenbasis and is therefore understood as an $n \times 1$ vector, while the Hamiltonian turns into a $n \times n$ matrix. The `Schrödinger` equation transforms into

$$i\frac{\partial}{\partial t}\begin{pmatrix} c_0(t) \\ c_1(t) \\ \vdots \\ c_n(t) \end{pmatrix} = \begin{pmatrix} \langle 0|\mathcal{H}(t)|0\rangle & \langle 0|\mathcal{H}(t)|1\rangle & \dots & \langle 0|\mathcal{H}(t)|n\rangle \\ \langle 1|\mathcal{H}(t)|0\rangle & \ddots & & \vdots \\ \vdots & & \ddots & \vdots \\ \langle n|\mathcal{H}(t)|0\rangle & \dots & \dots & \langle n|\mathcal{H}(t)|n\rangle \end{pmatrix} \begin{pmatrix} c_0(t) \\ c_1(t) \\ \vdots \\ c_n(t) \end{pmatrix}. \tag{30}$$

This is the matrix form of the `Schrödinger` equation and the beginning for numerical calculations. The $n \times 1$ vector $(c_0(t), c_1(t), \dots, c_n(t))^T$ is often called 'state vector'. Eigenvalues of the free Hamiltonian $\mathcal{H}_0$ are the diagonal entries, while the electric field influences the off-diagonal elements (contributed by $\mathcal{H}_{int}$), containing the transition amplitudes between two states of the considered system. However, in our case, we have not one, but two electric fields, an interaction with an XUV-pulse and one with an NIR-pulse. This is why we also split the interaction Hamiltonian into two parts:

$$\mathcal{H}_{int}(t) = \mathcal{H}_{int,XUV}(t) + \mathcal{H}_{int,NIR}(t), \tag{31}$$

whereby

$$\mathcal{H}_{int,XUV}(t) = \hat{\mathbf{d}}_{XUV} \cdot \mathcal{E}_{XUV}(t) \tag{32}$$

$$\mathcal{H}_{int,NIR}(t) = \hat{\mathbf{d}}_{NIR} \cdot \mathcal{E}_{NIR}(t). \tag{33}$$

Here, $\hat{\mathbf{d}}_{XUV}$ is the dipole moment that allows population transfer from the ground state X to the excited B-/C-/D- states caused by the XUV pulse. On the other hand, $\hat{\mathbf{d}}_{NIR}$ is the dipole moment that allows coupling from the EF-/H- states to the excited B-/C-/D- states, via the NIR-pulse. An in-depth explanation of constructing the Hamiltonian for the considered system can be found in section 4.2.

The solution of equation (30) is given by:

$$\begin{pmatrix} c_0(t) \\ c_1(t) \\ \vdots \\ c_n(t) \end{pmatrix} = e^{-i\mathcal{H}(t)\cdot t} \begin{pmatrix} c_0(t=0) \\ c_1(t=0) \\ \vdots \\ c_n(t=0) \end{pmatrix} \tag{34}$$

The algorithm to solve this equation numerically is described in the next section.

4 Numerical Implementation

In this section the algorithm for solving the `Schrödinger` equation for a few-level model, as discussed in the previous section, is presented. Afterwards the Hamiltonian of the considered system is constructed. The relevant parameters and the laser configuration used in the simulation are outlined as well. Also, the concept of *zero-padding* is introduced and its relevance for the simulation is pointed out.

4.1 Algorithm for Solving the Schrödinger Equation in the Few-Level Model

Since in numerical calculations one can only use finite time steps Δt, one needs to choose Δt sufficiently small. Later we will see in section 4.3 that $\Delta t = 0.5$a.u. is proven to be small enough. The error of the time discretization for sufficiently small Δt is negligible [13]. The problem of solving equation (34), is that the Hamiltonian is a sum of the free and interaction part. In second-order accuracy [14] the time propagation can be solved by splitting the operator via

$$e^{-i(\mathcal{H}_0(t)+\mathcal{H}_{int}(t))\cdot t} \approx e^{-i\mathcal{H}_0(t)\cdot\frac{t}{2}} \cdot e^{-i\mathcal{H}_{int}(t)\cdot t} \cdot e^{-i\mathcal{H}_0(t)\cdot\frac{t}{2}}. \tag{35}$$

Therefore, the first step in the algorithm is to apply half of a time propagation, caused by the free Hamiltonian, by multiplying a complex phase term with the eigenvalues $\lambda_{0,j}$ of $\mathcal{H}_0$ to the state vector:

$$|\Psi(t)\rangle \leftarrow e^{-i\cdot\lambda_{0,j}\cdot\frac{\Delta t}{2}} |\Psi(t)\rangle . \tag{36}$$

The next emerging problem is that not only $\mathcal{H}_{int}$ is a sum of two parts again (the XUV and NIR part), but also that both parts are non-diagonal, meaning the time propagation $\exp[-i\mathcal{H}_{int}(t)\cdot t]$ cannot be evaluated. To overcome both challenges, one splits $H_{int}(t) = \mathcal{H}_{int,XUV}(t) + \mathcal{H}_{int,NIR}(t)$ in the time propagation in first-order accuracy into

$$e^{-i(\mathcal{H}_{int,XUV}(t)+\mathcal{H}_{int,NIR}(t))\cdot t} \approx e^{-i\mathcal{H}_{int,XUV}(t)\cdot t} \cdot e^{-i\mathcal{H}_{int,NIR}(t)\cdot t}. \tag{37}$$

To evaluate both factors, one first diagonalizes both Hamiltonians, before applying an unitary transformation T into the diagonal basis of the respective Hamiltonians, such that

$$\mathcal{H}^D_{int,XUV}(t) = T^{-1}_{XUV}\mathcal{H}_{int,XUV}(t)T_{XUV}$$
$$\mathcal{H}^D_{int,NIR}(t) = T^{-1}_{NIR}\mathcal{H}_{int,NIR}(t)T_{NIR}.$$

The eigenvectors of the Hamiltonians are stored as columns in the transformation matrix T. This is first done for the XUV part - rotating the state vector into the diagonal basis of $\mathcal{H}_{int,XUV}(t)$:

$$|\Psi^D_{XUV}(t)\rangle = T^{-1}_{XUV} |\Psi(t)\rangle . \tag{38}$$

After that, the time evolution is applied, using the eigenenergies $\lambda_{XUV,j}$ of $\mathcal{H}^D_{int,XUV}(t)$ as phase terms

$$|\Psi^D_{XUV}(t)\rangle \leftarrow e^{-i\cdot\lambda^D_{XUV,j}\cdot\Delta t} |\Psi^D_{XUV}(t)\rangle , \tag{39}$$

before transforming back to the original basis

$$|\Psi(t)\rangle \leftarrow T_{XUV} |\Psi^D_{XUV}(t)\rangle . \tag{40}$$

Now the whole procedure needs to be repeated for the NIR part: basis transformation

$$|\Psi^D_{NIR}(t)\rangle = T^{-1}_{NIR}\,|\Psi(t)\rangle\,, \tag{41}$$

time evolution

$$|\Psi^D_{NIR}(t)\rangle \leftarrow e^{-i\cdot\lambda^D_{NIR,j}\cdot\Delta t}\,|\Psi^D_{NIR}(t)\rangle\,, \tag{42}$$

and back transformation

$$|\Psi(t)\rangle \leftarrow T_{NIR}\,|\Psi^D_{NIR}(t)\rangle\,. \tag{43}$$

After all this is done, the last step is to apply the second half of a time propagation of the free Hamiltonian:

$$|\Psi(t)\rangle \leftarrow e^{-i\cdot\lambda^D_{0,j}\cdot\frac{\Delta t}{2}}\,|\Psi(t)\rangle\,. \tag{44}$$

The reason to consider equation (37) is to simplify the expression, since there are two basis transformations, which results in less matrix multiplications and saved computation time. Nevertheless the results are satisfactory, as seen in section 5.

In a nutshell, the state vector $|\Psi_n(t)\rangle$ is calculated for each time step $t_n = t_{n-1} + \Delta t$ and is used subsequently as the new state vector for the following time step:

$$|\Psi_n(t_n)\rangle = e^{-i\cdot\lambda^D_{0,j}\cdot\frac{\Delta t}{2}}T_{NIR}e^{-i\cdot\lambda^D_{NIR,j}\Delta t}T^{-1}_{NIR}T_{XUV}e^{-i\cdot\lambda^D_{XUV,j}\Delta t}T^{-1}_{XUV}e^{-i\cdot\lambda^D_{0,j}\cdot\frac{\Delta t}{2}}\,|\Psi_{n-1}(t_{n-1})\rangle\,. \tag{45}$$

This iteration is implemented using a loop, until it reaches the end of the time propagation. The initial state the one where only the ground state is populated:

$$|\Psi(t=0)\rangle = (1,0,0,...,0)^T. \tag{46}$$

Also for each time step, the time-dependent dipole moment $d(t)$ of the system between the ground state $|0\rangle$ and the excited states $|i\rangle$, for $i = 1, 2, ..., n$ needs to be calculated

$$d(t) = \langle\Psi(t)|\hat{\mathbf{d}}|\Psi(t)\rangle = \sum_i c^*_0(t)c_i\,\langle 0|\hat{\mathbf{d}}|i\rangle + c.c. \tag{47}$$

The ground to excited dipole transition matrix elements are represented by $\langle 0|\hat{\mathbf{d}}|i\rangle$, while $\langle 0|\hat{\mathbf{d}}|0\rangle = 0$. By taking the Fourier transform of the time-dependent dipole moment, one gets a quantity $d(\omega)$ (dipole expectation value, as named for equation (9)) to calculate the OD from equation (10).

4.2 Building the Hamiltonian for the Simulation

The Hamiltonian contains the total energy of the considered system and also describes all possible interactions between the considered states. A short summary of our system for describing the Hamiltonian from the previous sections is presented:

1. The bright B-/C-/D-states can be excited from the ground electronic state X using an XUV pulse.

2. The dark EF-/H-states can couple to the bright states with an NIR-pulse.

First of all, the free Hamiltonian $\mathcal{H}_0$ is constructed. It contains all energy levels of all considered states as diagonal elements:

$$\mathcal{H}_0 = \text{diag}(E_X, E_{B_{1,0}}, E_{B_{1,1}}, ..., E_{B_{1,37}}, E_{C_{1,0}}, ..., E_{C_{1,13}}, E_{D_{1,0}}, ..., E_{D_{1,18}}, E_{EF_{1,0}}, ..., E_{EF_{1,11}}, E_{H_{1,0}}, ..., E_{H_{1,2}}). \tag{48}$$

The index $Y_{J,\nu}$ refers to a specific state with its quantum numbers. As shown in the level scheme in figure 5, we consider 38 B-, 14 C-, 19 D-, 12 EF- and 3 H- vibrational states. Including the ground state there are 1 ground state + 71 bright states + 15 dark states = 87 total states. So the Hamiltonian has a dimension of 87×87.

If one wants to consider decays, by adding a lifetime $1/\Gamma$ to the states, the energies must be modified to

$$E \leftarrow E - i\frac{\Gamma}{2}. \tag{49}$$

However, the ground electronic state energy (E_X) does not need to be modified, since it cannot decay. More details are explained in the next section (4.3).

In a second step we consider the interaction part. To allow transitions from the ground state to the bright states, one must fill up the first row and the first column of the Hamiltonian with the corresponding transition probabilities. Comparing to equation (32), the dipole moment operator $\hat{\mathbf{d}}_{XUV}$ has non-zero entries for $d_{1,j}, d_{i,1}$ with $i, j \leq 72$, so that $d_{i,j} = d^*_{j,i}$. Since the dark states cannot be excited using an XUV-pulse, the transition probabilities $d_{1,j}, d_{i,1}$ with $i, j \geq 73$ are $= 0$. From [11] there are experimental data, with transition amplitudes A from the excited state to the ground state. The dipole moment, is proportional to the square root of A [16]:

$$d_{i,j} \sim \sqrt{A_{i,j}}. \tag{50}$$

The interaction part of the Hamiltonian can now be evaluated by multiplying the electric field to the dipole moment operator: $\mathcal{H}_{int,XUV} = \hat{\mathbf{d}}_{XUV} \cdot \mathcal{E}(t)$, where $\mathcal{E}(t) = \mathcal{E}_{XUV}(t)$.

The same principle can be applied for $\mathcal{H}_{int,NIR}(t) = \hat{\mathbf{d}}_{NIR} \cdot \mathcal{E}(t)$, with $\mathcal{E} = \mathcal{E}_{NIR}(t)$: the EF-/H-states can couple to all of the B-/C-/D- states, meaning that the Hamiltonian must have non-zero entries in all rows and columns, where a transition can happen. See equation (51) for the written out total Hamiltonian. The colors of $\mathcal{H}_0$, $\mathcal{H}_{int,XUV}(t)$ and $\mathcal{H}_{int,NIR}(t)$ indicate, which element is contributed by which Hamiltonian part.

The dipole moments in $\hat{\mathbf{d}}_{NIR}$ are at first all set equal to 1. This is why also the dipole moments in $\hat{\mathbf{d}}_{XUV}$ are normalized to 1, relative to the maximum entry, so that all dipole moments have the same order of magnitude. Later we will consider cases, where we use `Franck-Condon` factors in $\hat{\mathbf{d}}_{NIR}$ for certain transitions.

$$\mathcal{H}(t) = \begin{pmatrix} E_X & d_{1,2}\mathcal{E}(t) & d_{1,3}\mathcal{E}(t) & \dots & d_{1,72}\mathcal{E}(t) & 0 & 0 & 0 & \dots & 0 \\ d_{2,1}\mathcal{E}(t) & E_{B_{1,0}} & 0 & \dots & 0 & d_{2,73}\mathcal{E}(t) & d_{2,74}\mathcal{E}(t) & d_{2,75}\mathcal{E}(t) & \dots & d_{2,87}\mathcal{E}(t) \\ d_{3,1}\mathcal{E}(t) & 0 & E_{B_{1,1}} & \dots & 0 & d_{3,73}\mathcal{E}(t) & d_{3,74}\mathcal{E}(t) & d_{3,75}\mathcal{E}(t) & \dots & d_{3,87}\mathcal{E}(t) \\ \vdots & \vdots & \vdots & \ddots & \vdots & \vdots & \vdots & \vdots & \dots & \vdots \\ d_{72,1}\mathcal{E}(t) & 0 & 0 & \dots & E_{D_{1,18}} & d_{73,73}\mathcal{E}(t) & d_{73,74}\mathcal{E}(t) & d_{73,75}\mathcal{E}(t) & \dots & d_{73,87}\mathcal{E}(t) \\ 0 & d_{73,2}\mathcal{E}(t) & d_{73,3}\mathcal{E}(t) & \dots & d_{73,72}\mathcal{E}(t) & E_{EF_{1,0}} & 0 & 0 & \dots & 0 \\ 0 & d_{74,2}\mathcal{E}(t) & d_{74,3}\mathcal{E}(t) & \dots & d_{74,72}\mathcal{E}(t) & 0 & E_{EF_{1,1}} & 0 & \dots & 0 \\ 0 & d_{75,2}\mathcal{E}(t) & d_{75,3}\mathcal{E}(t) & \dots & d_{75,72}\mathcal{E}(t) & 0 & 0 & E_{EF_{1,2}} & \dots & 0 \\ \vdots & \vdots & \vdots & \vdots & \vdots & \vdots & \vdots & \vdots & \ddots & \vdots \\ 0 & d_{87,2}\mathcal{E}(t) & d_{87,3}\mathcal{E}(t) & \dots & d_{87,72}\mathcal{E}(t) & 0 & 0 & 0 & \dots & E_{H_{1,2}} \end{pmatrix} \tag{51}$$

4.3 Configuration of the Laser Pulses and other Parameters

XUV and NIR pulses are ultrashort laser pulses. A brief mathematical treatment for these laser pulses is introduced, based on [2]. A detailed description can be found in [15].

The XUV and NIR pulses can be identified as time-dependent electric fields $\mathcal{E}(t)$ (in the time domain). The complex form can be written as

$$\mathcal{E}(t) = \mathscr{E}(t) \cdot e^{i\phi(t)}, \tag{52}$$

for an envelope $\mathscr{E}(t)$, defining the temporal structure of the pulse and a phase term $\phi(t)$. The real part of this electric field is the measurable quantity which interacts with a physical system.

Our simulation uses a Gaussian envelope, defined by

$$\mathscr{E}_G(t) = \mathscr{E}_0 \cdot e^{-(t/t_G)^2}, \tag{53}$$

where t_G depends on the FWHM pulse duration:

$$t_G = \frac{t_{\text{FWHM}}}{\sqrt{2\ln 2}}. \tag{54}$$

The phase term $\phi(t)$ is in our case characterized by the frequency ω with

$$\phi(t) = \omega t. \tag{55}$$

We use:

- $\mathscr{E}_{0,\text{XUV}} = 5 \cdot 10^{-5}$a.u.
- $t_{\text{FWHM, XUV}} = 0.5$fs
- $\hbar\omega_{\text{XUV}} = 14$eV for the XUV pulse and
- $\mathscr{E}_{0,\text{NIR}} = 3 \cdot 10^{-3}$a.u.
- $t_{\text{FWHM, NIR}} = 5$fs

- $\hbar\omega_{\text{NIR}} = 1.6\text{eV}$ for the NIR pulse.

The field strength may differ from the strength, which is used in an experiment, because we do not know the actual dipole moments, as mentioned in the section before. Therefore the couplings with an NIR field may be stronger, so that a weaker NIR pulse must be considered. By trial and error these parameters are found, giving us good results.

Obtaining the field by switching from time domain into the spectral (frequency) domain is related to the Fourier transform

$$\mathcal{E}^s(\omega) = \mathcal{FT}\{\mathcal{E}(t)\} = \int_{-\infty}^{+\infty} \mathrm{d}t\, \mathcal{E}(t) e^{-i\omega t}, \tag{56}$$

and the inverse transform is calculated via

$$\mathcal{E}(t) = \mathcal{FT}^{-1}\{\mathcal{E}^s(\omega)\} = \frac{1}{2\pi} \int_{-\infty}^{+\infty} \mathrm{d}\omega\, \mathcal{E}^s(\omega) e^{i\omega t}. \tag{57}$$

In the following, the propagation time T, the time steps Δt, the life time $1/\Gamma$ and the range of the time delay scan are discussed:

- $T = 100.000$ a.u. The propagation time T needs to be long for the investigated dynamics to fully evolve. The set value has proved to be sufficient.
- $\Delta t = 0.5$ a.u.: The time step increments Δt are chosen in an order of magnitude where natural electronic motion takes place. This indeed produced a satisfactory result.
- $\Gamma = 2 \cdot 10^{-4}$ a.u. By considering a lifetime $1/\Gamma$ for the states, a decay, e.g. due to spontaneous emission, can be simulated as well. According to [17], the time-dependent dipole moment $d(t)$ after an δ-function-like XUV-excitation at $t = 0$ becomes

  $$d(t > 0) \sim -ie^{-i\omega_r t - \frac{\Gamma}{2}t}. \tag{58}$$

  The value $\omega_r = E_r/\hbar$ is the resonance frequency, where E_r is the energy position or the elements of the free Hamiltonian $\mathcal{H}_0$ in equation (48). This is the reason, for why the energies are modified according to equation (49). As outlined also in [17], the imaginary part of the Fourier transform of $d(t)$ is associated to the spectral line shape with

  $$\text{Im } d(\omega) = \text{Im } \left(\int_{-\infty}^{+\infty} d(t) e^{-i\omega t} dt \right) \sim \text{Im } \left(\frac{1}{i(\omega_r - \omega) + \Gamma/2} \right). \tag{59}$$

  This shows a Lorentzian line profile, centered at ω_r with a full width at half maximum (FWHM) of Γ. The chosen value has shown that the decay is appropriate for the simulation and the Lorentzian profile could be observed. See more in section 5.1.2.
- Time delay scan from $\tau_{start} = -10\text{fs}$ to $\tau_{end} = 60\text{fs}$, in steps of $d\tau = 0.05\text{fs}$ are considered. These settings were determined because in that range one could observe a lot of dynamics. The step size and time range are regulated in a way to have a reasonable resolution, while the computation time is kept to a minimum.

If not mentioned otherwise, the above mentioned settings and parameters are used for all simulations.

4.4 Zero-Padding

When dealing with a discrete Fourier transform, in our case for calculating the OD, by taking the ratio of the time-dependent dipole moment and the electric field from time domain into frequency domain, the resolution $\Delta\omega$ depends on the propagation time T or also on the number of steps N [18]:

$$\Delta\omega_N = \frac{2 \cdot \pi}{\Delta t \cdot N} = \frac{2 \cdot \pi}{T}. \tag{60}$$

One can improve the resolution $\Delta\omega_N$, by adding zeros to the calculated signal, before taking the Fourier transform. This process is called *zero-padding*. It is easy to see that indeed

$$\Delta\omega_{N+M} = \frac{2 \cdot \pi}{\Delta t \cdot (N + M)} < \frac{2 \cdot \pi}{\Delta t \cdot N} = \Delta\omega_N, \tag{61}$$

if one adds M additional zeros to the signal.

In the simulation $N = 200.000$ ($T = 100.000$ a.u. in steps of $\Delta t = 0.5$ a.u., see section 4.3). From the calculated signal, we increased its length by a factor of five, meaning $M = 800.000$, so that $N' = N + M = 1.000.000$, since this factor is large enough to get a better resolution, while adding more zeros would not make a significant difference. This is because the line shape of the resonance lines for the chosen Γ is broad enough that a better resolution would not have a great impact on the shape.

5 Results and Data Analysis

This section covers the results of the numerical calculation of the laser-driven few-level system. It starts with reducing the whole system, consisting of 87 states, to a five-level system. The reduced complexity enables to gain an intuitive understanding of the behaviour of the state vectors. Following to this, the full 87-level system is considered. With only the XUV as excitation pulse, the resonant lines spectrum in absence of the NIR pulse is studied. By turning on the NIR pulse, time-delay scans are investigated systematically, to find the sources, which cause the occuring dynamics. Lastly, an intensity scan is studied, before an approach for using `Franck-Condon` factors to scale the transition probabilities between D- and EF-states is examined.

5.1 The Five-Level System

In this subsection, the following states are chosen for investigating their behavior under interaction with the XUV and NIR laser fields:

	X	B	C	D	EF
(ν, J)	$(0,0)$	$(4,1)$	$(1,1)$	$(1,1)$	$(9,1)$
photon energy [eV]	0	$11,81$	12.58	15.01	$13,40$
trans. amplitude to X	0	0.545	1	0.546	0

Table 1: The chosen states with their corresponding parameters for the five-level system

Since $\hbar\omega_{\mathrm{NIR}} = 1.6\mathrm{eV}$ (see section 4.3), there are resonant couplings between the B-/EF-states and the D-/-EF states, while the couplings between the C- and EF-states can also happen off-resonantly. Only one dark state is considered to further simplify the system. In atomic units, the associated Hamiltonian reads:

$$\mathcal{H}_{5\mathrm{L}}(t) = \begin{pmatrix} 0 & 0.545\mathcal{E}(t) & 1\mathcal{E}(t) & 0.546\mathcal{E}(t) & 0 \\ 0.545\mathcal{E}(t) & 0.434\text{-}0.0001\mathrm{i} & 0 & 0 & 1\mathcal{E}(t) \\ 1\mathcal{E}(t) & 0 & 0.462\text{-}0.0001\mathrm{i} & 0 & 1\mathcal{E}(t) \\ 0.546 & 0 & 0 & 0.552\text{-}0.0001\mathrm{i} & 1\mathcal{E}(t) \\ 0 & 1\mathcal{E}(t) & 1\mathcal{E}(t) & 1\mathcal{E}(t) & 0.492\text{-}0.0001\mathrm{i} \end{pmatrix}, \tag{62}$$

with electric fields as defined in section 4.3.

5.1.1 Time-Dependent Time Population of the Five-Level System

The absolute square of the state vectors for different time delays between the XUV and NIR pulses are plotted in figure 6. The rising population around time zero of the B-/C-/D-state indicates, how the XUV pulse rearranges the populations from the ground state to the bright states, before they start decaying exponentially. The C-state has the strongest population increase, because its transition amplitude from the ground state is the highest, as seen in table 1. Although the B- and D-state have a similar transition amplitude from the ground electronic state, the population of the D-state is higher than the population of the B-state. The reason for this is, because the D-state's energy at 15.01eV lays closer to the photon energy of the XUV pulse $\hbar\omega_{\mathrm{XUV}} = 14\mathrm{eV}$ (see section 4.3), so the excitation is higher than for a state with a photon energy farther away. The ground

electronic state's amplitude is subtracted by 1, so it has a minimum at $\sim -6 \cdot 10^{-6}$, which implicates that its population decreased from 1 and stays at $1 - 6 \cdot 10^{-6}$.

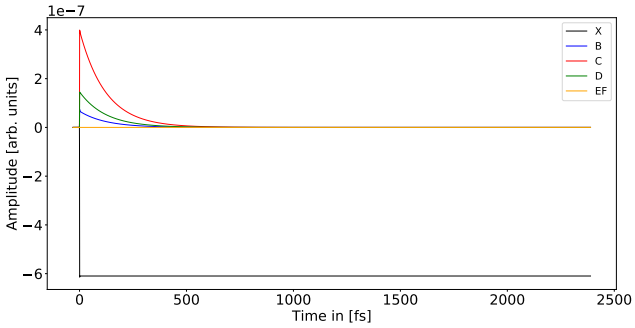

(a) $\tau = -10$fs, zoomed out, to see the ground state population

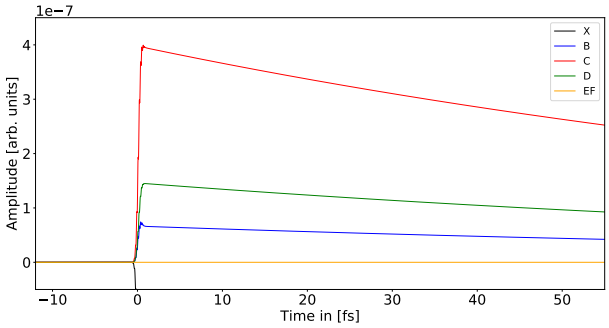

(b) $\tau = -10$fs

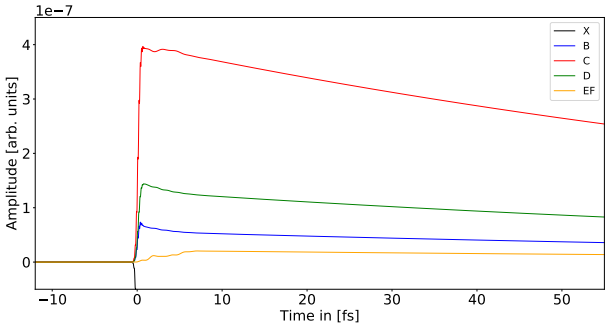

(c) $\tau = 0$fs

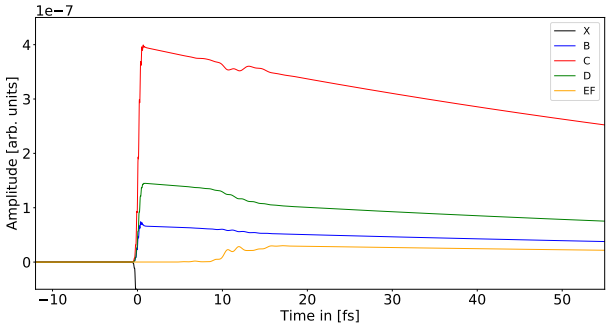

(d) $\tau = 10$fs

Figure 6: The population of the considered states in the five-level simulation is plotted. The XUV pulse arriving at $\tau = 0$fs can populate the bright states from the ground electronic state X. The amplitude of the X-state is subtracted by 1, with its minimum at around $-6 \cdot 10^{-6}$. While the effect of the NIR pulse is not visible for a negative time delay (b), one can see that the EF-state can couple to the bright states and gain population, when the resonant NIR coupling is switched on during and after the initial XUV population of the bright states, in (c) for $\tau = 0$fs and (d) for $\tau = 10$fs. Also it can loose its population back to the bright states. The states decay exponentially right after they got populated.

For a negative time delay $\tau = -10$fs (a), (b) where the NIR pulse arrives before the XUV pulse can interact with the system, and with this populate the excited B-/C-/D-states, the effect of the NIR pulse is not visible, because the EF-state cannot be populated from the X-state. With this the coupling to the not yet populated bright states is not existing. If both pulses arrive simultaneously (c), $\tau = 0$fs, the NIR pulse can couple the EF-state with the B-/C-/D- state, since the NIR pulse duration still lasts, even though the XUV pulse finished its interaction with the system. This is why the population of the EF-state in (c), $\tau = 0$fs, is smaller compared to (d), $\tau = 10$fs, where the NIR pulse can interact with the system for its full duration.

Another observed effect is that the EF-state can loose its population to the bright states again,

i.e. it can transfer its population back; in (c) the C-state rises a little bit at around 2.5fs, in (d) the same effect is seen at around 12.5fs. Whenever rise of the population of the C-state is observed, the EF-state becomes less populated. The population of the B- and D-state, on the other side, do not rise during the NIR interaction. This is the two-photon-transition, meaning that the EF-state acts like an intermediate step for further couplings to other bright states. Since both B- and D-state can couple resonantly with the EF-state, the two-photon-transition from B-to-EF-to-D and vice versa is about equally probable, meaning both states cannot get a population gain, because the loss to the first-photon-transition to the EF-state is equalized with the gain from the two-photon-transition. But two-photon-transitions from the C-state in one of the B-/D-state is less probable because of the off-resonant coupling. In reverse it happens with a higher probability, because the general probability to couple with the EF-state is higher from the B- or D-state, so there are more chances for a two-photon-transition to the C-state. This is why a population gain is only visible for the C-state.

All interactions need to happen within the decay time of the states, this is why a short time delay was chosen.

5.1.2 Resonant Line Shapes of the Spectrum

Since the XUV pulse is very short, its excitation can be considered almost δ-like, in accordance with the discussion in section 4.3, a Lorentzian line shape occurs, if the line spectrum is calculated in absence of an NIR pulse. This is shown for the D-state in figure 7. It is clearly visible that the line is centered at $\hbar\omega \approx 15.01$ eV, which is the resonant energy difference between the D-state energy and the ground state energy. The FWHM is geometrically found to be

$$\text{FWHM} = 0.00544 \text{ eV} = 0.00020 \text{ a.u.} = \Gamma. \tag{63}$$

This demonstrates the connection between the FWHM and the lifetime. If additionally the NIR pulse interacts with the system, the line shape turns to be asymmetrical (see. figure 8). Specifically for the considered D-state as above, the line's maximum shifts either to the left or to the right, creating a minimum and maximum. Here $\mathscr{E}_{0,\text{NIR}} = 1 \cdot 10^{-2}$ a.u. and for comparison, a weaker pulse with $\mathscr{E}_{0,\text{NIR}} = 0.5 \cdot 10^{-2}$ a.u. are used, since the interactions are very weak compared to if one considers all states. When more dark states are allowed to couple through the NIR pulse, the overall interaction strength is effectively enhanced. Since here only one EF-state is used, a stronger coupling could be achieved by using a higher field strength. The time delay is set to $\tau = 8$fs and $\tau = 10$fs.

The observed line shape in figure 8 is a `Fano` line shape and can be explained with the `Fano` formalism [19], which will not be discussed in detail in this thesis. However, the line can be fitted using

$$f(q, \epsilon(E)) = a \cdot \frac{|q + \epsilon(E)|^2}{1 + \epsilon^2(E)} + c, \tag{64}$$

for

$$\epsilon(E) = \frac{E - E_r}{\Gamma/2} \tag{65}$$

a scaling parameter a and a parameter for the non-resonant background part c. E_r is the resonance energy, or the position of the state on the photon energy axis, which is kept fix for the fit. The sign of the q-parameter decides, whether the line shape begins with a maximum switching to a minimum or vice versa. The following fit parameters are found:

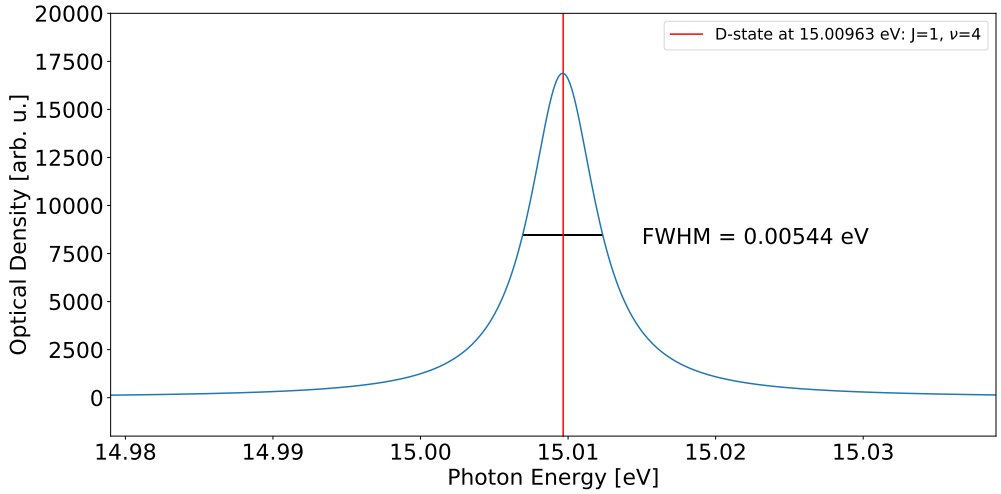

Figure 7: If only the XUV pulse interacts with the system, a Lorentzian line profile can be observed, here, for the considered D-state. The FWHM corresponds to the lifetime, where $\Gamma = 0.00544$ eV $= 0.0020$ a.u.

figure	q	a	c
8a	1.074	4262	-3661
8b	-1.618	2268	-1717
8c	7.204	219	6.682
8d	-9.962	127	63

Table 2: Fit parameters for the `Fano` lines in figure 8.

Here we see that the minus sign refers to a maximum switching to a minimum and vice versa for a plus sign.

5.2 The Full 87-Level System

After looking at the simplified five-level system, this subsection covers the full system consisting of all 87 considered states. In absence of the NIR field, the spectrum is shown, first, if one treats all couplings and transitions equal, by setting all dipole moments to 1, then by weighting the transition probabilities according to the experimental data, as described in section 4.2. After that, time-delay scans are investigated in section 5.2.2. Naturally, any coupling between dark states and bright states are possible. This shows many time-dependent structures and need to be investigated carefully. An approach by regarding a system, where only few couplings between certain bright and dark states are possible, is pursuit. By doing it systematically, one can find which couplings causes which structures. In section 5.2.3 an intensity scan is considered and its relevance is pointed out. Furthermore `Franck-Condon`-factors are used to weight the transition amplitudes between the D-

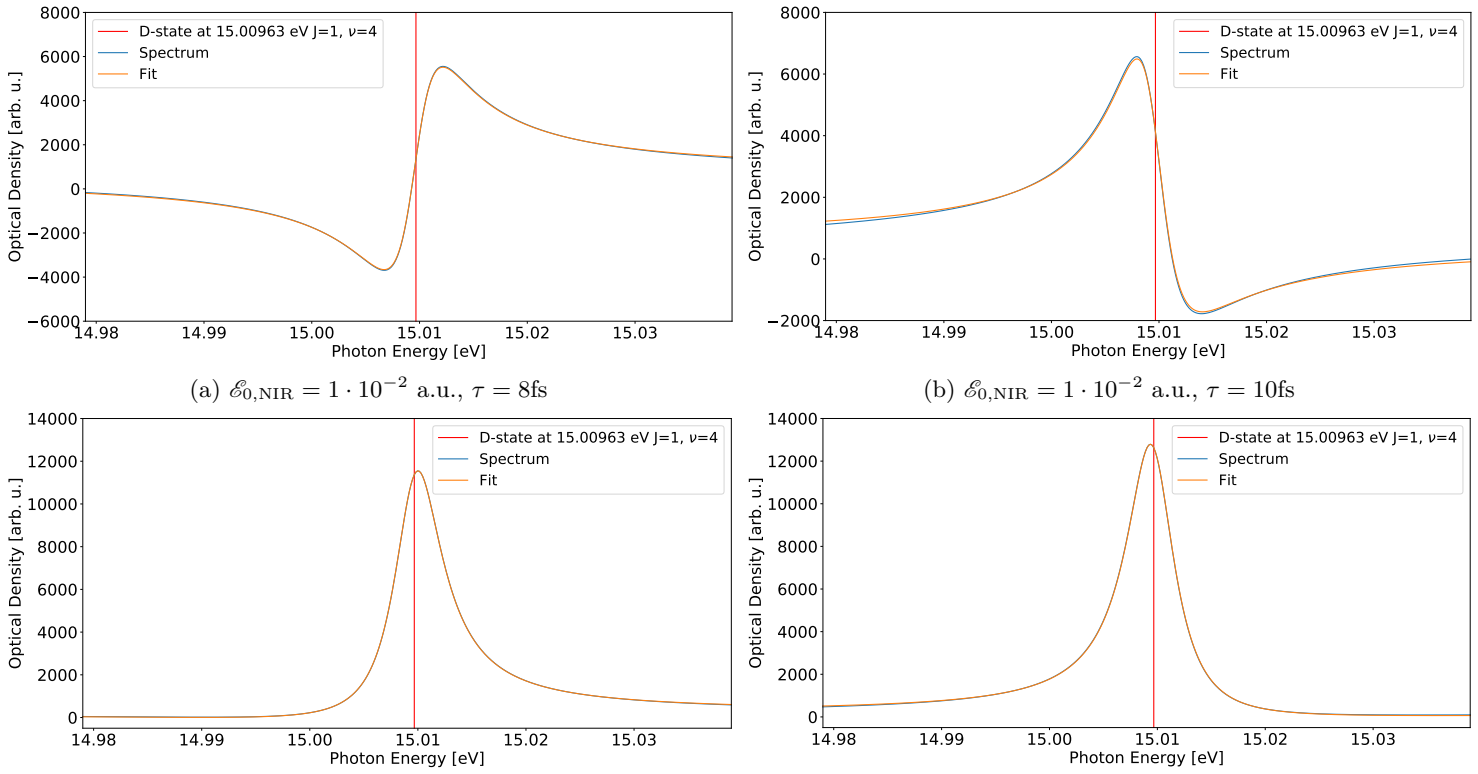

(a) $\mathscr{E}_{0,\mathrm{NIR}} = 1 \cdot 10^{-2}$ a.u., $\tau = 8$fs

(b) $\mathscr{E}_{0,\mathrm{NIR}} = 1 \cdot 10^{-2}$ a.u., $\tau = 10$fs

(c) $\mathscr{E}_{0,\mathrm{NIR}} = 0.5 \cdot 10^{-2}$ a.u., $\tau = 8$fs

(d) $\mathscr{E}_{0,\mathrm{NIR}} = 0.5 \cdot 10^{-2}$ a.u., $\tau = 10$fs

Figure 8: An asymmetric line shape can be observed for the same D-state as in figure 7, by using an NIR pulse with intensity of $\mathscr{E}_{0,\mathrm{NIR}} = 1 \cdot 10^{-2}$ a.u. for (a), (b) and $\mathscr{E}_{0,\mathrm{NIR}} = 0.5 \cdot 10^{-2}$ for (c), (d), each with time delay of $\tau = 8$fs and $\tau = 10$fs. The spectrum is fitted with a function according to equation (64). The fit parameters can be seen in table 2.

and EF-states. A time-delay scan is compared to a scan, where the scaling is not applied.

5.2.1 Resonant Lines Spectrum with XUV only

The first case for the investigation of the resonant line spectrum assumes that all transition amplitudes from the ground state X to the bright states are equal to 1. In other words, all non-zero entries of the dipole moment operator $\hat{d}_{XUV}$ are 1. This assumption serves as a sanity check to verify that the implementation for the full system is correct. Since all transition probabilities are equal, and according to equation (9) and (10)

$$OD(\omega) \sim \sigma(\omega) \sim \omega, \tag{66}$$

i.e. one would expect that the calculated OD is increasing linearly regarding the photon energy $E = \hbar\omega$. Indeed, in figure 9a the amplitude of the spectrum follows a linear behavior with higher photon energy. The spectrum also only shows the bright states, while the dark states do not give rise to any resonant absorption lines, since they cannot be excited from the ground state. For the sake of completeness, all resonant energy differences for all states are indicated. At around ~ 13.1eV, ~ 14.3eV, $\sim 14,8$eV and ~ 16.6eV larger peaks stand out. The reason for this is constructive interference between two or more states at around each of the mentioned energies. This is also why some lines near these peaks also have a higher amplitude, since they also can interfere with them.

After this sanity check, the dipole moments are weighted using experimental data, as explained in section 4.2. The spectrum for this configuration is shown in figure 9b. The linear rising behavior of the lines to higher energies vanishes, since the transition amplitudes from ground to exited state are not treated equal anymore. Also the larger peaks at around $\sim 14,8$eV and ~ 16.6eV do not dominate the line spectrum. The modulation of the amplitudes of the lines now reflects the change in the transition amplitudes according to the `Fracnk-Condon` factors between ground an excited vibrational states.

5.2.2 Time-Delay Scans with an NIR Pulse

In the following, we calculate the optical density for changing time delay τ between the XUV and NIR pulse. The obtained time-delay scans are analyzed in order to identify which dynamics signatures are caused by which interaction between the states, e.g. which couplings are important for the observed spectral line changes. This is accomplished by a systematic investigation, where we only allow couplings between certain bright and dark states. By *allowing, or turning on couplings between certain states* we mean the following: if the coupling between the B- and EF-states is allowed, that the associated dipole moments describing the coupling with an NIR pulse are non-zero. In this case, in the Hamiltonian, equation (51), $d_{73,2} = d_{73,3} = ... = d_{73,39} = 1$, because the couplings between $EF_{J=1,\nu=0}$ and all 38 B-states are allowed. Analogously for all the other EF-states. If a coupling is *not allowed* or *turned off*, the associated dipole moments describing the couplings with an NIR pulse equals zero, e.g. if the coupling of the B- and H-states is turned off, $d_{85,2} = d_{85,3} = ... = d_{85,39} = 0$, i.e. $H_{J=1,\nu=0}$-state cannot interact with any of the B-states.

A full time-delay scan by allowing all couplings between the bright and dark states is performed and is plotted in a 2D-plot in figure 10. The energy differences between all states and the ground

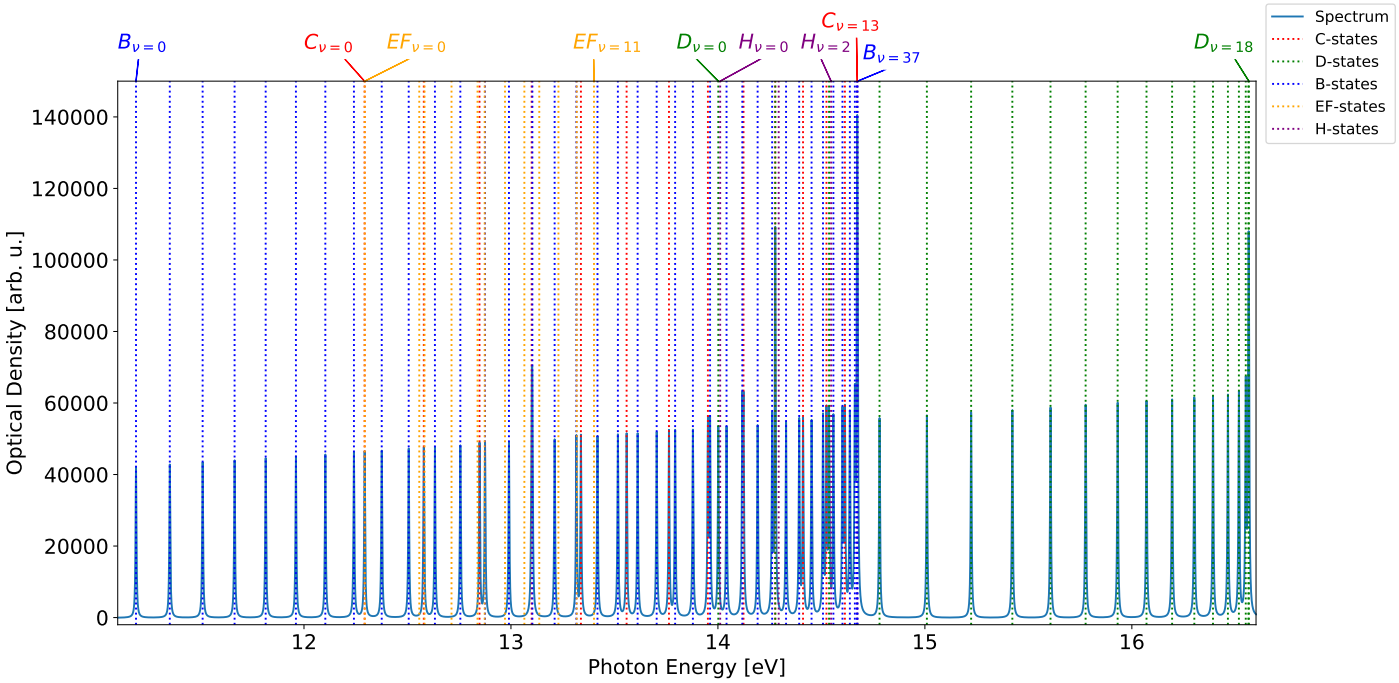

(a) All dipole moments are set to 1.

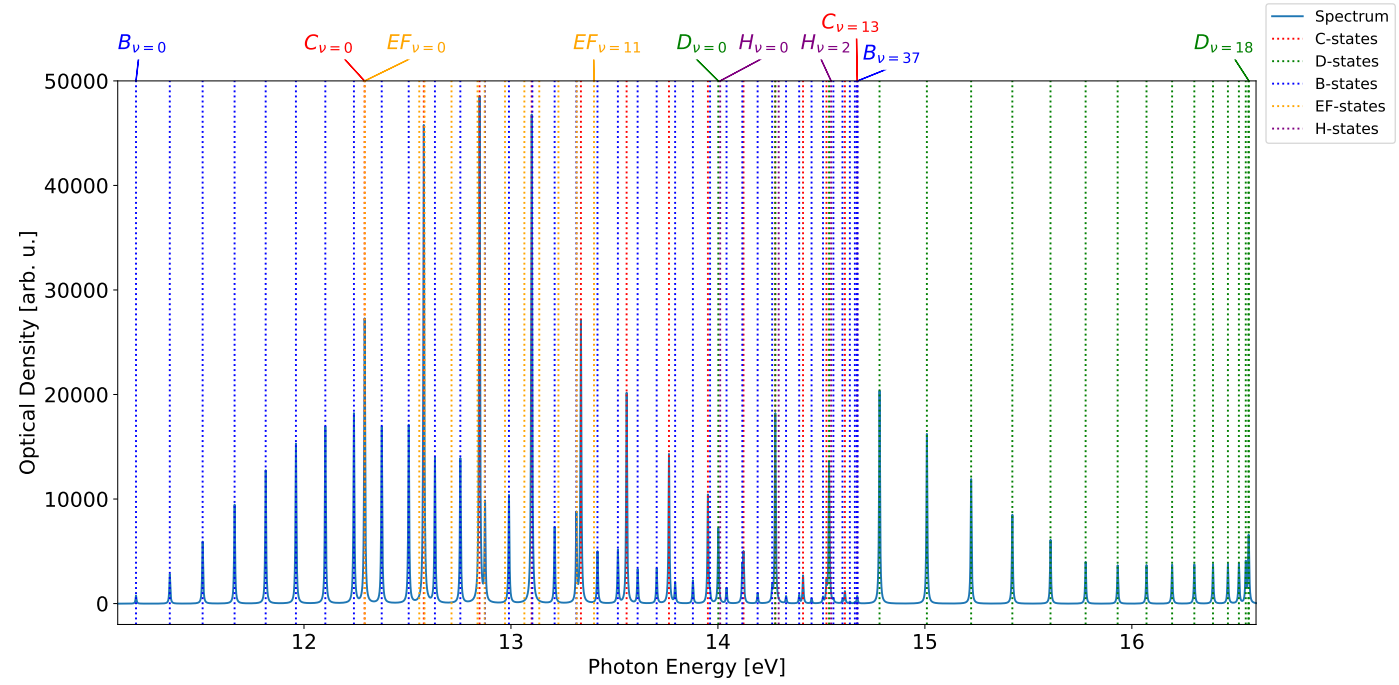

(b) Dipole moments weighted according to section 4.2.

Figure 9: The calculated resonant line spectrum for all states is plotted and the resonant energy difference between each state to the ground state are marked. Only the bright states are forming the line spectrum. In (a), where all transition amplitudes from ground to the excited states are equal to 1, the amplitudes show a linear rising behavior for higher photon energies. By weighting them according to section 4.2, the amplitudes are proportional to the weighting factors, as seen in (b).

electronic state are marked as well. This time-delay scan shows rich dynamics: a lot oscillations and energy shifts can be observed. To understand the reason behind the dynamics and which coupling causes them, a systematic approach by performing time-delay scans for different coupling scenarios is pursued. Specifically, the cases for turning on the coupling between the B- and EF-states, and considering the coupling between B-/EF-states and the D-/EF-states are investigated in detail. All other cases considered in the simulation can be discussed analogously to the two mentioned cases. This is why we do not discuss their time-delay scans in this thesis, but only their contribution to the case, where all couplings between all bright and dark states are allowed, is indicated. But the scans with the associated Fourier plot are found in appendix A.

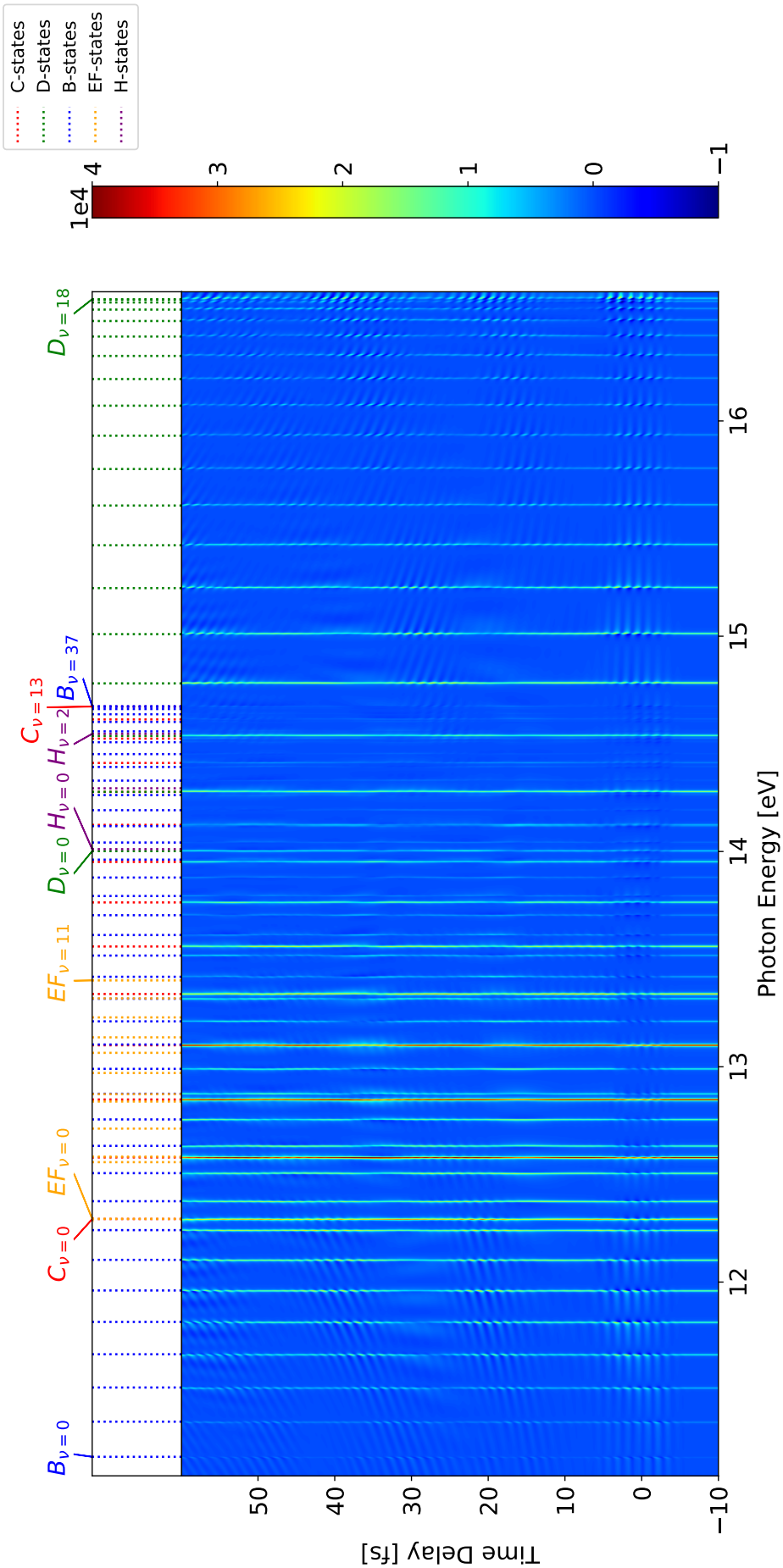

Figure 10: A time-delay scan is performed for the case that all couplings between the bright and dark states are allowed. The scan show a rich dynamical behavior, like oscillations and intensity shifts. The reason behind it and from where they arise, will be discussed later.

Case 1: Only couplings between the B-/EF-states are allowed

The full time-delay scan for this case is shown figure 11. Around $\tau \approx -5$fs to $\tau \approx 5$fs, one can see oscillations between ≈ 11.1eV to ≈ 12.6eV for the B-states. These are caused by the modulation of the NIR pulse. After the B-states are excited with the XUV-pulse at $\tau = 0$fs, the NIR pulse starts to transfer populations to the EF-states. It is observed that the period of these oscillation is ≈ 1.3fs. Taking into account that the NIR pulse frequency is given via $\hbar\omega_{\mathrm{NIR}} = 1.6$eV and using

$$\omega = \frac{2\pi}{T} \tag{67}$$

for the period T, one finds

$$T = \frac{2\pi}{\omega_{\mathrm{NIR}}} = \frac{2\pi\hbar}{1.6\mathrm{eV}} \approx 2.6\mathrm{fs}. \tag{68}$$

This showss that the oscillations are half-cycle periodic. The factor of $\frac{1}{2}$ can be explained by the fact that the absolute square of the NIR pulse is considered for the calculation of the OD, meaning that negative amplitudes of the NIR pulse also give rise to a maximum in the oscillations. Thus the oscillation period is half of a period of the laser frequency.

Also the oscillations are stronger for the B-states, which can couple resonantly to the EF-states, here in the range of ≈ 11.1eV to ≈ 12.6eV. Between ≈ 12.6eV to 13.6eV there is almost no oscillation, while between ≈ 13.6eV to ≈ 14.7eV the oscillations are visible again, but weaker, because here the B-states can couple off-resonantly to the EF-states.

Another effect that enhances the couplings are two-photon-transitions. A B-state can couple to one of the EF-state, which can then couple back to the same B-state or couple to another B-state. This effect is also stronger for resonant couplings. By taking the Fourier transform of the time-delay scan along the time delay axis, these two-photon-transitions are visible on a straight line with slope ± 1, crossing the resonant line at around the double photon energy at 3.2eV. The Fourier plot is shown in figure 12. Some B-states can couple through the EF-state to many different other B-states, this is why there are more straight lines slightly above or below the double photon energy, indicating the two-photon-transitions. This is observed e.g. for the B-states at ≈ 14eV to ≈ 14.5eV. The double photon energy peak is also not sharp at exactly 3.2eV but has a certain width, reflecting the spectral width of the NIR pulse.

Due to the two-photon-transition phase shifts are occurring. These phase shifts lead to interference and depend on the time delay. In this case, at $\tau \gtrsim 5$fs the oscillations vanishes due to the dephasing. The phase shifts can be better observed in figure 13. For the B-states with $\nu = 2, 4, 6$ the OD of the associated spectral line is averaged within ± 0.02eV of the line's position along the time delay axis. A vertical line in black is positioned at the minimum of the $B_{J=1,\nu=2}$ state. The related minima of the higher energetic states are indeed shifted to higher time delays.

Another structure e.g. at $\tau \approx 25$fs to $\tau \approx 32$fs and $\tau \gtrsim 55$fs, for the B-states in the range of ≈ 11.1eV to ≈ 12.6eV in the time-delay scan is seen. The spectral lines seem to shift to higher or lower energies. It is assumed that this is caused by the AC Stark effect. Briefly summarized, it describes the splitting and shifting of spectral lines under the influence of an external electric field. Here the NIR pulse is the electric field, which may shift the energy due to that effect.

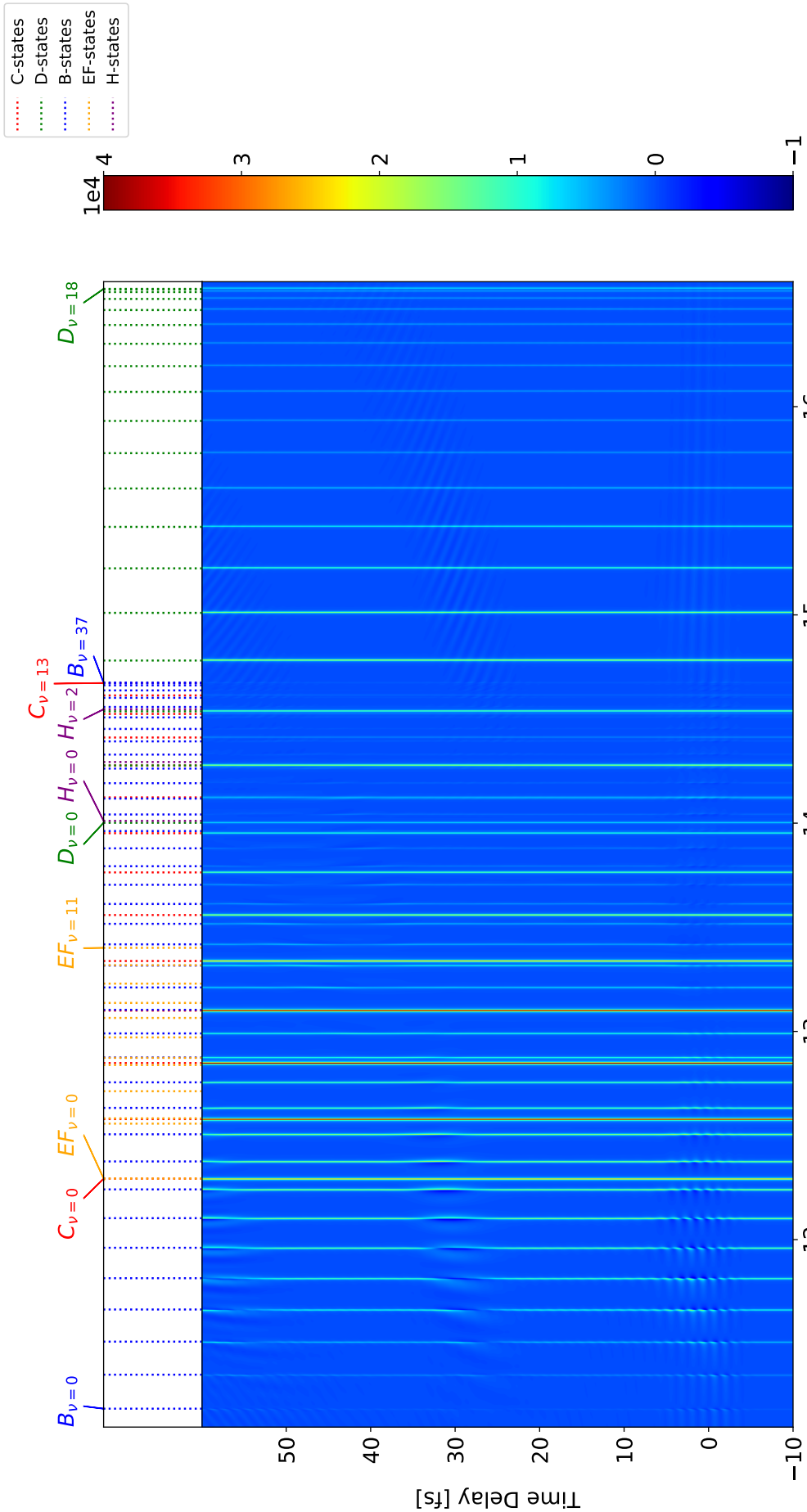

Figure 11: Time-delay scan, where only the couplings between the B- and EF-states are allowed. The strongest visible structures are the 2ω-oscillations, due to the modulation of the NIR pulse at ≈ 11.1eV to ≈ 12.6eV for $\tau \approx -5$fs to $\tau \approx 5$fs. An energy shift in the same energy range at $\tau \approx 25$fs to $\tau \approx 32$fs is observed. It is suspected that this is caused by the AC Stark effect.

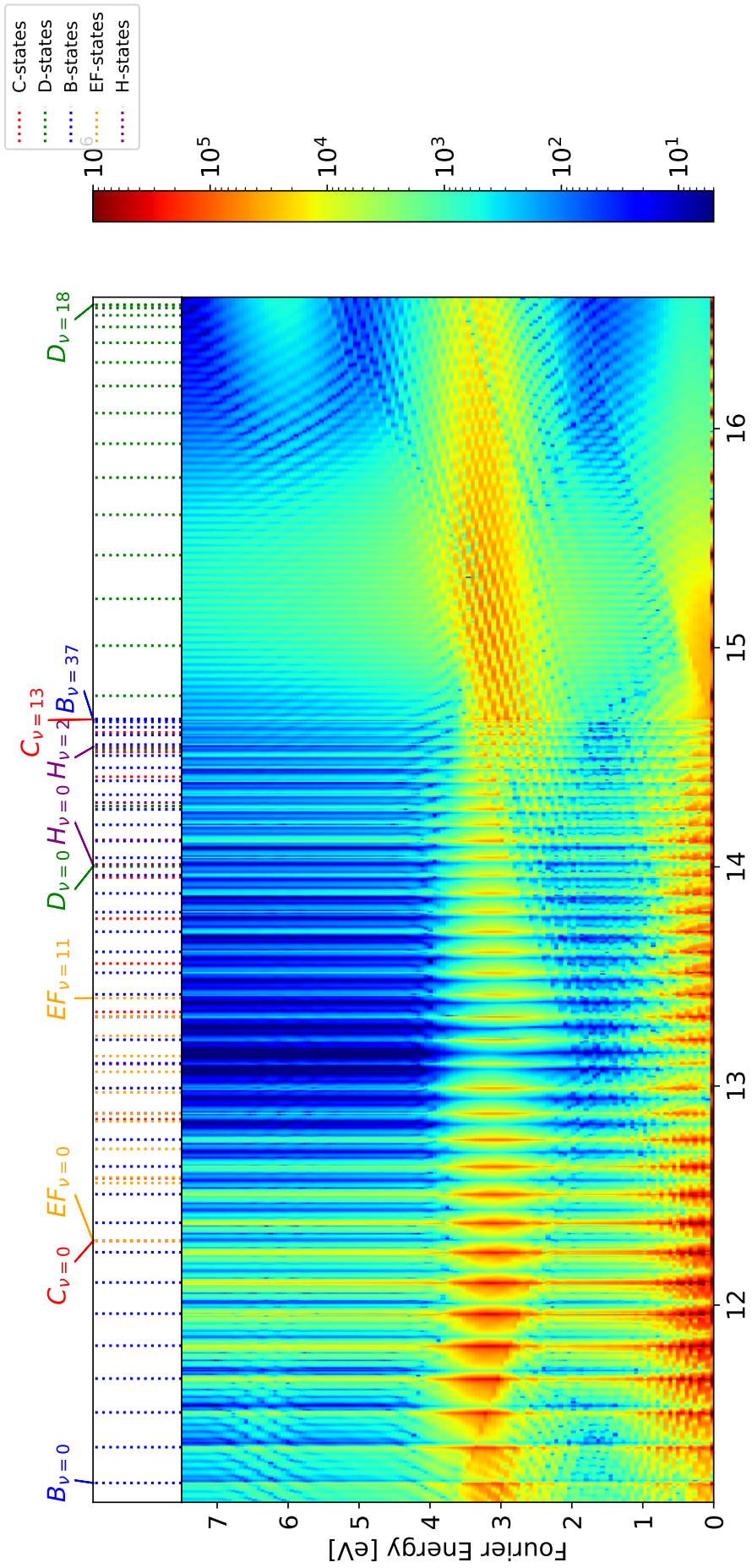

Figure 12: Fourier plot, where only the couplings between the B- and EF-states are allowed. The straight lines crossing the resonant lines at around the double photon energy 3.2eV, have each a slope of ±1. They indicate two-photon-transitions. The B-states from between ≈ 14eV to ≈ 14.5eV show multiple lines, meaning they can couple via the EF-state to different other B-states.

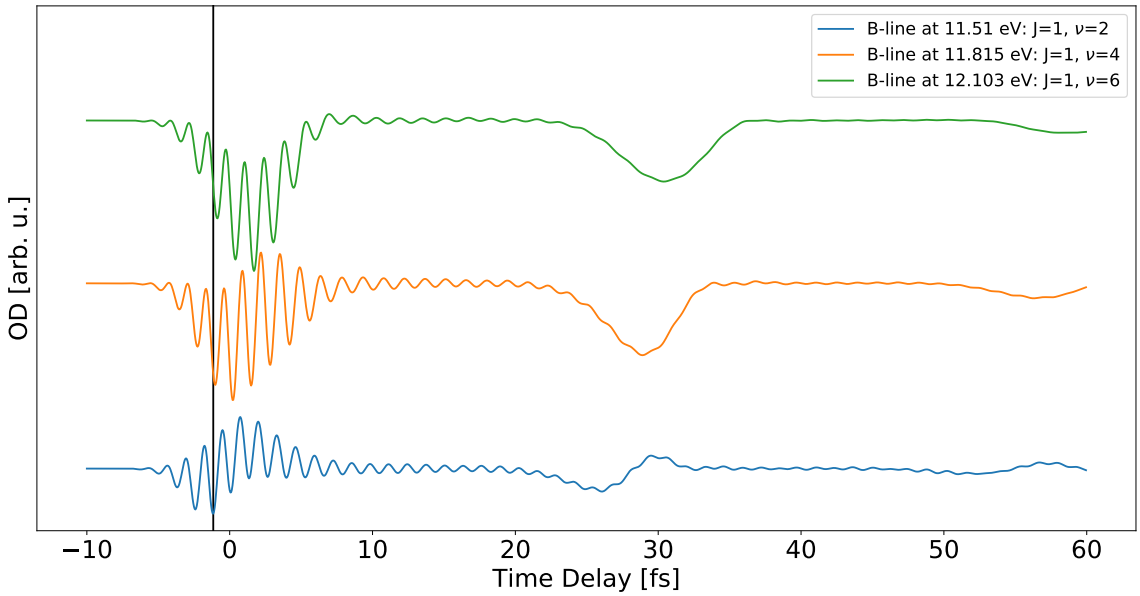

Figure 13: The averaged OD within ±0.02eV of each spectral line along the time delay axis is plotted. A phase shift can be observed. The vertical black indicates the minimum of the $B_{J=1,\nu=2}$-state; the related minima of the other two B-states with higher ν are shifted to higher time delays.

Case 2: Couplings between B-/EF- and D-/EF-states are allowed

The time-delay scan for this case is shown in figure 14. Here, more time-dependent features can be observed compared to case 1, where only interactions between the B- and EF states were allowed. In the range of $\tau \approx -5$fs to $\tau \approx 5$fs, not only the B-states can interact with the NIR pulse, but also the D-states for $\gtrsim 14.5$eV can couple resonantly to the EF-states, showing oscillations due to the NIR laser modulation. The last two D-states are laying closely together, and thus the oscillations are enhanced due to constructive interference. The spectral lines of the B-states between ≈ 12.6eV to 13.6eV are showing a weak oscillation. In the previous case, the oscillation in that area was almost non-existing; these B-states can only couple off-resonantly to the 12 EF-states between ≈ 12.3eV and ≈ 13.4eV. Since the D-states also are allowed to couple to the EF-states, the populations of the EF-states are larger, due to the additional coupling. This is the reason that two-photon-transitions can couple off-resonantly to the less preferred B-states between ≈ 12.6eV to 13.6eV with a higher probability. The D-states between ≈ 14.0eV and ≈ 14.5eV also show no visible interaction with the system, since they couple only off-resonantly, too. Looking to the associated Fourier plot, figure 15, the two-photon-transitions dominate for the D-states $\gtrsim 14.5$eV. Compared to the case above, for the B-states, which can couple resonantly, the two-photon-transitions are more common likewise.

For higher time delays, the oscillations are returning, but in a diagonal shape. In this case, for the B-states, between ≈ 11eV and ≈ 12.6eV, from $\tau \approx 10$fs to $\tau \approx 25$fs, $\tau \approx 25$fs to $\tau \approx 45$fs and $\tau \gtrsim 45$fs are the first, second and third returning oscillations, respectively. For the D-states, between ≈ 14.8eV and ≈ 16.6eV, 2ω-oscillations happen in the range of $\tau \approx 22$fs to $\tau \approx 50$fs and $\tau \gtrsim 50$fs. The reason for the returning oscillation could be a quantum mechanical revival of the wave function. After a certain time during the time evolution, the wave function occurs in a periodic recurrence, back to its initial form or in multiple scaled fractions of its initial form. This can happen multiple times, as seen in the time-delay scan. The diagonal shape can be explained by phase shifts, as mentioned in the previous case, caused by two-photon-transitions. However, the phase shifts are much stronger, which needs to be further studied. A possible explanation is that the suspected Stark effect can cause additional phase shifts, also through two-photon-transitions, but with a shifted energy. The previously mentioned suspected energy shift at $\tau \approx 25$fs to $\tau \approx 32$fs and $\tau \gtrsim 55$fs, for the B-states between ≈ 11.1eV to ≈ 12.6eV appear approximately at the same time delay range, where the revival structures of the D-states lay. Looking closely to the area right above and beneath the first revival structure of the D-states, there are also energy shifts in the time delay range corresponding to the first two revival structures of the B-states. This is also seen for both revival structures at around $\tau \approx 50$fs. Also since the wave function had more time to evolve, its phase becomes larger the higher the photon energy of the considered state is.

When looking to the recurring oscillations it is also interesting to inspect the evolution of a spectral line shape for different time delays. We choose the $D_{J=1,\nu=5}$-state at ≈ 15.22eV, because the oscillations there are strong. In figure 16, the spectral line is investigated for $\tau = 30.4$fs to $\tau = 31.6$fs in steps of $\Delta\tau = 0.05$fs. The asymmetrical line shape, beginning with a minimum transitioning to a maximum, is rising until $\tau = 30.95$fs. At $\tau = 31.0$fs, the minimum becomes a maximum and vice versa, meaning the q-parameter describing the `Fano` line (see also section 5.1.2) flips from positive to negative, before the line descends.

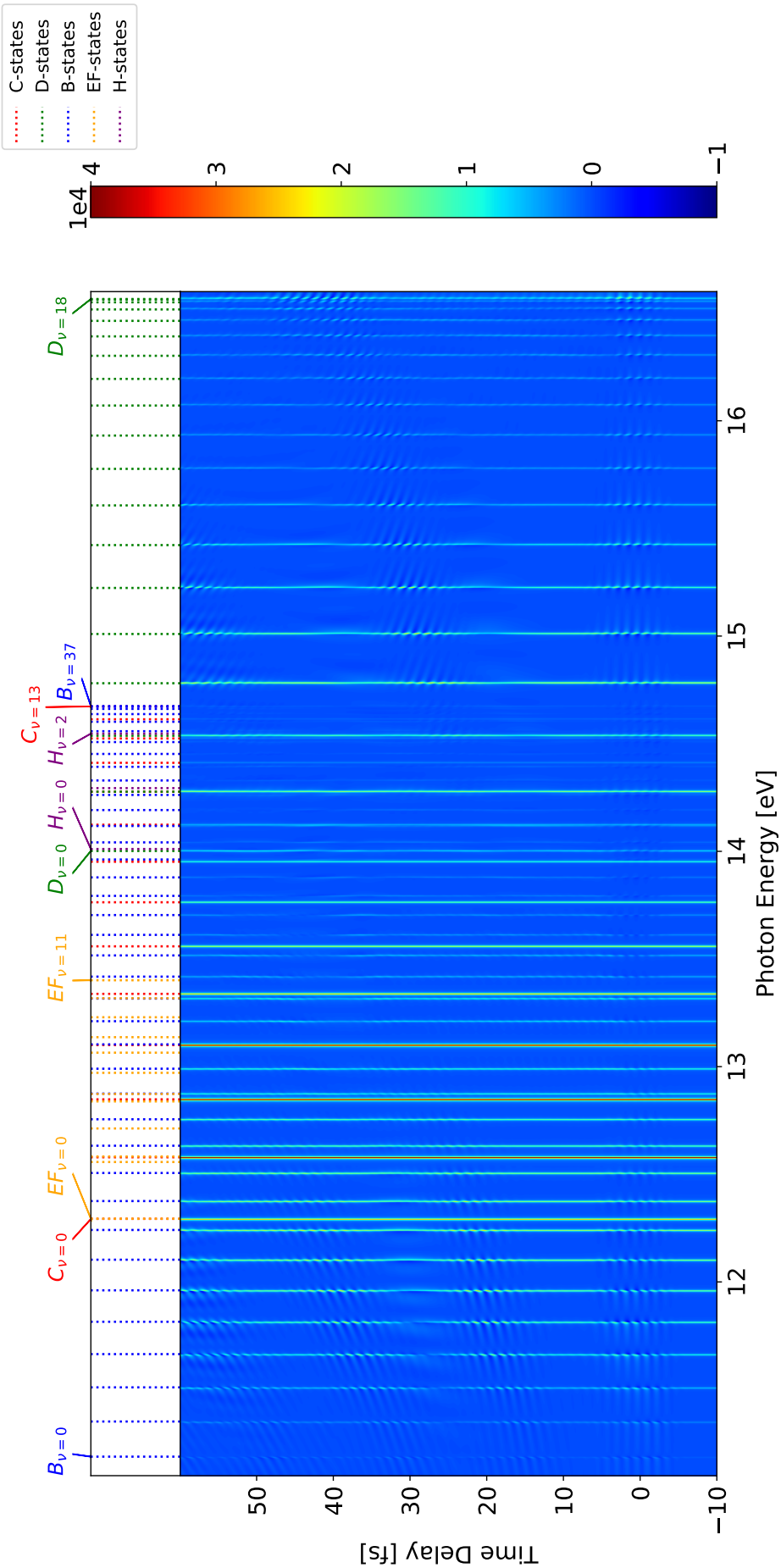

Figure 14: Time-delay scan, where the couplings between the B-/EF- and D-/EF-states are allowed. Here the main differences to the previous considered case are that the D-state $\gtrsim 14.5$eV also show 2ω-oscillation for $\tau \approx -5$fs to $\tau \approx 5$fs. A revival structure can be seen for both the D-states and the B-states between ≈ 12.6eV to 13.6eV for higher time delays.

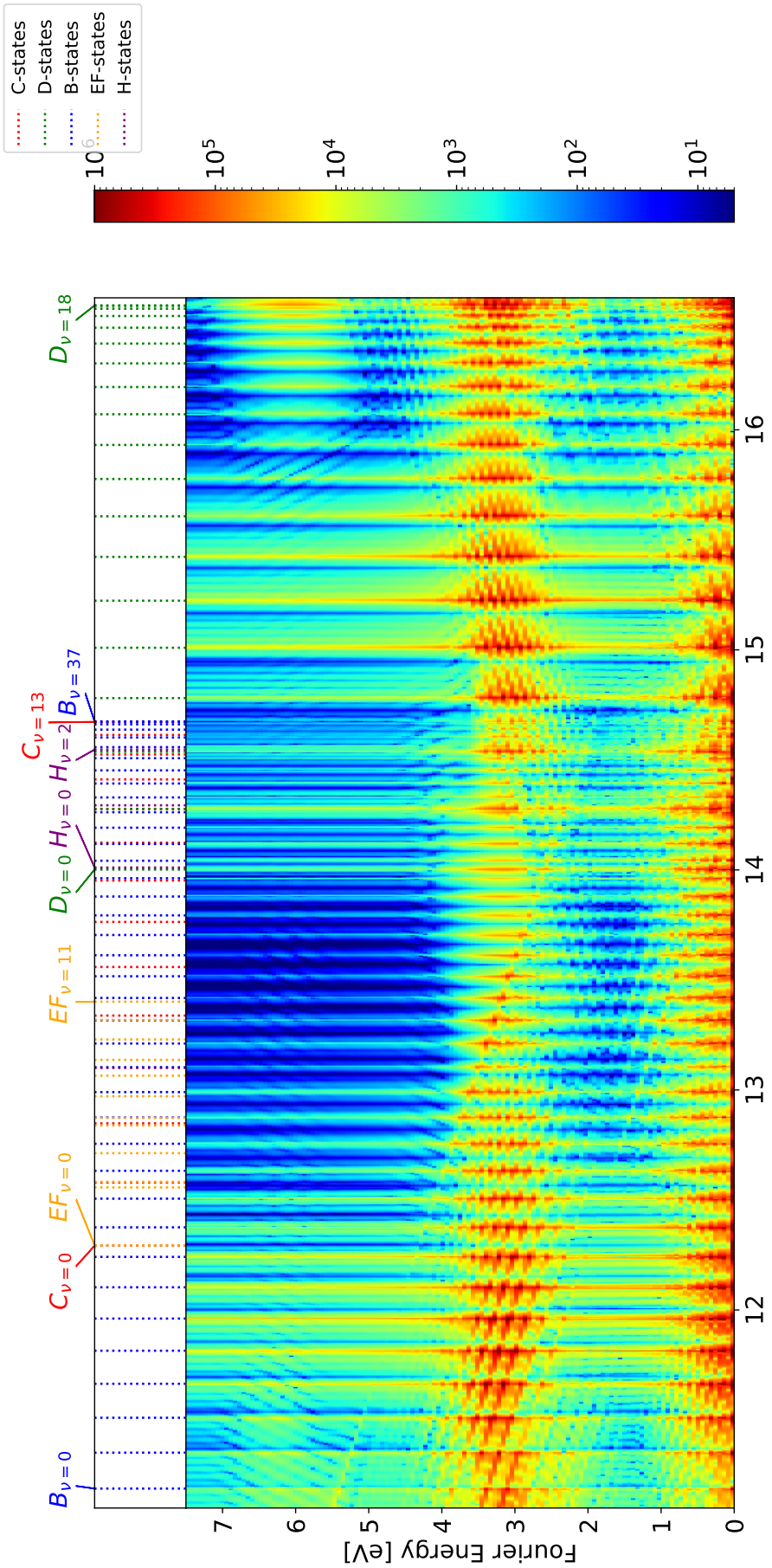

Figure 15: Fourier plot, where the couplings between the B-/EF- and D-/EF-states are allowed. Compared to the previous case, more straight lines are visible, indicating more two-photon-transitions are happening. Since the coupling to the D-states are allowed, the probability for such a transition is in general higher.

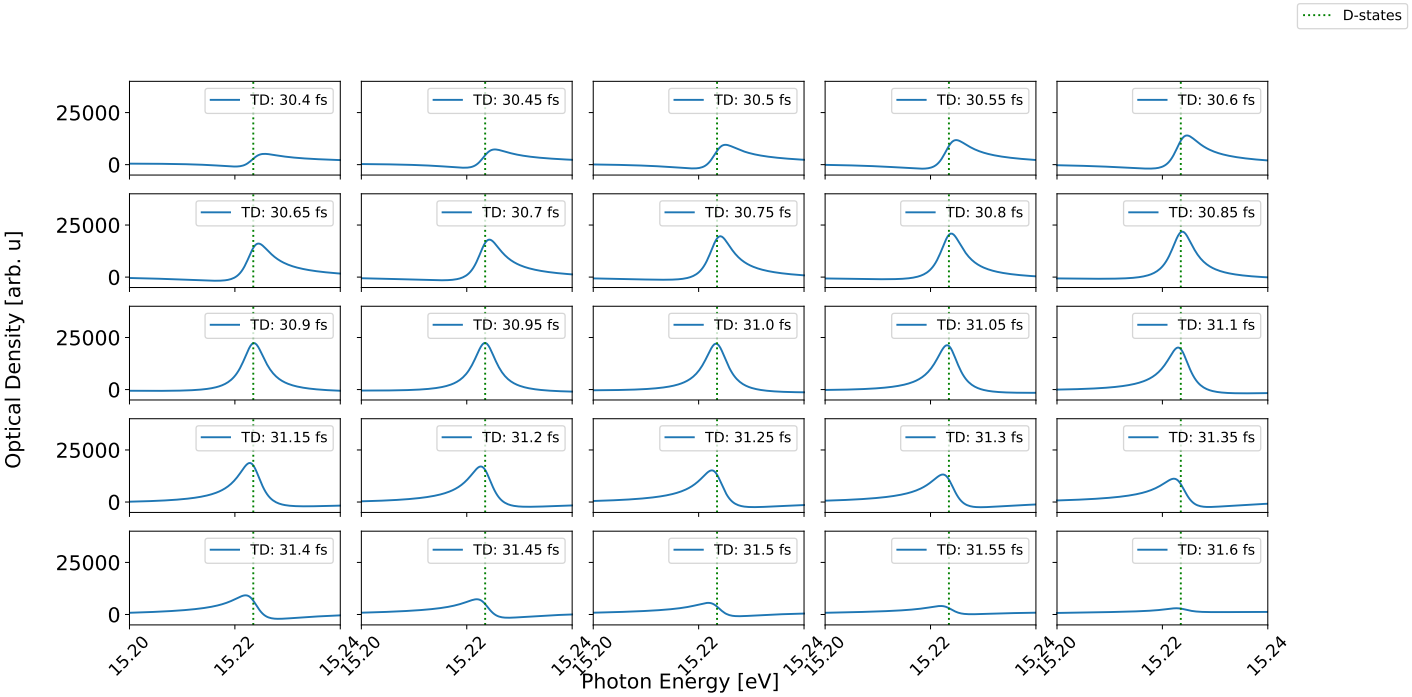

Figure 16: The resonant line of the $D_{J=1,\nu=5}$-state is plotted for $\tau = 30.4$fs to $\tau = 31.6$fs with $\Delta\tau = 0.05$fs. The line switches its sign of the q-parameter at $\tau = 31.0$fs, in this case the transition from a minimum to a maximum of the asymmetrical line is changed to a transition from a maximum to a minimum.

Couplings between all dark and bright states are allowed

A systematical investigation for different configurations of allowed couplings between certain bright and dark states is performed. Breaking down the time-delay scan using few couplings allows one to deduce the causes for distinct time-dependent structures in the time-delay scan, where couplings between all dark and bright states (from now on: all couplings) are allowed, as introduced earlier in figure 10. The notation e.g. "B-EF" is used, if the couplings between the B- and EF-states are allowed.

The time-delay scan where all couplings are allowed, is modified and divided in sections, so it is easier to follow, which features in the scan are addressed (figure 17). When talking about a section, it is always referred to the same section in the time-delay scan of the respective case. All considered time-delay scans using different coupling configurations and the associated Fourier plot can be found in the appendix A. Their contribution to the time-delay scan using all couplings are summarized in a tabular form:

Allowed Couplings	Contribution in Section	Comment
B-EF	(a), (c), (e), (h)	(a), (c): energy shifts, (h): weaker energy shifts, (e): 2ω oscillations by resonant couplings. Additionally at the end of (i): weak 2ω oscillations by off-resonant couplings.
C-EF	(g), (h), (i)	(g): weak 2ω-oscillations by the first two C-states, (h): energy shifts, (i): weak 2ω-oscillations by the last few C-states. Couplings between C-EF happen mostly off-resonantly.
D-EF	(h), (k), (m), (s)	(h), (k), (m): energy shifts, (s): weak 2ω-oscillations.
B-H	(c), (e), (f), (g)	(c), (f): weak energy shifts, (e), (g): weak 2ω-oscillations.
C-H	(f), (g)	(f): energy shifts, (g): weak 2ω-oscillations. The states there can couple resonantly to the H-states between $\approx$ 14eV and $\approx$ 14.5eV.
D-H	(s)	(s): weak 2ω-oscillations. Additionally in the areas (n)-(q), very weak energy shifts can be observed.
B-EF and D-EF	(a) - (e), (g)-(n), (q), (s)	(a), (b), (d), (e), (j), (l), (n), (q), (s): moderately strong to strong 2ω-oscillations, (g), (i): weaker 2ω-oscillations, (c), (h), (k), (m): energy shifts
B-H and D-H	—"—	Mostly the same effects as in the case B-EF and D-EF but only weaker; because only the H-states can couple, the oscillations shifts to right - it is less possible for the energetically lower B-states $\lesssim$ 12.4eV to couple with the H-states beg. from 14.0eV. The same applies to the D-states with energy $\lesssim$ 15.4eV - this is why in (l), (n) the 2ω-oscillations are barely visible.
C-EF and D-EF	(f)-(s)	(f), (g), (i): weak 2ω-oscillations, (n)-(s): moderately strong 2ω-oscillations, in (h), (j)-(m) energy shifts for both C- and D-states can be observed.
C-H and D-H	—"—	Mostly the same effects as in case above, but weaker, analogue argumentation like in the B-H and D-H case.

Table 3: A systematic investigation for identifying the contribution of different coupling configuration for the time-dependent structures in figure 17 is performed.

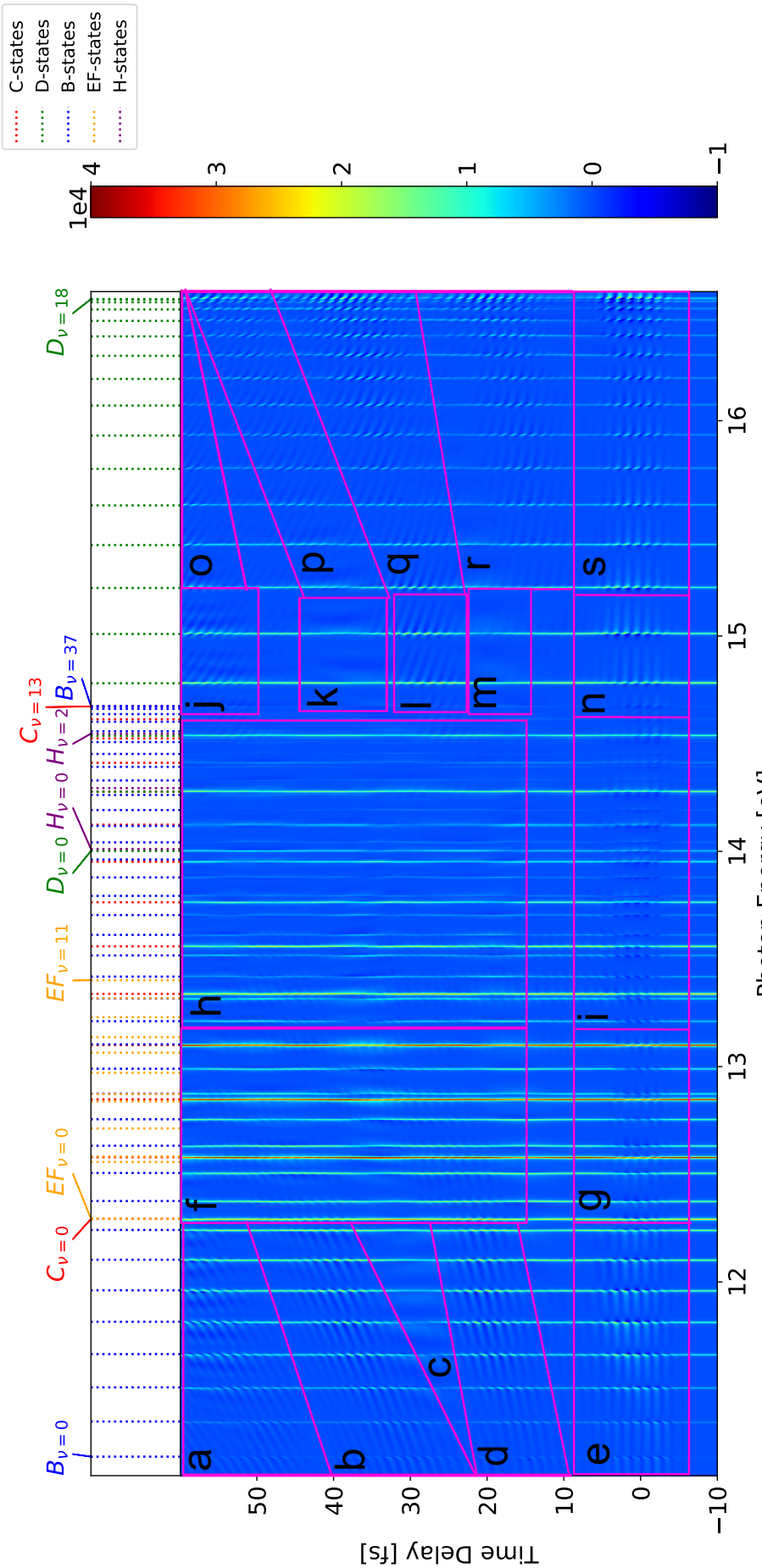

Figure 17: Time-delay scan, where couplings between all dark and bright states are allowed. The figure is divided in sections (a)-(s), where different time-dependent structures can be observed. Mostly there are 2ω-oscillations in (a), (b), (d), (e), (g), (i), (j), (l), (n)-(s) and energy shifts in (c), (f), (h), (k), (m), but also in (a). In table 3 a systematic approach for investigating different coupling configurations between certain dark and bright states, is performed, searching the causes of the structures.

The energy shifts indicated in (a), (c), (k) and (m) were discussed earlier in the previous cases, suggesting an AC stark effect could have caused them. Taking a closer look at section (h), figure 18, one can observe, how every shown line is shifted either to higher or lower energies. Since in the range of $\approx$ 12.6eV to $\approx$ 14.5 many of the B- and C-states are laying energetically very close to each other, so that interference effects may also cause energy shifts. The same argument can be applied for section (f). The behavior that the lines are not "straight" is only observed in the energy range of section (f) and (h). Weak 2ω-oscillations are observed, too, for the states between $\approx$ 13.2eV to $\approx$ 13.6eV, throughout almost the complete visible time-delay axis. But compared to figure 17, they are not that dominant as the oscillations that are pointed out explicitly.

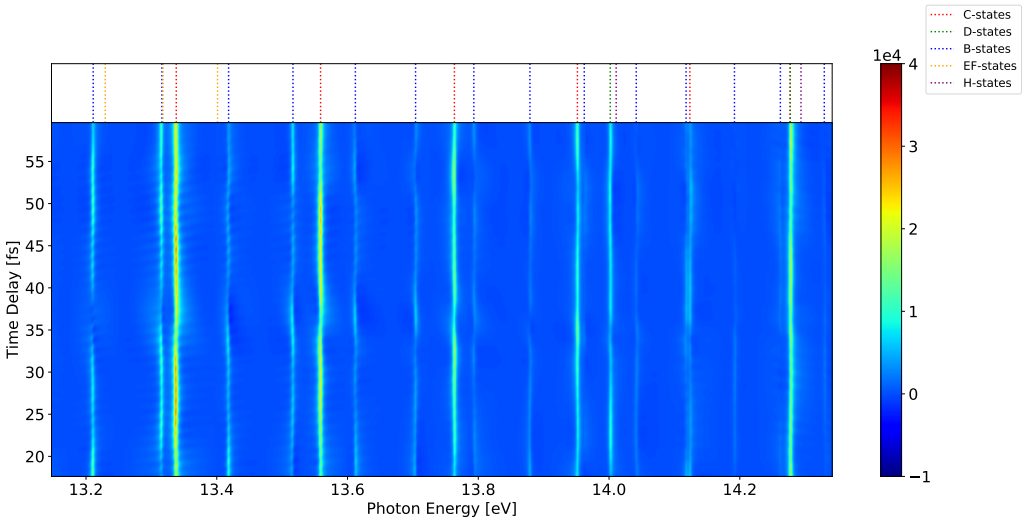

Figure 18: Zoomed in view of section (h). The spectral lines are shifted either to higher or lower energies. Between $\approx$ 13.2eV to $\approx$ 13.6eV, 2ω-oscillations occur, but they are not as dominant as the oscillations as e.g. in section (e).

If 2ω-oscillations are contributed by different kind of couplings configurations, e.g. in section (e) the B-EF and B-H coupling causes this effect, these oscillations are enhanced for the case, that all couplings are allowed.

Comparing to recent experimental works [21, 22], some structures could be reproduced, especially the oscillations in in (a), (b), (d), (e). This shows that our simulation could predict experimental results.

The associated Fourier plot to the time-delay scan using all couplings can be found in the appendix A as well.

5.2.3 Outlook: Intensity Scans and Franck-Condon Factors for the Couplings with NIR

Intensity scans for a fixed time delay τ are not only used to see their influences on the line shapes of the spectrum, but also to observe energy shifts, due to the Stark effect. Using this information one can make an estimate, how the couplings are influenced depending on the intensity. For $\tau = 5$fs, meaning in the overlap of the XUV and NIR pulses, an intensity scan was performed, where all couplings are allowed, see figure 19. The considered range starts from $\mathscr{E}_{0,\mathrm{NIR}} = 1 \cdot 10^{-4}$a.u. to $\mathscr{E}_{0,\mathrm{NIR}} = 5 \cdot 10^{-2}$a.u. in steps of $\Delta\mathscr{E}_{0,\mathrm{NIR}} = 2 \cdot 10^{-4}$a.u.

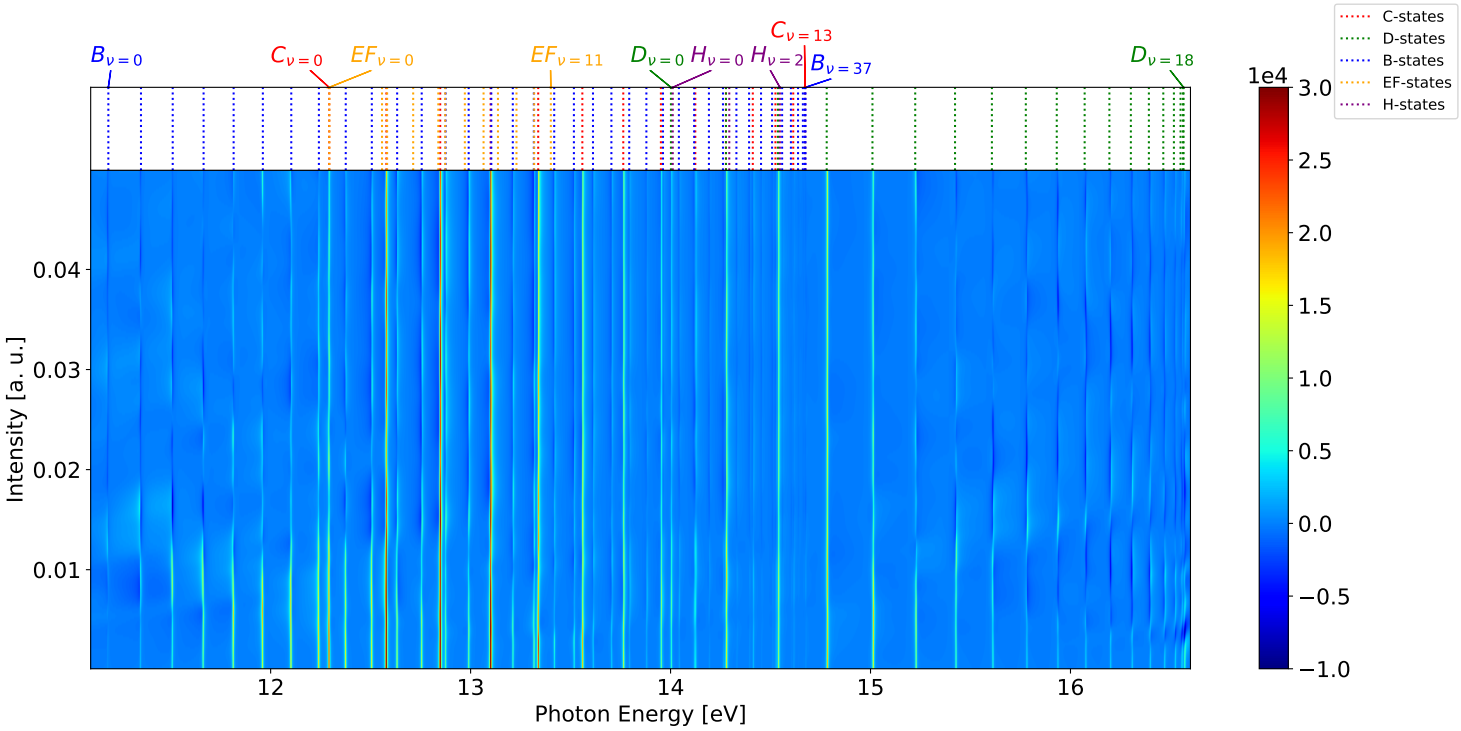

Figure 19: An intensity scan is performed at a time delay $\tau = 5$fs, where all couplings are allowed. The range of the scan is between $\mathscr{E}_{0,\mathrm{NIR}} = 1 \cdot 10^{-4}$ a.u. to $\mathscr{E}_{0,\mathrm{NIR}} = 5 \cdot 10^{-2}$a.u. in steps of $\Delta\mathscr{E}_{0,\mathrm{NIR}} = 2 \cdot 10^{-4}$a.u.

From this scan, one can observe how the line shape is changing, e.g. at ≈ 11.5eV, the line of the $B_{J=1,\nu=2}$-state is flipping from positive (yellow in the scale) to negative (dark blue in the scale), for $\mathscr{E}_{0,\mathrm{NIR}} \approx 0.015$a.u.

So far, the simulation sets all transition amplitudes from the dark states to the bright states equal to 1. However, in reality these amplitudes obey the `Franck-Condon`-principle. Briefly summarized, it quantifies the transition probabilities during a vibronic transition. This means that certain vibronic transition are more likely to happen, so that the non-zero entries in dipole moment operator $\hat{\mathbf{d}}_{NIR}(t)$ need to be adjusted. In [20] `Franck-Condon` factors are found for the hydrogen molecule. A time delay scan for using these factors by scaling the transition probabilities between

D- and EF-states is performed, where the couplings between B-/EF and D-/EF is allowed (figure 20 and figure 21 for the associated `Fourier` plot). Allowing B-EF increases the probability that more two-photon-transitions are happening, which can be observed better in the `Fourier` plot. Also the same case without scaling the transition probabilities is studied in section 5.2.2, so one can compare the scans with each other. In doing so, we use the same section classification as used in figure 17.

It is striking that the 2ω-oscillations of the D-states are almost non-existent in the sections (j), (o), (l), (q), (n), (s), as well for the B-states in (a), (b), (d), compared to figure 14 (B-EF and D-EF couplings are allowed). The scan looks very similar to the case, where only the B-EF coupling is allowed, figure 11. This is due to the `Franck-Condon` factors: most of the factors have a order of magnitude between 10^{-2} to 10^{-7}, while the maximum amplitude is at 0.9757 for the transition between the ground vibronic states. So the couplings with the NIR pulse is really unlikely, while the couplings between the B- and EF-states are dominating. For future calculations, one should consider the `Franck-Condon` factors for other couplings as well, to get a better understanding of how the system is really evolving and to have a system where the strength of the considered interactions are more similar to those in the real hydrogen system.

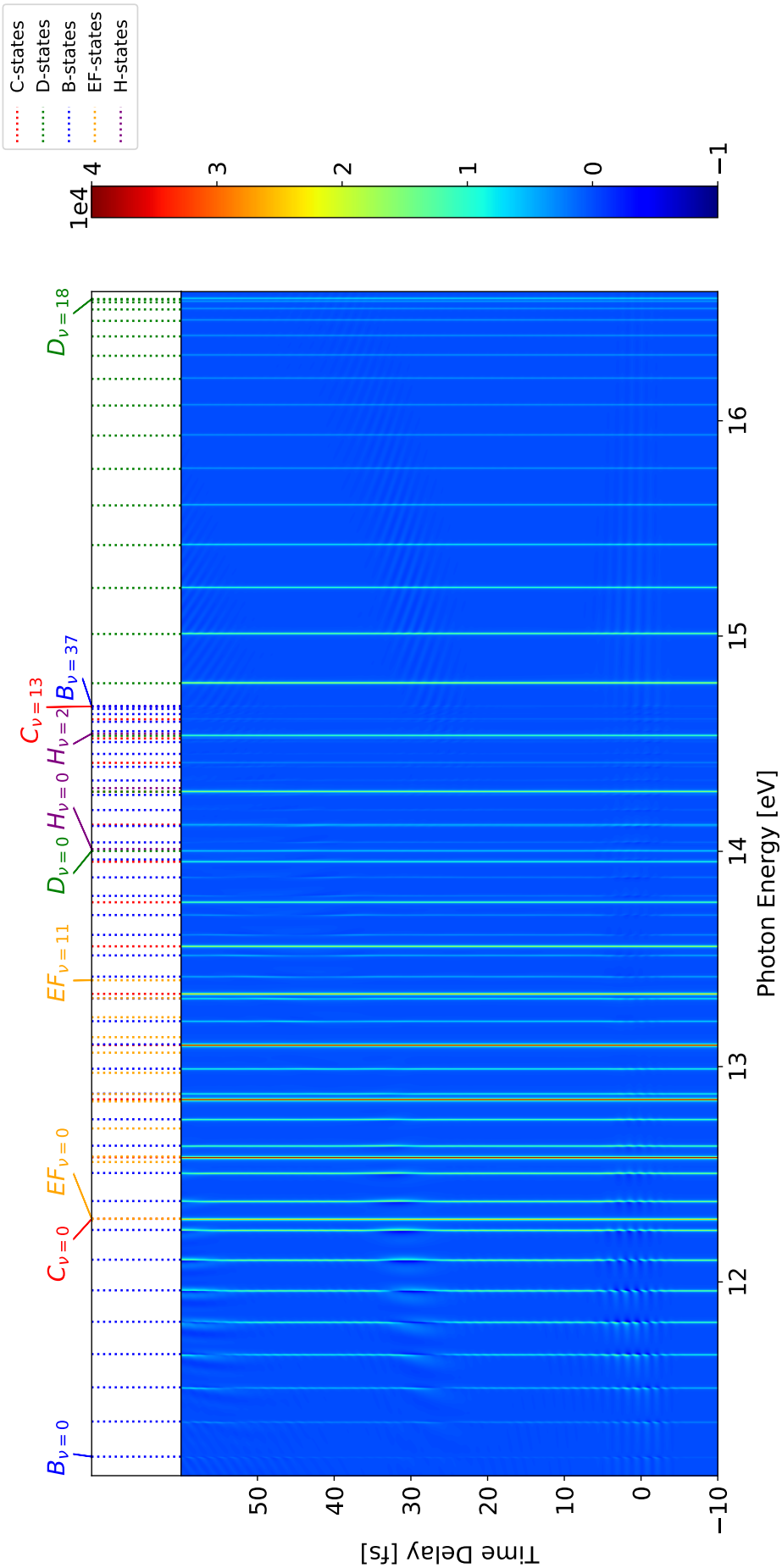

Figure 20: Time-delay scan, where couplings between B-EF and D-EF are allowed. `Franck-Condon` factors are used for the transition amplitudes for the D-EF coupling. The dominant 2ω-oscillations, as compared to case 2, are mostly not visible.

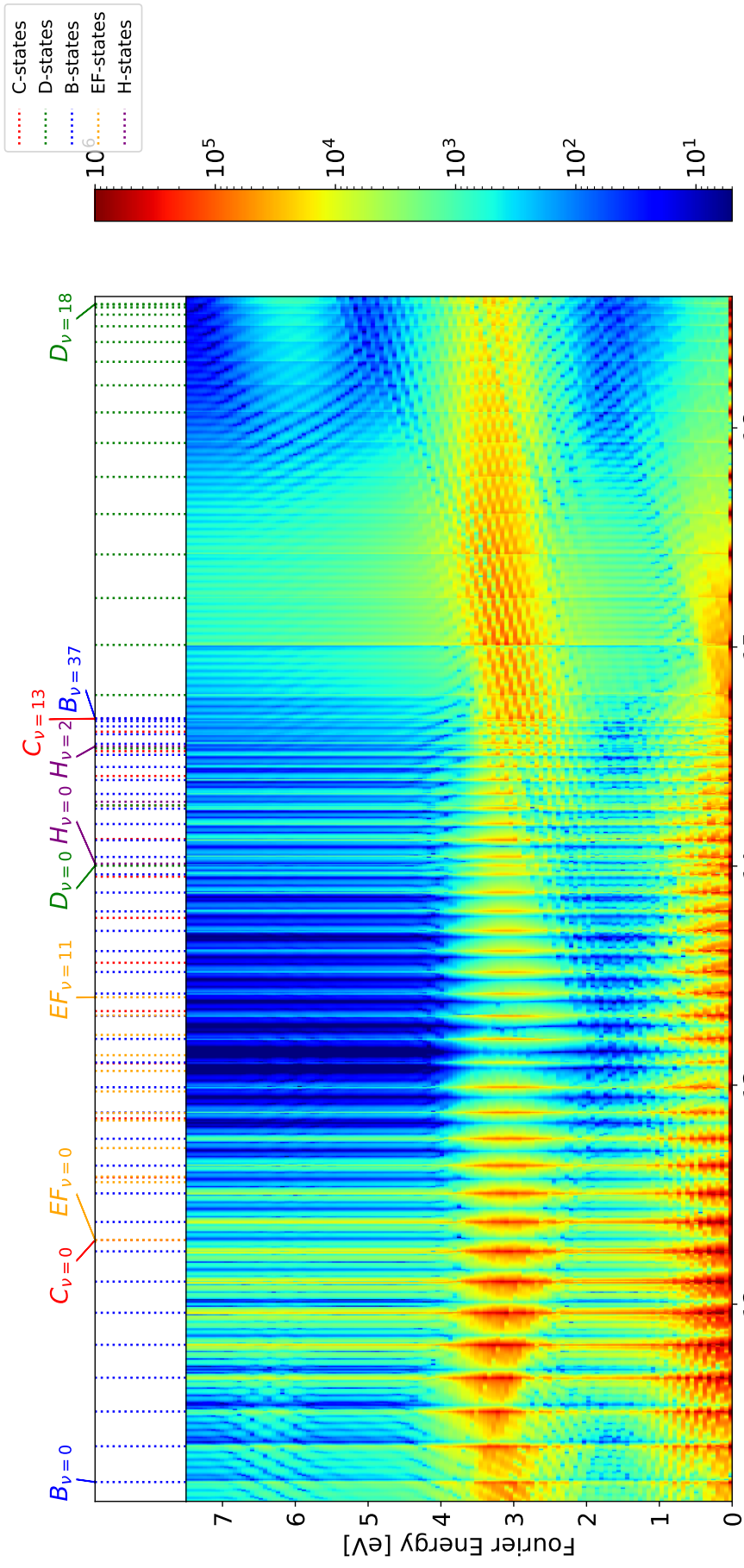

Figure 21: Associated Fourier Plot to figure 20. The probability for two-photon-transitions is greatly decreased, so that almost no straight lines indicating the transitions are visible.

6 Conclusion

The aim of the thesis was to get insights on dynamical processes in the molecular hydrogen system. Signatures of electronic and nuclear degrees of freedom imprinted on singly excited resonances of molecular hydrogen, are investigated theoretically. More specifically an NIR pulse is used to examine the couplings between different vibronic states. Selection rules limit certain transitions, this is why all considered bright states can be excited from the ground electronic state, and couplings between the excited bright states with the considered dark states are possible.

A numerical calculation was implemented in order to investigate the hydrogen system, assuming a few-level model. This model aims to solve the `Schrödinger` equation for the considered system, with known energies of the included eigenstates. The Hamiltonian used in the equation is built with respect to experimental data for the resonances and as well for the dipole moments, describing the transition amplitudes from the considered bright states to the ground electronic state, while the dipole moments describing the couplings via an NIR pulse are initially set all equally. The full Hamiltonian contains 87 states.

To get an intuitive understanding of how the system works, first, a simplified system with less degrees of freedom was considered. Only the ground electronic state, three bright states and one dark state were included. Using this five-level model, we were able to understand how populations transfer from the ground state to the bright states and via the NIR interaction to the dark state as well, for different time delays between the excitation pulse and the coupling pulse. The resonant line shapes were also examined. In absence of the NIR pulse, the spectral lines show a Lorentzian shape and under the influence of an NIR field they transform into asymmetrical `Fano` lines.

By considering all 87 states, not only the resonant lines spectrum using XUV only was observed, but also time-delay scans were performed in order to make predictions about their time-evolution. The time-delay scans of the dynamics of that many states shows rich dynamical behavior, if the couplings between all dark and bright states are possible. Thus, a systematic approach for identifying the time-dependent structures was considered. The idea was to look at time-delay scans, where only couplings between few selected states is allowed. Knowing which coupling contributes to which structure, we were able to conclude what causes the dynamics in the initially considered time-delay scan.

Nevertheless, only a real experiment reveals the true natural behavior of the considered system. However, recent studies [21, 22] about wave packet dynamics of molecular hydrogen, showed similar structures in their time-delay scans, compared to our calculations. Since our implementation did not consider `Franck-Condon` factors for all the transition amplitudes between dark and bright states, it is open to investigate, if one can produce similar results as well. Another possible extension to this work is to include more states that are energetically in the same range. Ionized hydrogen, H_2^+, has states in the considered energy range, which can be seen as additional population loss channel, leading to a kind of a discrete continuum. It would be interesting to investigate, in which way the dynamics in such a system would change.

A Appendix

The time-delay scans (TDS) and Fourier plots (FP) for different allowed coupling configurations can be found:

- C-EF. TDS: figure 22, FP: 23
- D-EF. TDS: figure 24, FP: 25
- B-H. TDS: figure 26, FP: 27
- C-H. TDS: figure 28, FP: 29
- D-H. TDS: figure 30, FP: 31
- B-H and D-H. TDS: figure 32, FP: 33
- C-EF and D-EF. TDS: figure 34, FP: 35
- C-H and D-H. TDS: figure 36, FP: 37
- Couplings between all bright and dark states. FP: 38

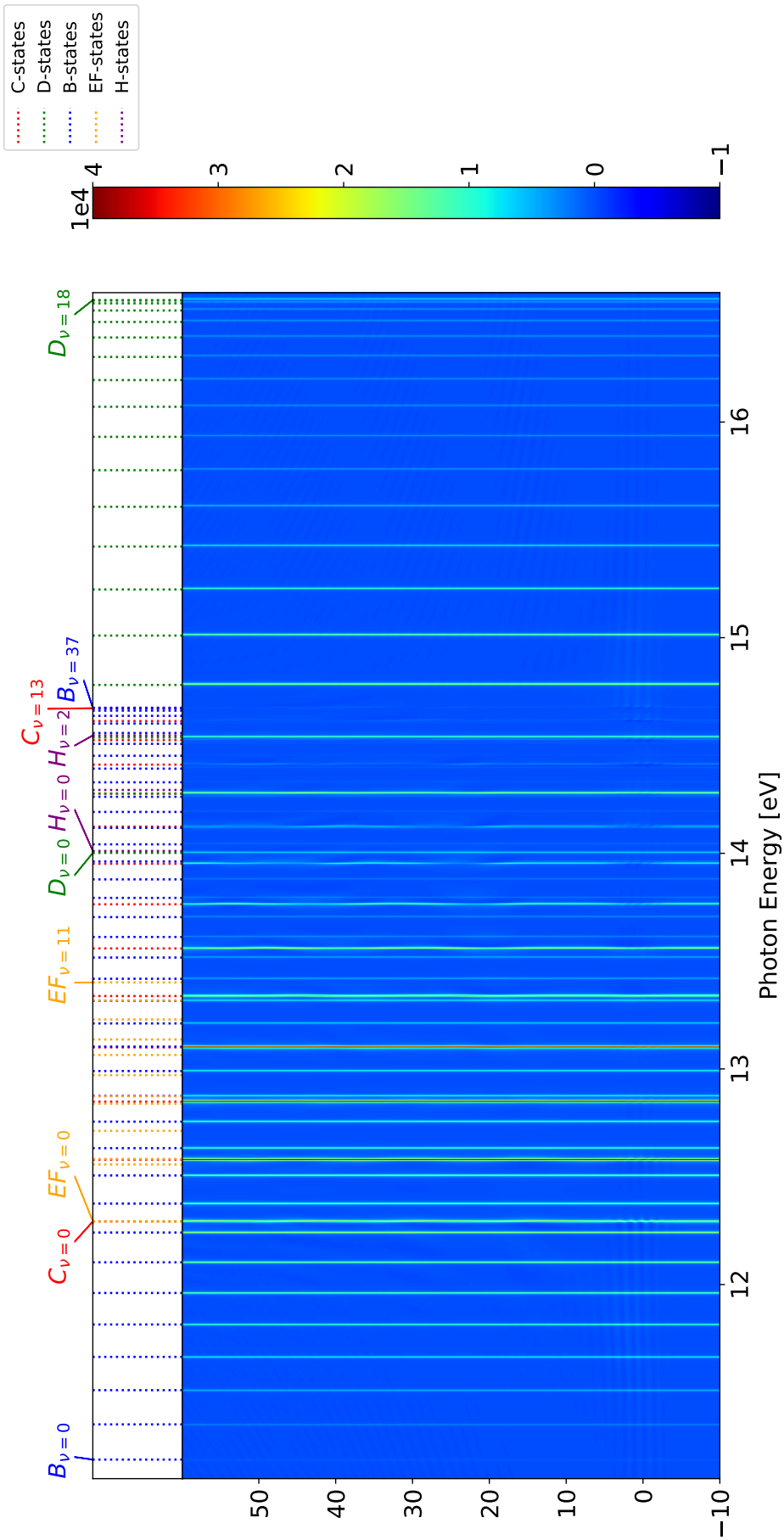

Figure 22: Time-delay scan, where couplings between the C-/EF-states are allowed.

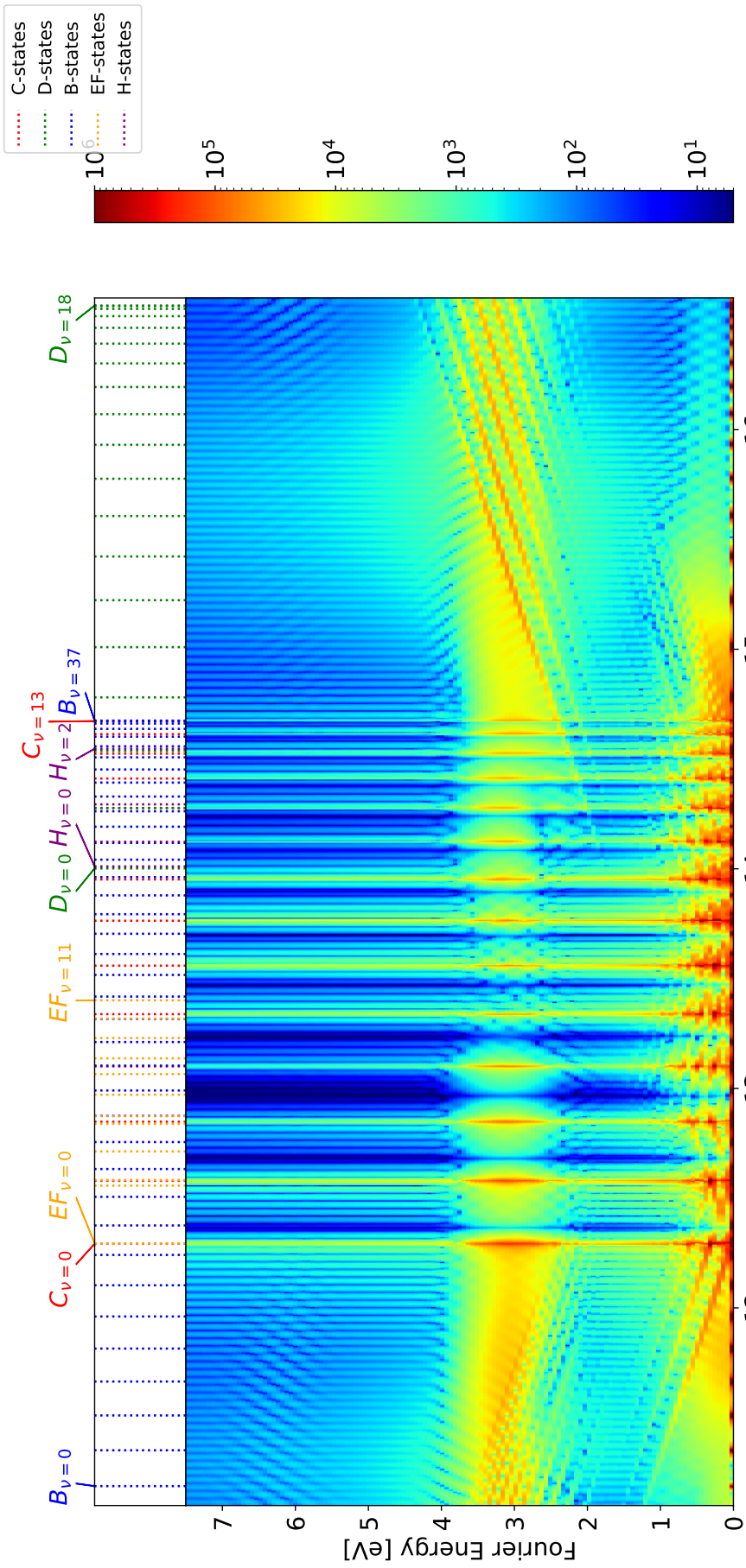

Figure 23: Fourier plot, where couplings between the C-/EF-states are allowed.

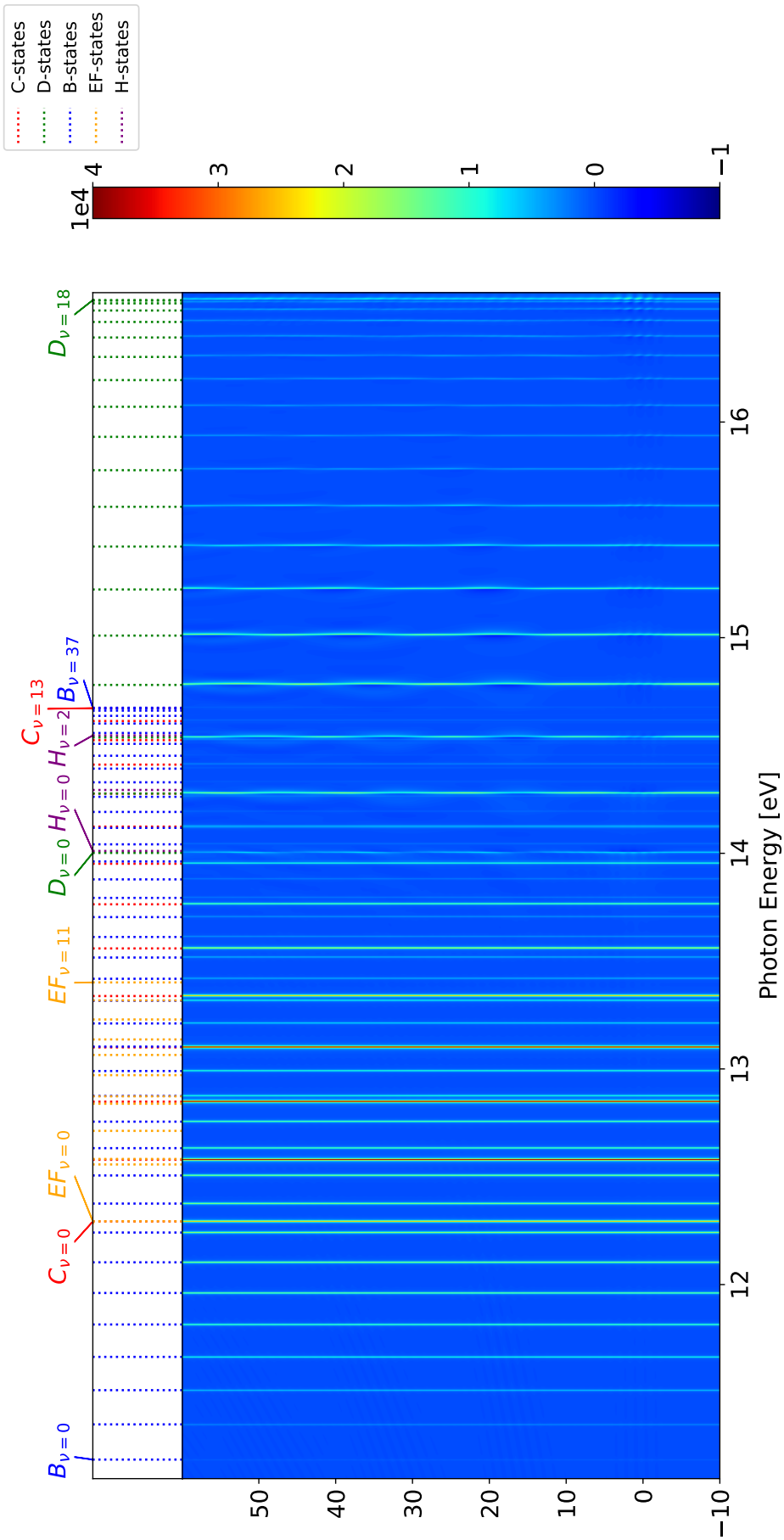

Figure 24: Time-delay scan, where couplings between the D-/EF-states are allowed.

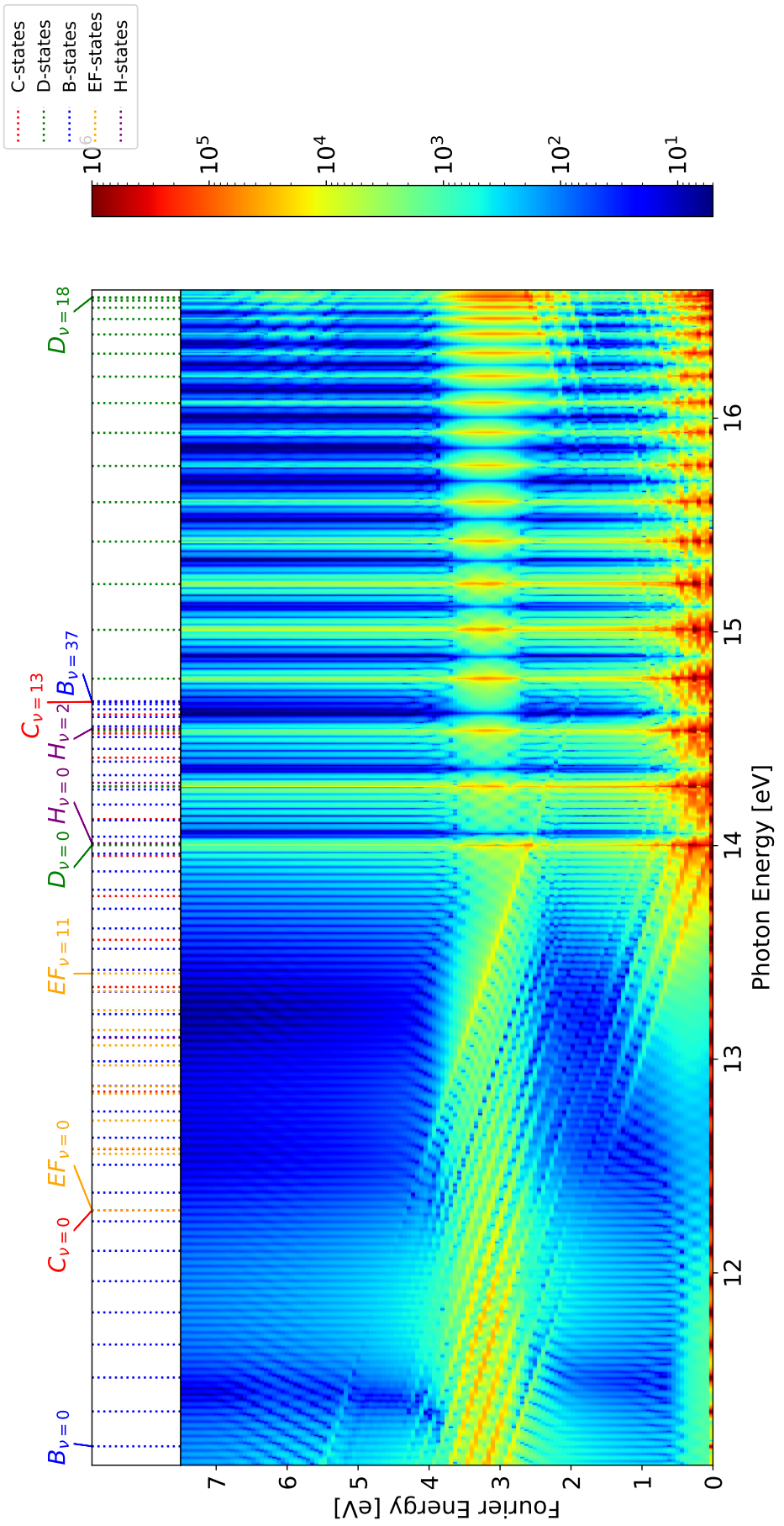

Figure 25: Fourier plot, where couplings between the D-/EF-states are allowed.

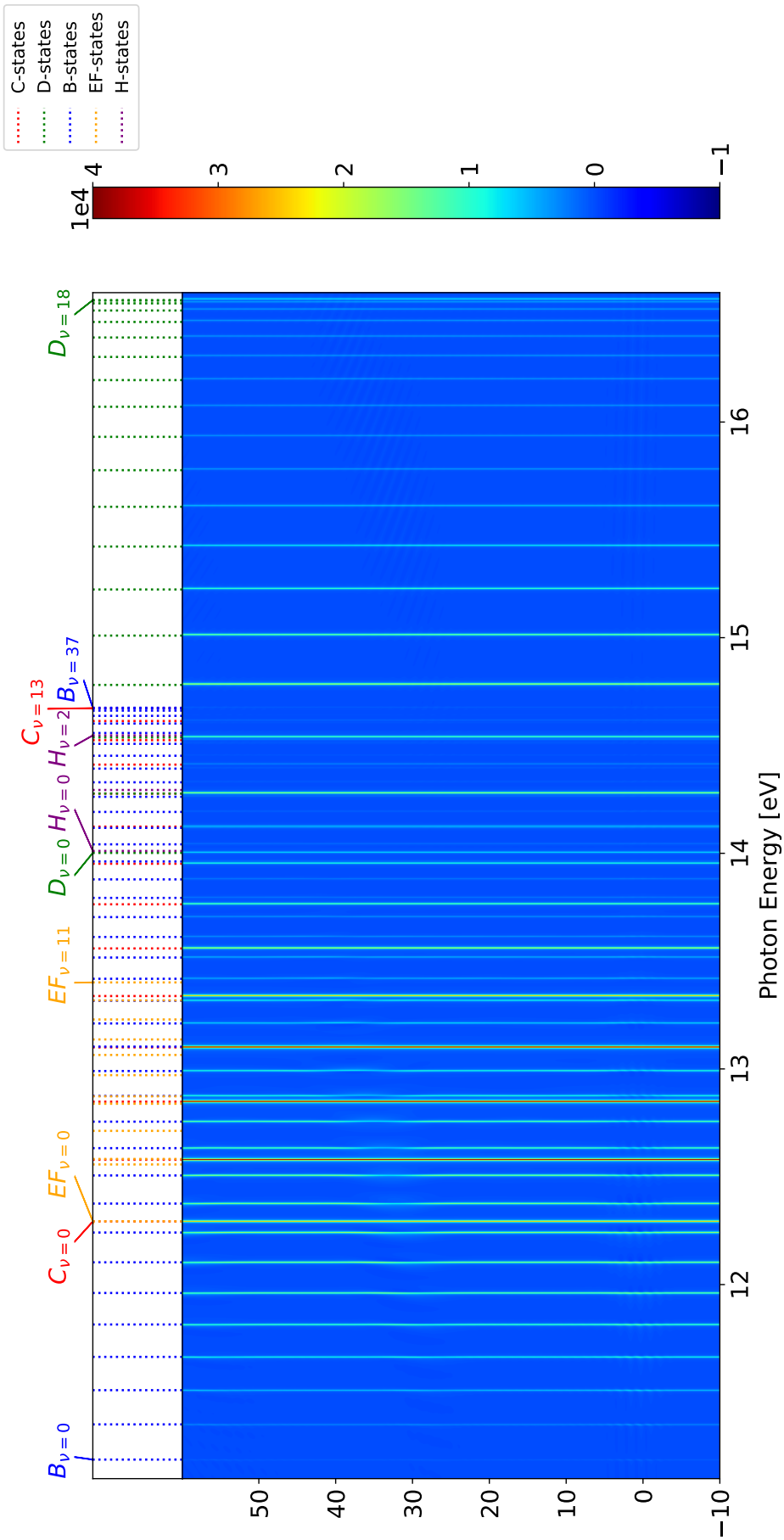

Figure 26: Time-delay scan, where couplings between the B-/H-states are allowed.

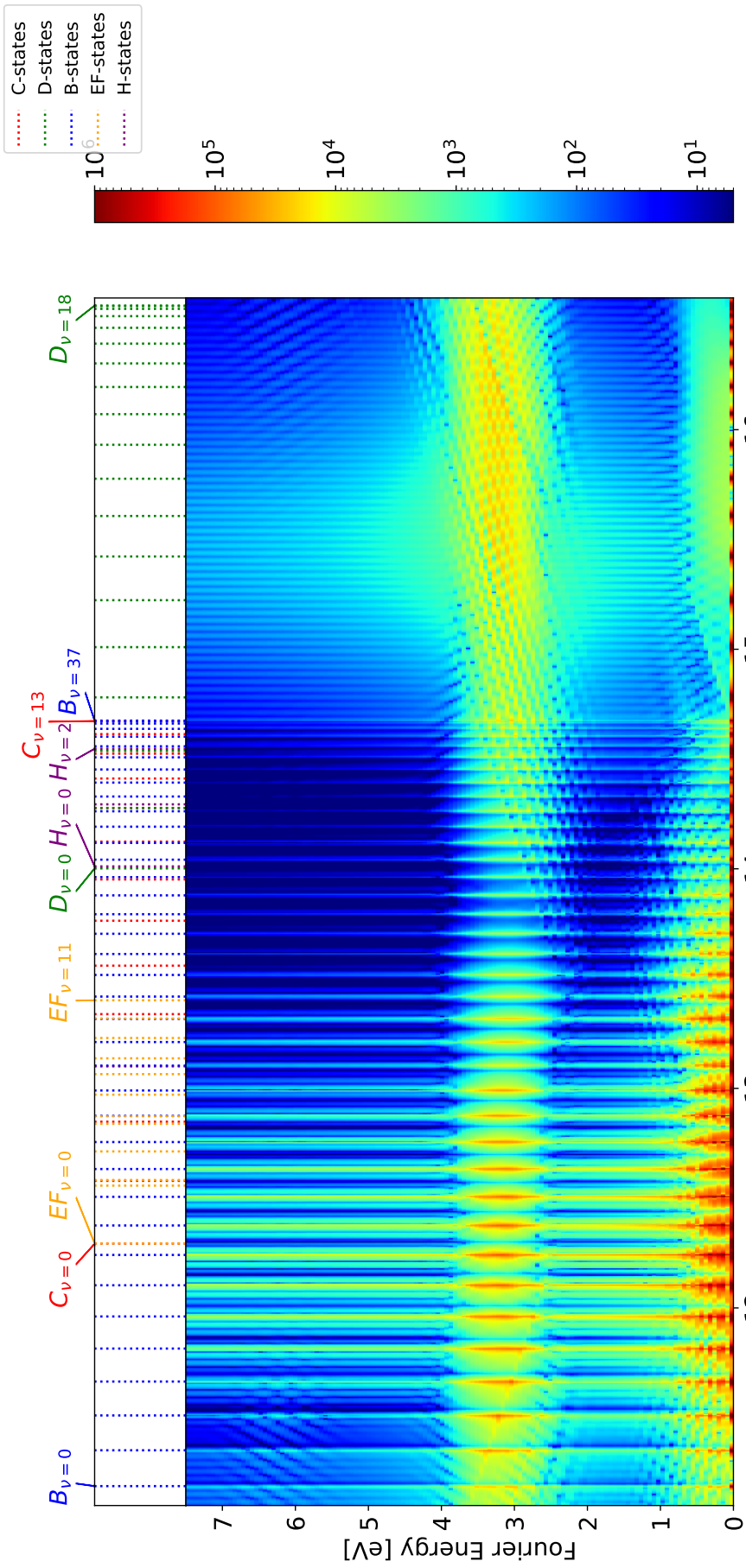

Figure 27: Fourier plot, where couplings between the B-/H-states are allowed.

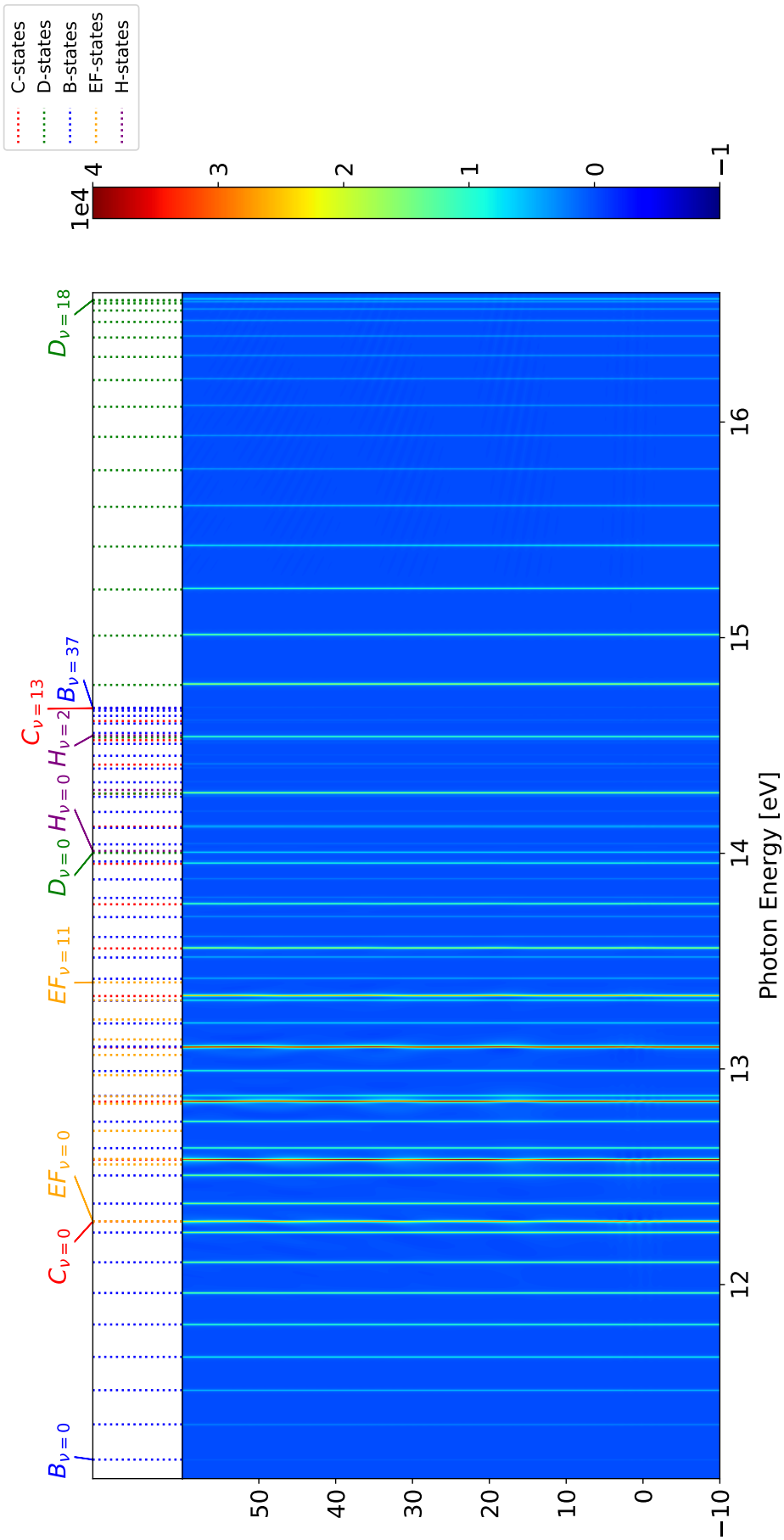

Figure 28: Time-delay scan, where couplings between the C-/H-states are allowed.

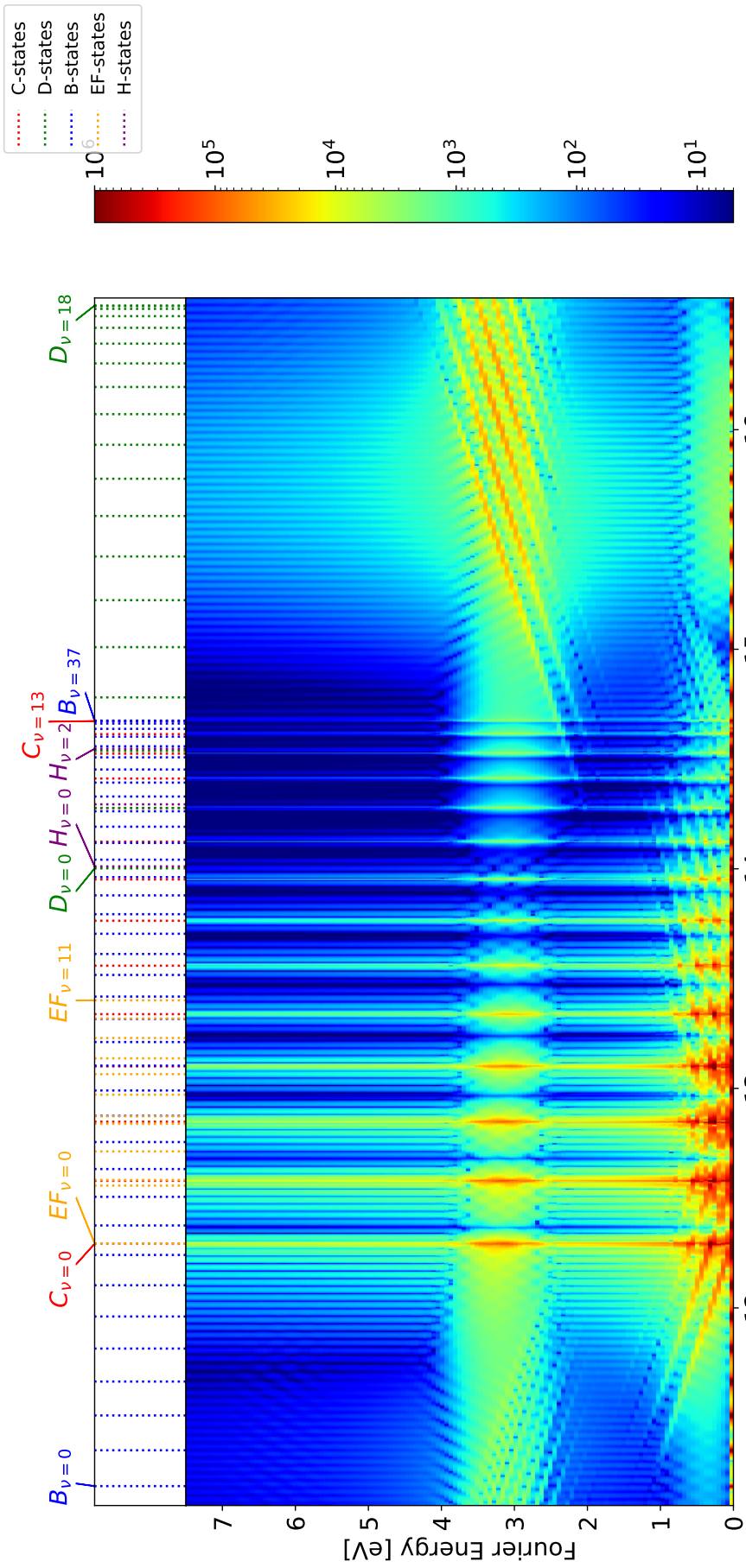

Figure 29: Fourier plot, where couplings between the C-/H-states are allowed.

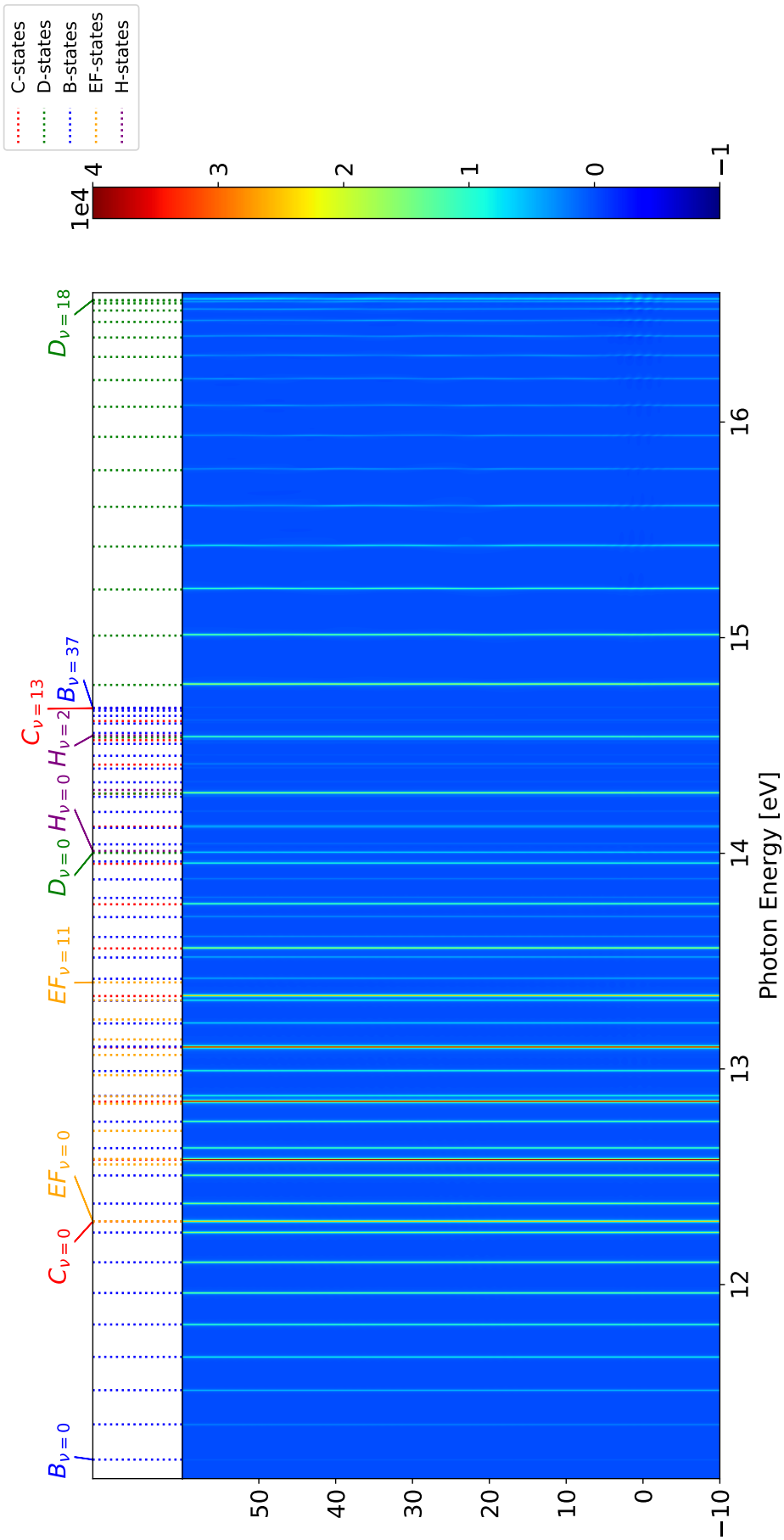

Figure 30: Time-delay scan, where couplings between the D-/H-states are allowed.

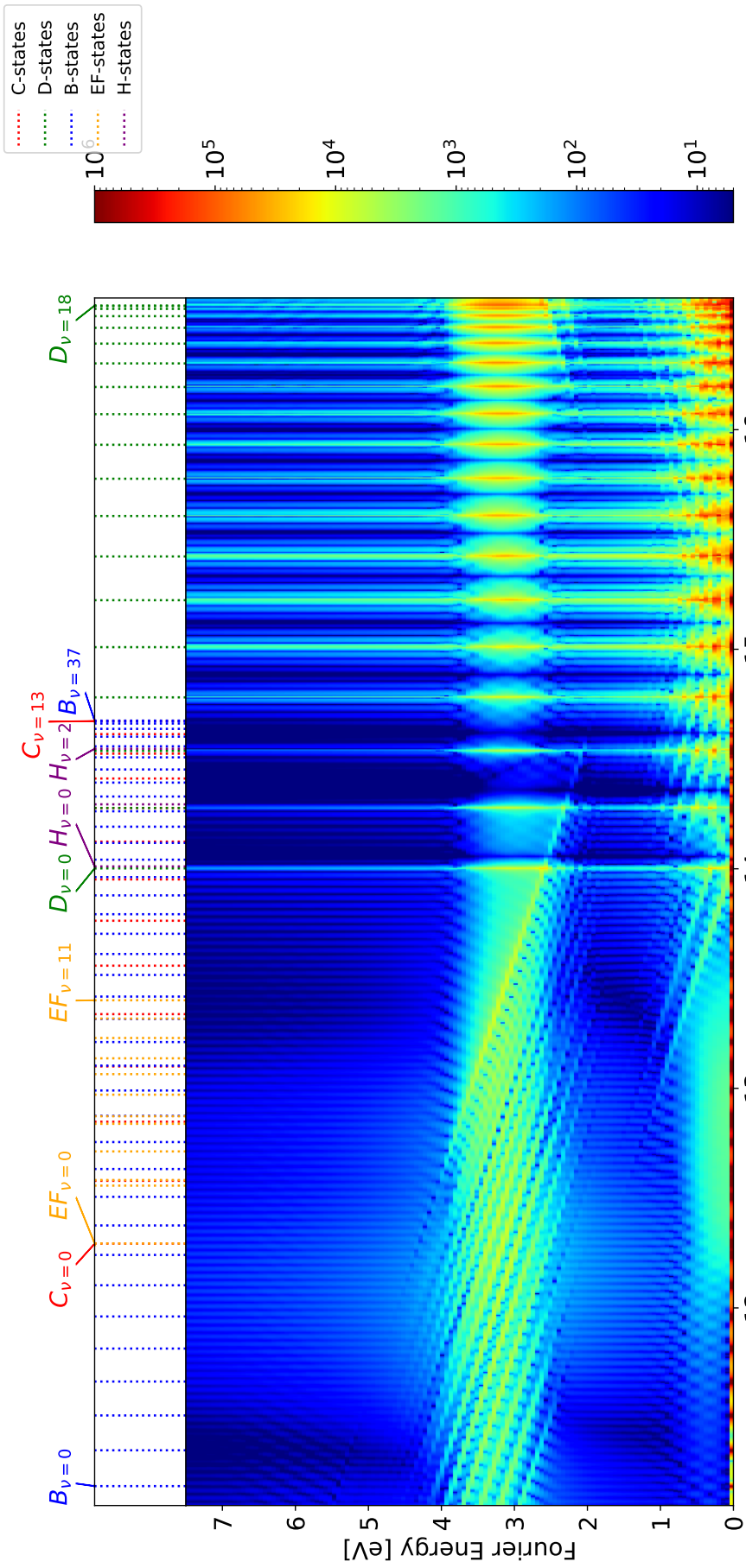

Figure 31: Fourier plot, where couplings between the D-/H-states are allowed.

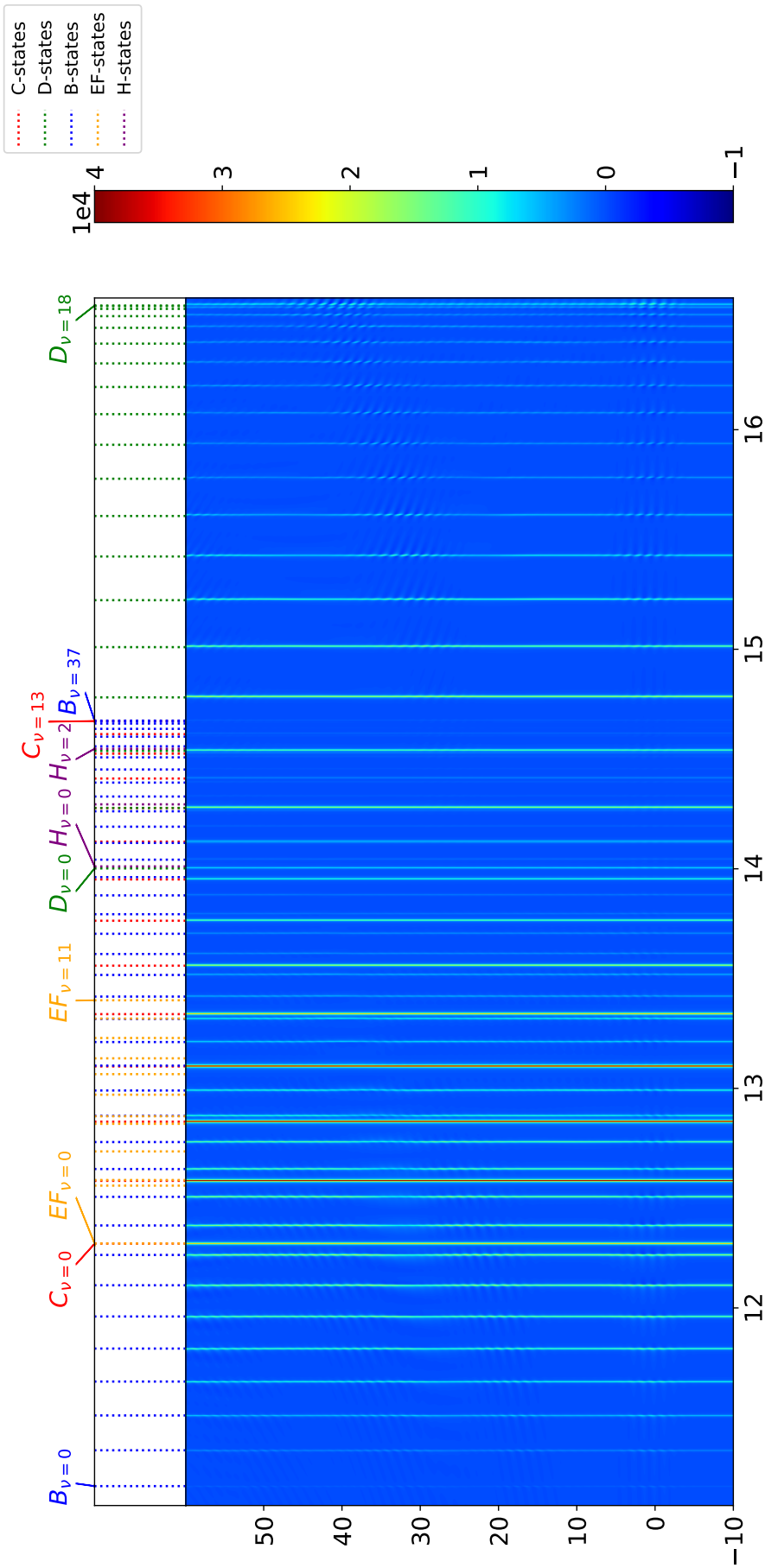

Figure 32: Time-delay scan, where couplings between the B-/H-states and D-/H-states are allowed.

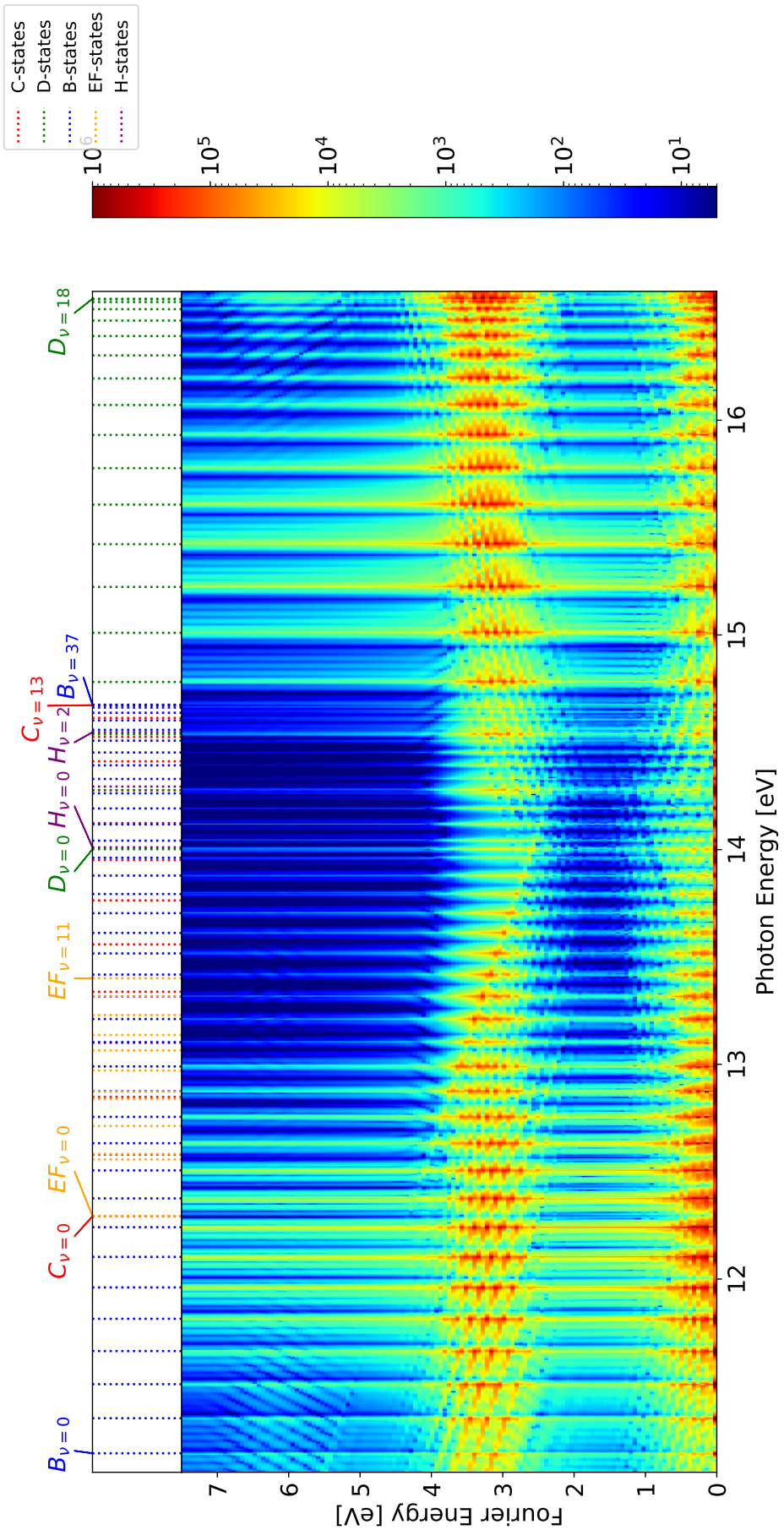

Figure 33: Fourier plot, where couplings between the B-/H-states and D-/H are allowed.

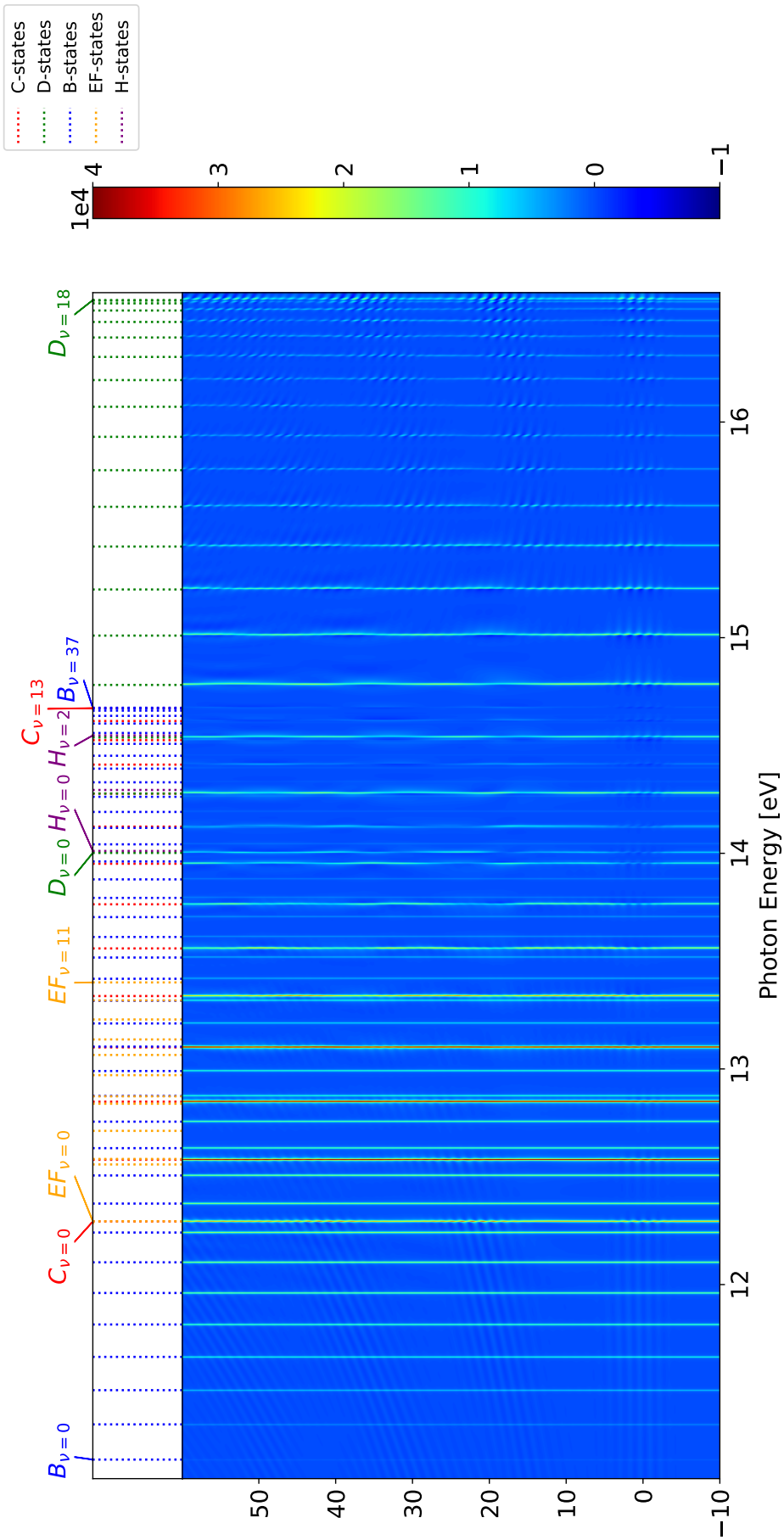

Figure 34: Time-delay scan, where couplings between the C-/EF-states and D-/EF-state are allowed.

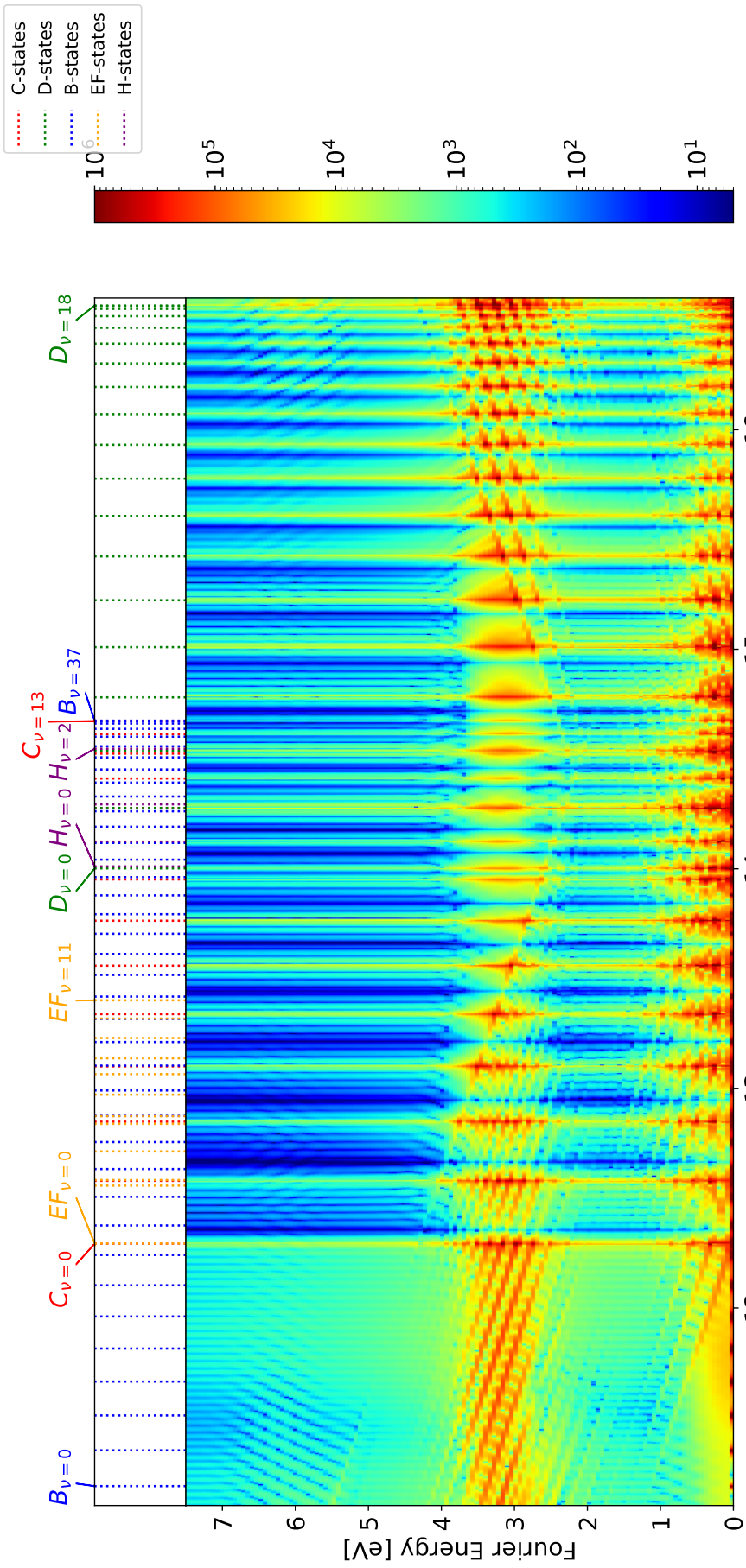

Figure 35: Fourier plot, where couplings between the C-/EF-states and D-/EF-states are allowed.

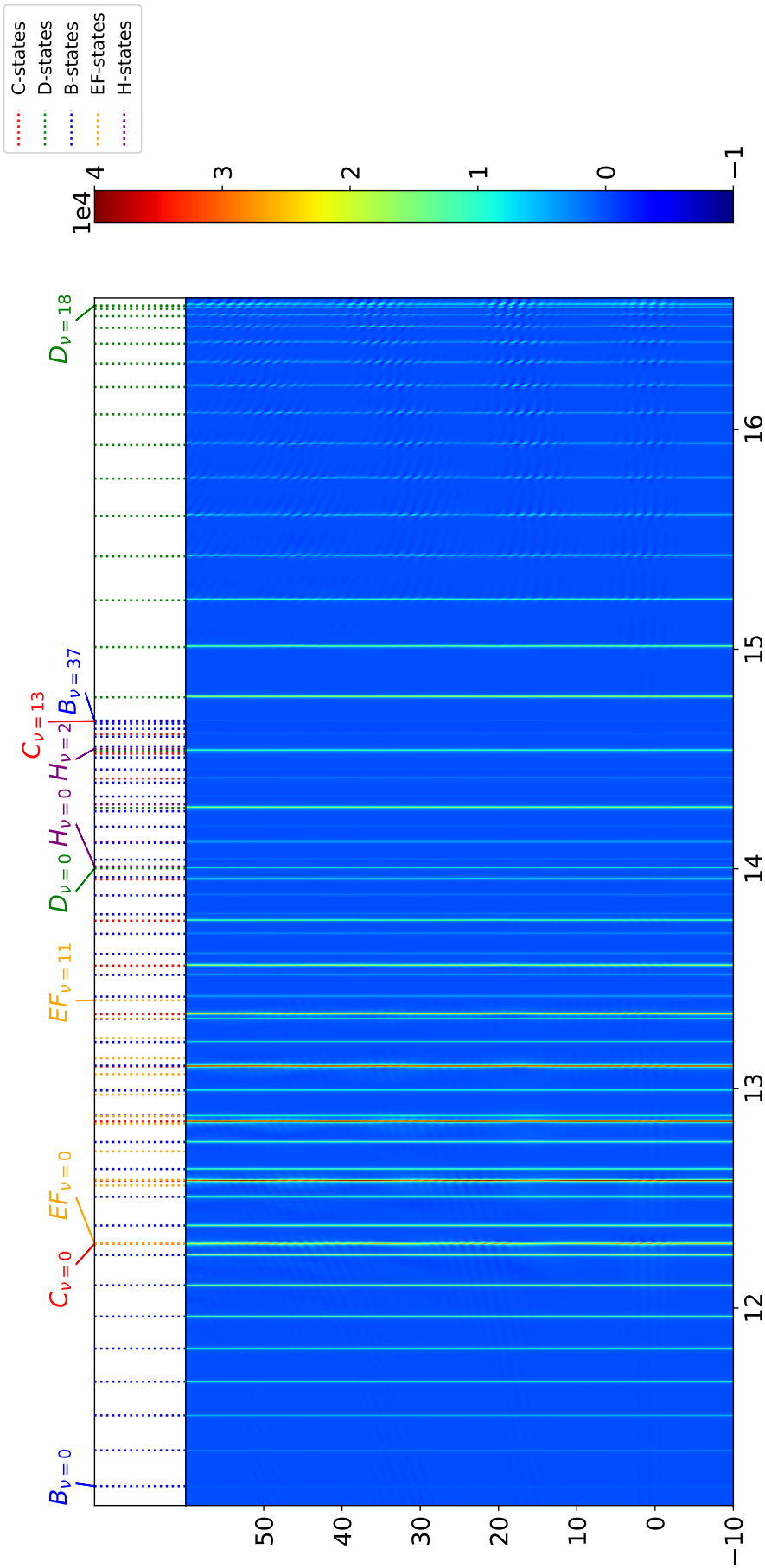

Figure 36: Time-delay scan, where couplings between the C-/H-states and D-/H-states are allowed.

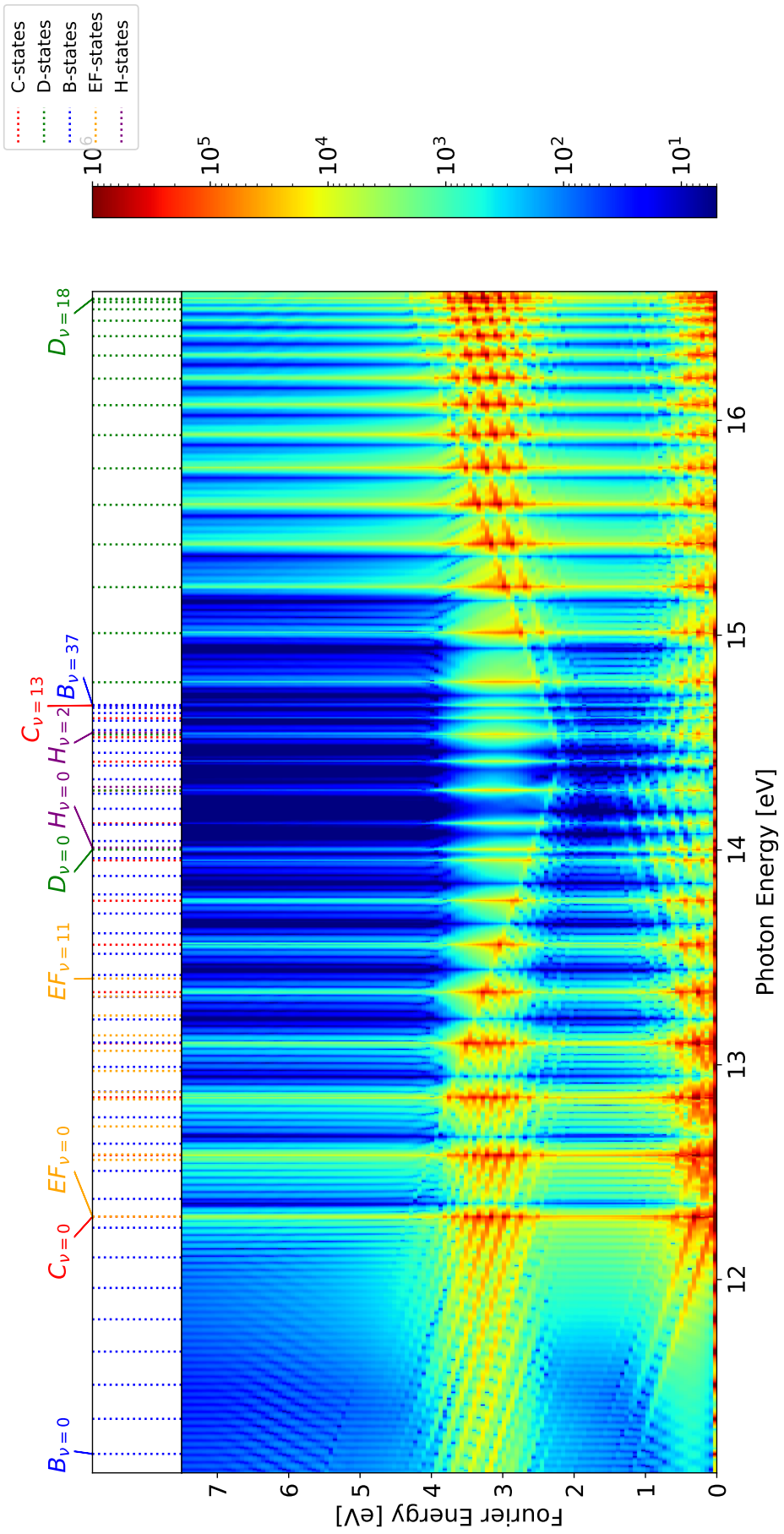

Figure 37: Fourier plot, where couplings between the C-/H-states and D-/H-states are allowed.

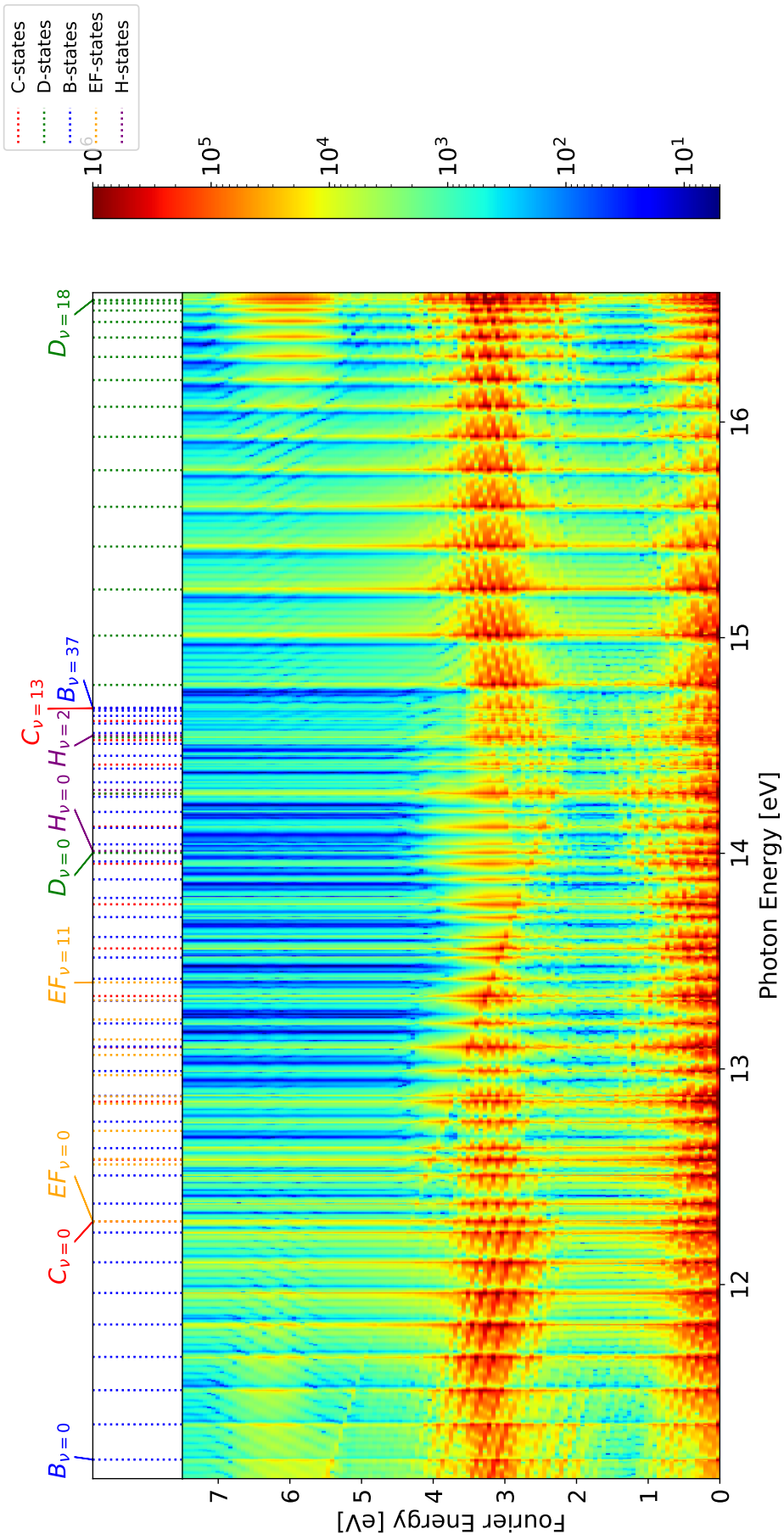

Figure 38: Fourier plot, where couplings between all bright and dark states are allowed.

References

[1] E. Rutherford. *The Scattering of α and β Particles by Matter and the Structure of the Atom.* Philosophical Magazine, Series 6, vol. 21, May 1911, p. 669-688

[2] C. Ott. *Attosecond multidimensional interferometry of single and two correlated electrons in atoms.* PhD Thesis, University of Heidelberg, 2012

[3] V. Stooß et al. *XUV-beamline for attosecond transient absorption measurements featuring a broadband common beam-path time-delay unit and in situ reference spectrometer for high stability and sensitivity.* Review of Scientific Instruments 90, 053108, 2019

[4] T. Ding et al. *Nonlinear Coherence Effects in Transient-Absorption Ion Spectroscopy with Stochastic Extreme-Ultraviolet Free-Electron Laser Pulses.* Physical Review Letters 123, 103001, 2019

[5] G. D. Borisova. *Theoretical and Experimental Studies of XUV Multielectron (Auto-) Ionization Dynamics in Helium and Molecular Hydrogen.* MSc Thesis, University of Heidelberg, 2017

[6] I. V. Hertel, C. Schulz. *Atoms, Molecules and Optical Physics 2: Molecules and Photons - Spectroscopy and Collisions.* Springer-Verlag Berlin Heidelberg, 2015

[7] M. Born, J. R. Oppenheimer. *Zur Quantentheorie der Molekeln.* Annalen der Physik 389 (20): 457–484, 1927.

[8] T. Ding. *Quantum dynamics in weak and strong fields measured by XUV nonlinear spectroscopy.* PhD Thesis, University of Heidelberg, 2018

[9] J. Evers. *Theoretical Quantum Optics.* Lecture notes from summer semester 2020, University of Heidelberg

[10] T. E. Sharp. *Potential-energy curves for molecular hydrogen and its ions.* Atomic Data 2, 119-169, 1971

[11] MOLAT, Atomic and Molecular Data. *Line emission Probabilities for B-X (Lyman), C-X (Werner), B'-X and D-X bands of the H2 molecule.* Website of l'Observatoire de Paris. https://molat.obspm.fr/index.php?page=pages/Molecules/H2/H2can94.php

[12] G. H. Dieke *The Molecular Spectrum of Hydrogen and Its Isotopes.* Journal of molecular spectroscopy 2, 494-517, 1958

[13] A. D. Bandruck, H. Shen. *Exponential split operator methods for solving coupled time-dependent Schrödinger equations.* The Journal of Chemical Physics 99, 1185–1193, 1993

[14] A. D. Bandruck, H. Shen. *Improved exponential split operator method for solving the time-dependent Schrödinger equation.* Chemical Physics Letters, Volume 176, Issue 5, 1991, Pages 428-432.

[15] J. Diels, R. Wolfgang. *Ultrashort Laser Pulse Phenomena, 2nd Edition.* Academic Press, 2006

[16] T. Pfeifer. Personal discussion on a zoom meeting, 06.10.2020

[17] A. Blättermann et al. *Two-dimensional spectral interpretation of time-dependent absorption near laser-coupled resonances.* Journal of Physics B: Atomic, Molecular and Optical Physics, Volume 47, Number 12, 2014

[18] Systemtheorie Online. *Frequenzauflösung der diskreten-Fourier-Transformation - Zero-Padding.* Website of Hochschule Karlsruhe Technik und Wirtschaft https://www.eit.hs-karlsruhe.de/mesysto/teil-b-zeitdiskrete-signale-und-systeme/diskrete-fourier-transformation/frequenzaufloesung-der-diskreten-fourier-transformation-zero-padding/zero-padding-im-zeitbereich.html

[19] U. Fano. *Effects of configuration interaction on intensities and phase shifts.* Physical Review 124, 1866-1878, 1961

[20] U. Fantz, D. Wünderlich. *Franck–Condon Factors, Transition Probabilities and Radiative Lifetimes for Hydrogen Molecules and Their Isotopomeres.* Atomic Data and Nuclear Data Tables Volume 92, Issue 6, November 2006, Pages 853-973

[21] W. Cao et al. *Excited-state vibronic wave-packet dynamics in H_2 probed by XUV transient four-wave mixing.* Physical Review A 97, 023401, 2012

[22] Y. Cheng et al. *Reconstruction of an excited-state molecular wave packet with attosecond transient absorption spectroscopy.* Physical Review A 94, 023403, 2016

Danksagung

Das Wichtigste in dieser Arbeit ist es sich bei allen zu bedanken, die mich während der Zeit unterstützt haben.

An erster Stelle bedanke ich mich bei **Thomas Pfeifer**, der es mir ermöglicht hat, die Arbeit in seiner Abteilung zu schreiben und mir durch seinen Input in den Diskussionen fachlich zur Seite stand.

Ein herzliches Dankeschön gebührt **Robert Moshammer**, der so freundlich war und die Zweitkorrektur übernommen hat.

Ebenfalls möchte ich mich zutiefst bei **Christian Ott** bedanken, der mich herzlich in seiner Gruppe aufgenommen hat. Er hatte immer einen aufmerksamen Blick für meine Simulation, und hat viele Verbesserungsvorschläge gegeben. Dadurch konnte ich viele Hintergründe besser verstehen.

Mein größter Dank gilt aber **Gergana Borisova**. Du hast mich tagtäglich betreut und warst immer jeder Zeit für neue Fragen und für Diskussionen neuer Ergebnisse für mich da. Du hattest viele Ideen und Vorschläge gehabt, wie man gewisse Probleme angehen kann - von dir habe ich eine Menge gelernt! Auch bei der Literatursuche hast du mir geholfen. Zum Schluss hast du dir auch noch viel Mühe beim Korrekturlesen gegeben und diverse Fehler gefunden, sowie Formulierungsvorschläge gegeben. Eine bessere Betreuung hätte ich mir nicht wünschen können!

Ein Dankeschön geht auch an **Felicitas Franke** und **Frederike Hanisch**, die ebenfalls Korrektur gelesen haben.

Des Weiteren möchte ich mich noch bei **Paul Birk** bedanken, dessen Code ich als Grundlage für meine Implementierung nutzen durfte und er mir auch erklärt hat, wie der Code funktioniert.

Auch möchte ich mich beim Personal der Mensa bedanken, deren Essen mir im Laufe des Studiums stets die nötige Kraft gegeben haben.

Zu guter Letzt gilt mein Dank an meine Freunde, meinen Eltern und meiner Schwester, **Nina Fan**, die immer hinter mir standen und mich auf meinem Weg begleitet haben.

Erklärung

Ich versichere, dass ich diese Arbeit selbstständig verfasst und keine anderen als die angegebenen Quellen und Hilfsmittel benutzt habe.

Heidelberg, den 24.08.2020 .....